

**Sensitivity of Tropical Cyclone Mahasen to Physical Parameterization
Schemes using Weather Research & Forecasting (WRF) model**

BY

SAMIR KUMAR DEBNATH

Roll No: 1155554

Session: July 2011

A thesis submitted in partial fulfillment of the requirements for the degree of Master of
Philosophy in the Department of Physics, Khulna University of Engineering &
Technology, Khulna-9203



DEPARTMENT OF PHYSICS

Khulna University of Engineering & Technology


Khulna-9203, Bangladesh

January 2018

DECLARATION

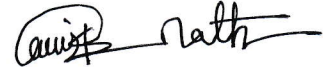
This is to certify that the thesis work entitled as "*Sensitivity of Tropical Cyclone Mahasen to Physical Parameterization Schemes using Weather Research & Forecasting (WRF) model*" has been carried out by SAMIR KUMAR DEBNATH in the Department of Physics, Khulna University of Engineering & Technology, Khulna-9203, Bangladesh. The above research work or any part of this work has not been submitted to anywhere for the award of any degree or diploma.

Signature of Supervisor



Professor Dr. Md. Abdullah Elias Akhter

Signature of Candidate



SAMIR KUMAR DEBNATH

DEDICATED

TO

**THOSE WHO LOST THEIR LIVES BY MAHASEN AND THEIR
FAMILIES**

ACKNOWLEDGEMENT

I have had a lot of help with this thesis work from many individuals in various selfless Ways. With my great manner it is great pleasure for me to express my deepest sense of gratitude, indebtedness and honor to my respected supervisors Professor Dr. Md. Abdullah Elias Akhter, Department of Physics, Khulna University of Engineering & Technology, Khulna for suggesting me the problem and for his able guidance, encouragement and constant consultation throughout the course of the research work without which it would not be possible on my part to complete the work.

It is a matter of great pleasure for me to record the deepest sense of gratitude to Professor Dr. Shibendra Shekher Sikder, Head of the Department, Physics, Khulna University of Engineering & Technology, Khulna, who has given me a strong support in various ways during the entire period of my study in this department.

I am indebted also to Professor Dr. Md. Mahbub Alam, who also has given me a strong support in various ways during the entire period of my study in this department. Professor, Dr. Jolly Sultana, Department of Physics, KUET for their invaluable suggestions and inspiration during my study and thesis period in this department.

I gratefully acknowledge Mr. Md. Kamrul Hasan Reza, Mr. Sujit Kumar Shil, Md. Alamgir Hossain, Assistant Professors and Mr. Sumon Halder, Sumon Deb Nath, Lecturer, Department of Physics, KUET for their co-operation regarding writing the thesis.

I convey my sincere thanks to Principal Refat Jahan Khan, Gabkhali Magura United Degree College, Avoyagar, Jessore who extended his helping hands and gave me potential administrative supports and constant encouragements during this research work.

My personal thankful greetings are to my good friends and well-wishers for their help and cooperation. I am highly grateful to my parents, brothers, sisters and wife and nearest relatives for their inspiration, encouragement and support to carry out this M. Phil thesis work.

My thanks are due to research staff of SMRC and Bangladesh Meteorological Department (BMD) for providing necessary data with other necessary help.

I also wish to thank the authority of Khulna University of Engineering & Technology (KUET), for providing me with the necessary permission and financial assistance for conducting this thesis work.

Finally, All thanks and gratitude is due to Almighty God whose blessings are always with me.

Samir Kumar Debnath

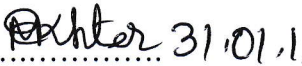
**KHULNA UNIVERSITY OF ENGINEERING & TECHNOLOGY
DEPARTMENT OF PHYSICS**

Approval

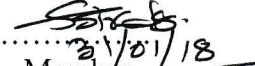
This is to certify that the thesis work submitted by Samir Kumer Debnath entitled **“Sensitivity of Tropical Cyclone Mahasen to Physical Parameterization Schemes using Weather Research & Forecasting (WRF) model”** has been accepted by the board of examiners in partial fulfillment of the requirements for the degree of Master of Philosophy in the Department of Physics, Khulna University of Engineering & Technology, Khulna, Bangladesh on 31 January 2018.

Board of Examiners

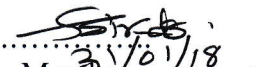
1. Prof. Dr. Md. Abdullah Elias Akhter
Department of Physics
Khulna University of Engineering & Technology


..... 31.01.18
Chairman & Supervisor


2. Head
Department of Physics
Khulna University of Engineering & Technology


..... 31/01/18
Member


3. Prof. Dr. Shibendra Shekher Sikder
Department of Physics
Khulna University of Engineering & Technology


..... 31/01/18
Member

4. Prof. Dr. Md. Mahbub Alam
Department of Physics
Khulna University of Engineering & Technology


..... 31.01.18
Member

5. Prof. Dr. Md. Abdul Mannam Chowdhury
Department of Physics
Jahangirnagar University, Savar. Dhaka


..... 31/1/18
Member (External)

Abstract

In this study, the sensitivity of numerical simulations of tropical cyclone to physical parameterizations is carried out with a view to determine the best set of physics options for prediction of cyclones originating in the north Indian Ocean. For this purpose, the tropical cyclone Mahasen that formed in the Bay of Bengal and crossed Bangladesh-Myanmar coast in the month of May, 2013 has been simulated by the advanced (or state of science) mesoscale Weather Research and Forecasting (WRF) model with the available physical parameterizations. To determine on the prediction of track and intensity of Tropical Cyclone Mahasen has been used single domain with latitude from 2.045° N to 26.480° N and longitude from 73.96° E to 97.04° E. Domain has been used 12 km horizontal resolution. Different run and different physical parameterizations have been used available in the model. The different physical parameterizations schemes are KF, BMJ, GF, OSAS and Grell-3 for Cumulus; YSU, MYJ, GBM, MYNN3, ACM2, MYNN2, BouLac, UW, TEMF and MRF for Planetary Boundary Layer; WSM6, Kessler, Purdue Lin, WSM3, WSM5, Eta, Thompson, Morrison 2-mom, CAM5.1, SBU-Ylin, WDM5, WDM6, NSSL 2-mom, NSSL 2-mom-CCN, NSSL 1-mom and NSSL 1-momlfo for Microphysics; UNLS, TDS, RUC, NLS, CLM4.0 and PXS for Land surface model; Dudhia, GSFC ARW+Chem(τ), CAM, RRTMG, New Goddard and FLG for Short Wave Radiation; RRTM, CAM Long wave (CAM), RRTMG, New Goddard FLG and Held-Suarez for Long Wave Radiation that have been used for the purpose to test the Sensitivity of Tropical Cyclone Mahasen to Physical Parameterization Schemes using Weather Research & Forecasting (WRF) model. Three parameters track, wind speed and CSLP has been used for calculating Root Mean Square Error (RMSE) to find the best physical made using parameterizations option with respect to observed. Finally Betts Miller Janjic (BMJ) for Cumulus, Medium Range Forecast Model (MRF) for Planetary Boundary Layer (PBL), WRF Single Moment 3-class simple ice scheme (WSM3) for Microphysics (MP), Unified Noah land-Surface Model (UNLS) for Land surface model (LSM), Dudhia (MM5) for Short Wave Radiation (SWR) and Rapid Radiative Transfer Model (RRTM) for Long Wave Radiation (LWR) were found the best among available physics option.

Contents

Description	Page No
Title Page	i
Declaration	ii
Acknowledgement	iv
Abstract	vi
Contents	vii
List of Tables	xii
List of Figures	xiii
Nomenclature	xx
CHAPTER I: Introduction	
1.1 General Introduction	1
1.2 Objectives and Scope of the Research Work	4
1.3 Social and Economic Benefit of the Research Work.	4
1.4 Structure of the Thesis	5
CHAPTER II: Literature Review	
2.1 Tropical Cyclone	6
2.1.1 Classification of tropical cyclones	7
2.1.2 Different Name of Tropical Cyclones	7
2.1.3 Structure of Tropical Cyclone	8
2.2 Weather Research & Forecasting Model	9
2.2.1 Map Projection Considerations	10
2.2.2 Initial Conditions	10
2.2.3 Cumulus parameterization	11
2.2.3.1 Kain-Fritsch scheme	11
2.2.3.2 Betts-Miller-Janjic scheme	11
2.2.3.3 Grell-Freitas (GF) Scheme	12
2.2.3.4 Old Simplified Arakawa-Schubert scheme (OSAS)	12
2.2.3.5 Grell-3 scheme	13
2.2.4 Planetary Boundary Layer	13
2.2.4.1 Yonsei University scheme (YSU)	14

2.2.4.2	Mellor-Yamada-Janjic scheme (MYJ)	14
2.2.4.3	Grenier-Bretherton-Mc Caa scheme (GBM)	14
2.2.4.4	The Mellor-Yamada-Nakanishi-Niino (MYNN) (Level 2 & 3)	15
2.2.4.5	Asymmetrical Convective Model version 2 (ACM2)	15
2.2.4.6	Bougeault-Lacarrère (BouLac) scheme	16
2.2.4.7	University of Washington (UW)	16
2.2.4.8	Total Energy-Mass Flux (TEMF) scheme	16
2.2.4.9	Medium Range Forecast Model (MRF) scheme	17
2.2.5	Microphysics schemes in WRF-ARW Model	17
2.2.5.1	Kessler scheme	18
2.2.5.2	Purdue Lin scheme	18
2.2.5.3	WRF Single-Moment 3-class (WSM3) scheme	18
2.2.5.4	WRF Single-Moment 5-class (WSM5) scheme	18
2.2.5.5	WRF Single-Moment 6-class (WSM6) scheme	19
2.2.5.6	Eta Grid-scale Cloud and Precipitation (2001) scheme	19
2.2.5.7	Thompson <i>et al.</i> scheme	20
2.2.5.8	Morrison <i>et al.</i> 2-Moment scheme	20
2.2.5.9	CAM 5.1 scheme	21
2.2.5.10	SBU-Ylin scheme	22
2.2.5.11	The WRF Double Moment 5-class (WDM5) scheme	22
2.2.5.12	WRF double-moment 6-Class (WDM6) scheme	22
2.2.5.13	NSSL 2-moment scheme	23
2.2.6	Land-Surface Model	23
2.2.6.1	5-layer Thermal Diffusion Scheme (TDS)	23
2.2.6.2	Noah Land Surface (NLS) Model	24
2.2.6.3	Rapid Update Cycle (RUC) Model	24
2.2.6.4	Pleim-Xiu Scheme (PXS)	25
2.2.6.5	Community Land Model (CLM4)	25
2.2.6.6	Unified Noah land surface (UNLS) model	26
2.2.7	Shortwave Radiation	26
2.2.7.1	MM5 (This scheme is based on Dudhia (1989) and is taken from MM5. Dudhia) Shortwave	26

2.2.7.2	Goddard and New Goddard (shortwave and long wave)	26
2.2.7.3	CAM Shortwave	27
2.2.7.4	Radiative and Rapped Transfer Model Gu/Gas (RRTMG) shortwave	27
2.2.7.5	Fu-Liou-Gu Radiative Transfer Model (FLG) (shortwave and long wave)	28
2.2.8	Long Wave Radiation	28
2.2.8.1	Rapid Radiative Transfer Model (RRTM) Long wave	28
2.2.8.2	CAM Long wave	28
2.2.8.3	Radiation and Radiative Transfer Model Gu/ Gas (RRTMG) long wave	28
2.2.8.4	Held-Suarez scheme	29
CHAPTER III: Model Description and Methodology		
3.1	Model Description	30
3.2	Model Domain and Configuration	32
3.3	Data and Methodology	32
3.4	Experimental procedure and scheme selection	34
3.5	Synoptic history of Mahasen	35
CHAPTER IV: Result and Discussion		
4.0	Tropical Cyclone Mahasen	40
4.1	Experiment with first set	40
4.1.1	Cumulus parameterization	40
4.1.1.1	Effect of Cumulus parameterization on track	40
4.1.1.2	Effect of Cumulus parameterization on wind speed	42
4.1.1.3	Effect of Cumulus parameterization on CSLP	44
4.1.2	Planetary boundary layer (PBL)	46
4.1.2.1	Effect of PBL on Track	46
4.1.2.2	Effect of PBL on wind speed	48
4.1.2.3	Effect of PBL on CSLP	50
4.1.3	Microphysics (MP) parameterization	52
4.1.3.1	Effect of Microphysics on track	52
4.1.3.2	Effect of Microphysics parameterization on wind speed	54

4.1.3.3	Effect of Microphysics Parameterization on CSLP	57
4.1.4	Land surface model (LSM)	59
4.1.4.1	Effect of land surface model on track	59
4.1.4.2	Effect of land surface model on wind speed	61
4.1.4.3	Effect of land surface model on CSLP	63
4.1.5	Short wave radiation (SWR) schemes	65
4.1.5.1	Effect of the short wave radiation on track	65
4.1.5.2	Effect of the short wave radiation schemes on wind speed	67
4.1.5.3	Effect of the short wave radiation schemes on CSLP	69
4.1.6	Long wave radiation (LWR) schemes	72
4.1.6.1	Effect of the long wave radiation on track	72
4.1.6.2	Effect of the long wave radiation schemes on wind speed	74
4.1.6.3	Effect of the long wave radiation schemes on CSLP	76
4.2	Discussion experiment with 2 nd set of Tropical Cyclone Mahasen	78
4.2.1	Microphysics parameterization	78
4.2.1.1	Effect of the microphysics on track	79
4.2.1.2	Effect of the microphysics schemes on wind speed	81
4.2.1.3	Effect of the microphysics schemes on CSLP	83
4.2.2	Land surface model (LSM)	85
4.2.2.1	Effect of the land surface model on track	85
4.2.2.2	Effect of the land surface model on wind speed	87
4.2.2.3	Effect of the land surface model on CSLP	89
4.2.3	Short wave radiation (SWR) schemes	91
4.2.3.1	Effect of the short wave radiation on track	91
4.2.3.2	Effect of the short wave radiation schemes on wind speed	93
4.2.3.3	Effect of the short wave radiation schemes on CSLP	95
4.2.4	Long wave radiation (LWR) schemes	97
4.2.4.1	Effect of the long wave radiation on track	97
4.2.4.2	Effect of the long wave radiation schemes on wind speed	99

4.2.4.3	Effect of the long wave radiation schemes on CSLP	101
CHAPTER V:	Conclusions	105
	References	107

LIST OF TABLES

Table No	Description	Page No
2.1	Local name of tropical cyclones in different basin	8
3.1	WRF Model and Domain Configurations	32
3.2	Observed information of Simulated Tropical Cyclones in the Bay of Bengal	34
3.3	Procedure for track prediction of 1 st set	36
3.4	Experimental procedure for track prediction of second set	38
4.1.1	Final result of these experiments	78
4.2.1	Compare final result of the two experiments	103

LIST OF FIGURES

Figure No	Description	Page No
2.1	Satellite view eye and eye wall of TC	6
2.2	Structure of the tropical cyclone on the Satellite image.	8
3.1	The WRF–ARW domain set up for the study	32
4.1.1.1(a)	Model simulated track with IMD observed of TC Mahasen by using five different cumulus schemes	41
4.1.1.1(b)	Model simulated track error with respect to IMD observed of TC Mahasen by using five different cumulus schemes	41
4.1.1.1(c)	Model simulated track error in the 24, 48, and 72-hr forecasts with respect to IMD observed of TC Mahasen by using five different cumulus schemes	42
4.1.1.2(a)	Model simulated wind speed with IMD observed of TC Mahasen by using five different cumulus schemes	42
4.1.1.2(b)	Model simulated wind speed error with respect to IMD observed of TC Mahasen by using five different cumulus schemes	43
4.1.1.2(c)	Model simulated wind speed error in the 24, 48, and 72-hr forecasts with respect to IMD observed of TC Mahasen by using five different cumulus schemes	43
4.1.1.3(a)	Model simulated CSLP with IMD observed of TC Mahasen by using five different cumulus schemes	44
4.1.1.3(b)	Model simulated CSLP error with respect to IMD observed of TC Mahasen by using five different cumulus schemes	45
4.1.1.3(c)	Model simulated CSLP error in the 24, 48, and 72-hr forecasts with respect to IMD observed of TC Mahasen by using five different cumulus schemes	45
4.1.2.1(a)	Model simulated track with IMD observed of TC Mahasen by using ten different PBL schemes	47
4.1.2.1(b)	Model simulated track error with respect to IMD observed of TC Mahasen by using ten different PBL schemes	47

4.1.2.1(c)	Model simulated track error in the 24, 48, and 72-hr forecasts with respect to IMD observed of TC Mahasen by using ten different PBL schemes	48
4.1.2.2(a)	Model simulated wind speed with IMD observed of TC Mahasen by using ten different PBL schemes	49
4.1.2.2(b)	Model simulated wind speed error with respect to IMD observed of TC Mahasen by using ten different PBL schemes	49
4.1.2.2(c)	Model simulated wind speed error in the 24, 48, and 72-hr forecasts with respect to IMD observed of TC Mahasen by using ten different PBL schemes	50
4.1.2.3(a)	Model simulated CSLP with IMD observed of TC Mahasen by using ten different PBL schemes	51
4.1.2.3(b)	Model simulated CSLP error with respect to IMD observed of TC Mahasen by using ten different PBL schemes	51
4.1.2.3(c)	Model simulated CSLP error in the 24, 48, and 72-hr forecasts with respect to IMD observed of TC Mahasen by using ten different PBL schemes	52
4.1.3.1(a)	Model simulated track with IMD observed of TC Mahasen by using sixteen different MP schemes	53
4.1.3.1(b)	Model simulated track error with respect to IMD observed of TC Mahasen by using sixteen different MP schemes	54
4.1.3.1(c)	Model simulated track error in the 24, 48, and 72-hr forecasts with respect to IMD observed of TC Mahasen by using sixteen different MP schemes	54
4.1.3.2(a)	Model simulated wind speed with IMD observed of TC Mahasen by using sixteen different MP schemes	55
4.1.3.2(b)	Model simulated wind speed error with respect to IMD observed of TC Mahasen by using sixteen different MP schemes	56
4.1.3.2(c)	Model simulated wind speed error in the 24, 48, and 72-hr forecasts with respect to IMD observed of TC Mahasen by using sixteen different MP schemes	56
4.1.3.3(a)	Model simulated CSLP with IMD observed of TC Mahasen by using sixteen different MP schemes	57

4.1.3.3(b)	Model simulated CSLP error with respect to IMD observed of TC Mahasen by using sixteen different MP schemes	58
4.1.3.3(c)	Model simulated CSLP error in the 24, 48, and 72-hr forecasts with respect to IMD observed of TC Mahasen by using sixteen different MP schemes	58
4.1.4.1(a)	Model simulated track with IMD observed of TC Mahasen by using six different LSM schemes	60
4.1.4.1(b)	Model simulated track error with respect to IMD observed of TC Mahasen by using six different LSM schemes	60
4.1.4.1(c)	Model simulated track error in the 24, 48, and 72-hr forecasts with respect to IMD observed of TC Mahasen by using six different LSM schemes	61
4.1.4.2(a)	Model simulated wind speed with IMD observed of TC Mahasen by using six different LSM schemes	61
4.1.4.2(b)	Model simulated wind speed error with respect to IMD observed of TC Mahasen by using six different LSM schemes	62
4.1.4.2(c)	Model simulated wind speed error in the 24, 48, and 72-hr forecasts with respect to IMD observed of TC Mahasen by using six different LSM schemes	62
4.1.4.3(a)	Model simulated CSLP with IMD observed of TC Mahasen by using six different LSM schemes	63
4.1.4.3(b)	Model simulated CSLP error with respect to IMD observed of TC Mahasen by using six different LSM schemes	64
4.1.4.3(c)	Model simulated CSLP error in the 24, 48, and 72-hr forecasts with respect to IMD observed of TC Mahasen by using six different LSM schemes	64
4.1.5.1(a)	Model simulated track with IMD observed of TC Mahasen by using six different SWR schemes	66
4.1.5.1(b)	Model simulated track error with respect to IMD observed of TC Mahasen by using six different SWR schemes	66
4.1.5.1(c)	Model simulated track error in the 24, 48, and 72-hr forecasts with respect to IMD observed of TC Mahasen by using six different SWR schemes	67

4.1.5.2(a)	Model simulated wind speed with IMD observed of TC Mahasen by using six different SWR schemes	68
4.1.5.2(b)	Model simulated wind speed error with respect to IMD observed of TC Mahasen by using six different SWR schemes	68
4.1.5.2(c)	Model simulated wind speed error in the 24, 48, and 72-hr forecasts with respect to IMD observed of TC Mahasen by using six different SWR schemes	69
4.1.5.3(a)	Model simulated CSLP with IMD observed of TC Mahasen by using six different SWR schemes	70
4.1.5.3(b)	Model simulated CSLP error with respect to IMD observed of TC Mahasen by using six different SWR schemes	70
4.1.5.3(c)	Model simulated CSLP error in the 24, 48, and 72-hr forecasts with respect to IMD observed of TC Mahasen by using six different SWR schemes	71
4.1.6.1(a)	Model simulated track with IMD observed of TC Mahasen by using five different LWR schemes	72
4.1.6.1(b)	Model simulated track error with respect to IMD observed of TC Mahasen by using five different LWR schemes	73
4.1.6.1(c)	Model simulated track error in the 24, 48, and 72-hr forecasts with respect to IMD observed of TC Mahasen by using five different LWR schemes	73
4.1.6.2(a)	Model simulated wind speed with IMD observed of TC Mahasen by using five different LWR schemes	74
4.1.6.2(b)	Model simulated wind speed error with respect to IMD observed of TC Mahasen by using five different LWR schemes	75
4.1.6.2(c)	Model simulated wind speed error in the 24, 48, and 72-hr forecasts with respect to IMD observed of TC Mahasen by using five different LWR schemes	75
4.1.6.3(a)	Model simulated CSLP with IMD observed of TC Mahasen by using five different LWR schemes	76
4.1.6.3(b)	Model simulated CSLP error with respect to IMD observed of TC Mahasen by using five different LWR schemes	77

4.1.6.3(c)	Model simulated CSLP error in the 24, 48, and 72-hr forecasts with respect to IMD observed of TC Mahasen by using five different LWR schemes	77
4.2.1.1(a)	Model simulated track with IMD observed of TC Mahasen by using sixteen different MP schemes	79
4.2.1.1(b)	Model simulated track error with respect to IMD observed of TC Mahasen by using sixteen different MP schemes	80
4.2.1.1(c)	Model simulated track error in the 24, 48, and 72-hr forecasts with respect to IMD observed of TC Mahasen by using sixteen different MP schemes	80
4.2.1.2(a)	Model simulated wind speed with IMD observed of TC Mahasen by using sixteen different MP schemes	81
4.2.1.2(b)	Model simulated wind speed error with respect to IMD observed of TC Mahasen by using sixteen different MP schemes	82
4.2.1.2(c)	Model simulated wind speed error in the 24, 48, and 72-hr forecasts with respect to IMD observed of TC Mahasen by using sixteen different MP schemes	82
4.2.1.3(a)	Model simulated CSLP with IMD observed of TC Mahasen by using sixteen different MP schemes	83
4.2.1.3(b)	Model simulated CSLP error with respect to IMD observed of TC Mahasen by using sixteen different MP schemes	83
4.2.1.3(c)	Model simulated CSLP error in the 24, 48, and 72-hr forecasts with respect to IMD observed of TC Mahasen by using sixteen different MP schemes	84
4.2.2.1(a)	Model simulated track with IMD observed of TC Mahasen by using six different LSM schemes	85
4.2.2.1(b)	Model simulated track error with respect to IMD observed of TC Mahasen by using six different LSM schemes	86
4.2.2.1(c)	Model simulated track error in the 24, 48, and 72-hr forecasts with respect to IMD observed of TC Mahasen by using six different LSM schemes	86
4.2.2.2(a)	Model simulated wind speed with IMD observed of TC Mahasen by using six different LSM schemes	87

4.2.2.2(b)	Model simulated wind speed error with respect to IMD observed of TC Mahasen by using six different LSM schemes	88
4.2.2.2(c)	Model simulated wind speed error in the 24, 48, and 72-hr forecasts with respect to IMD observed of TC Mahasen by using six different LSM schemes	88
4.2.2.3(a)	Model simulated CSLP with IMD observed of TC Mahasen by using six different LSM schemes	89
4.2.2.3(b)	Model simulated CSLP error with respect to IMD observed of TC Mahasen by using six different LSM schemes	90
4.2.2.3(c)	Model simulated CSLP error in the 24, 48, and 72-hr forecasts with respect to IMD observed of TC Mahasen by using six different LSM schemes	90
4.2.3.1(a)	Model simulated track with IMD observed of TC Mahasen by using six different SWR schemes	92
4.2.3.1(b)	Model simulated track error with respect to IMD observed of TC Mahasen by using six different SWR schemes	92
4.2.3.1(c)	Model simulated track error in the 24, 48, and 72-hr forecasts with respect to IMD observed of TC Mahasen by using six different SWR schemes	93
4.2.3.2(a)	Model simulated wind speed with IMD observed of TC Mahasen by using six different SWR schemes	93
4.2.3.2(b)	Model simulated wind speed error with respect to IMD observed of TC Mahasen by using six different SWR schemes	94
4.2.3.2(c)	Model simulated wind speed error in the 24, 48, and 72-hr forecasts with respect to IMD observed of TC Mahasen by using six different SWR schemes	94
4.2.3.3(a)	Model simulated CSLP with IMD observed of TC Mahasen by using six different SWR schemes	95
4.2.3.3(b)	Model simulated CSLP error with respect to IMD observed of TC Mahasen by using six different SWR schemes	96
4.2.3.3(c)	Model simulated CSLP error in the 24, 48, and 72-hr forecasts with respect to IMD observed of TC Mahasen by using six different SWR schemes	96

4.2.4.1(a)	Model simulated track with IMD observed of TC Mahasen by using five different LWR schemes	98
4.2.4.1(b)	Model simulated track error with respect to IMD observed of TC Mahasen by using five different LWR schemes	98
4.2.4.1(c)	Model simulated track error in the 24, 48, and 72-hr forecasts with respect to IMD observed of TC Mahasen by using five different LWR schemes	99
4.2.4.2(a)	Model simulated wind speed with IMD observed of TC Mahasen by using five different LWR schemes	100
4.2.4.2(b)	Model simulated wind speed error with respect to IMD observed of TC Mahasen by using five different LWR schemes	100
4.2.4.2(c)	Model simulated wind speed error in the 24, 48, and 72-hr forecasts with respect to IMD observed of TC Mahasen by using five different LWR schemes	101
4.2.4.3(a)	Model simulated CSLP with IMD observed of TC Mahasen by using five different LWR schemes	101
4.2.4.3(b)	Model simulated CSLP error with respect to IMD observed of TC Mahasen by using five different LWR schemes	102
4.2.4.3(c)	Model simulated CSLP error in the 24, 48, and 72-hr forecasts with respect to IMD observed of TC Mahasen by using five different LWR schemes	102

Nomenclature

ACM	Asymmetrical Convective Model
AFWA	Air Force Weather Agency
API	Application Program Interface
ARPS	Advanced Regional Prediction System
ARW	Advanced Research WRF
BMJ	Betts-Miller-Janjic
CAM	Community Atmosphere Model
CAPE	Convectively Available Potential Energy
CCM2	Community Climate Model Version 2
CLM	Community Land Model
COAMPS	Coupled Ocean / Atmosphere Mesoscale Prediction System
CP	Cumulus Parameterization
CSLP	Central sea level pressure
DFI	Digital Filtering Initialization
EMC	Environmental Modeling Center
FLG	Fu-Liou-Gu
FNL	Final Reanalysis / Final analysis
GBM	Grenier–Bretherton–McCaa
GD	Grell-Devenyi ensemble
GF	Grell–Freitas
GFS	Global Forecast System
GRIB	Gridded Binary
IMD	India Meteorological Department
JTWC	Join typhoon warning center
KF	Kain-Fritch
KS	Kessler
LSM	Land Surface Model
MKS	Meter Kilogram Second
MM5	Pennsylvania State / NCAR Mesoscale Model Version 5
MP	Microphysics

MRF	Medium Range Forecast Model
MYNN	The Mellor–Yamada–Nakanishi–Niino scheme
MYJ	Mellor-Yamada-Janjic scheme
NCAR	National Center for Atmospheric Research
NCEP	National Centers for Environmental Prediction
NLS	Noah Land Surface
NMM	Non hydrostatic Mesoscale Model
NOAA	National Oceanographic and Atmospheric Administration
NWP	Numerical Weather Prediction
OSAS	Old Simplified Arakawa-Schubert scheme
OSU	Oregon State University
PBL	Planetary Boundary Layer
RRTM	Rapid Radiative Transfer Model
RRTMG	Radiation and Radiative Transfer Model Gu/ Gas
RUC	Rapid Update Cycle
SI (WRF)	Standard Initialization
SST	Sea Surface Temperature
TC	Tropical Cyclones
TEMF	Total Energy–Mass Flux scheme
TKE	Turbulent Kinetic Energy
UNLS	Unified Noah Land Surface
UTC	Universal Time Co-ordinate
UW	University of Washington
YSU	Yonsei University Scheme (Korea)
WDM5	The WRF Double Moment 5-class scheme
WDM6	The WRF Double Moment 6-class scheme
WSM6	WRF Single-moment 6-class
WRF	Weather Research and Forecasting Model

CHAPTER I

Introduction

1.1 General Introduction

Tropical cyclones (TC) are important weather phenomena that cause heavy wind, torrential rain and enormous damage to life and property when they cross the coastal regions. A single storm in Bangladesh in 1970 killed nearly half a million people, Choudhury (2009). The cyclones formed over the Bay of Bengal generally move in the northwest direction and crossed Bangladesh, Myanmar and eastern coast of India. Understanding tropical cyclone genesis, development and associated characteristic features has been a challenging subject in meteorology over the last several decades. For this coastal regions are particularly vulnerable to damage from a tropical cyclone as compared to inland regions. Heavy rain, significant flooding inland, and storm surges can produce extensive coastal flooding up to 40 km from the coastline. The importance of the sea surface temperature (SST) in the genesis and intensity of tropical cyclones has become well established. It is known that tropical cyclones usually develop over waters in which the SST is 26°C or higher. In recent years, attempts to associate tropical cyclone trends with climate change resulting from greenhouse warming has led to additional attention being paid to tropical cyclone prediction Evans (1992) and Lighthill *et al.* (1994).

A TC is the generic term for a non-frontal warm core synoptic scale low-pressure system originating over tropical or sub-tropical waters with organized convection and definite cyclonic surface wind circulation- counter clock wise. It is a low-pressure system with maximum sustainable winds over 62 km/hr, which can go up to around 300 km/hr. A mature tropical cyclone has a horizontal dimension of around 500-1500 km and extends through the depth of the troposphere, about 15 km Ali (1999a).

The well-developed system vertically extents up to 100 hPa level with several towers of cumulus clouds organized in a number of spiral bands. The mature cyclone often has a clear region around its center with diameter of about 5 to 50 km, which is called the eye of the cyclone and is characterized by descending motion. Away from the center the system has strong upward motion due to large-scale convergence of moist air within the boundary layer. The convective clouds are formed due to adiabatic ascent of this highly moist air and

enormous energy in the form of latent heat is released through condensation of water vapor. This condensation heat allows the pre-existing atmospheric lows to develop into the tropical cyclones provided all other conditions are favorable. The tropical cyclones are formed in the tropical warm ocean with sea surface temperature (SST) higher than 26.5°C and with latitudes higher than 5°N in an atmosphere with low vertical wind Choudhury (2009) and Henderson *et al.* (1998). Such a high surface temperature is necessary to produce a steep lapse rate for maintaining the vertical circulation in a cyclone.

Tropical convert the heat energy of the tropical ocean into winds and waves. They can produce extremely strong winds, tornadoes, torrential rain, high waves, and storm surges. The heavy rains and storm surges can produce extensive flooding. Tropical cyclones on the open sea cause large waves, heavy rain, and high winds, disrupting international shipping. The strong wind of the tropical cyclone exerts frictional force on the water surface which is proportional to the square of the wind speed. This frictional force causes high gravity waves with heights of up to 10-12 meters. These waves cause water to flow inland and flash everything in its path. The ultimate effect is the heavy loss of lives, properties and damages to ecosystem and environment.

The tropical cyclones being formed in the Bay of Bengal frequently hit the coastal regions of Bangladesh, India, and Myanmar and to a lesser extent, Sri Lanka. The Bay of Bengal basin is highly vulnerable to strong tropical cyclone genesis because it generally maintains a temperature between 28°C to 30°C during the tropical cyclone seasons. The distribution of the average SST temperature of the Bay of Bengal is sufficiently warm and has high potential for tropical cyclone genesis.

Accurate predictions of TC track and intensity with timely warning to people will minimize loss of life and property. Availability of state-of-the-art numerical weather prediction (NWP) models along with efficient computing facilities to carry out simulations has made possible the prediction of the mesoscale weather events. The prediction of TCs using mesoscale NWP models is highly influenced by initial/boundary conditions and physical parameterizations employed in the model. In view of this, 'fixing' the one best combination of physics schemes in the mesoscale NWP models for the whole globe is formidable. Further, the NWP model performance is very sensitive to grid sizes and the geographical region of interest. The best set of schemes for one region may not be suitable for some other region. The horizontal and vertical resolutions are also very important factors, since different parameterization schemes

can give different results for different model resolutions. Sensitivity experiments are the only logical way to identifying the best set of physics schemes for a particular region.

Srinivas *et al.* (2007) conducted a sensitivity study of the Andhra severe cyclone (2003) by using the National Center for Atmospheric Research (NCAR) fifth generation non-hydrostatic mesoscale model (MM5). They reported that the planetary boundary Layer (PBL) schemes and convective parameterization schemes (CPS) play an important role in predicting both the intensity and movement of the model simulated storms. They also concluded that the combination of Mellor Yamada (MY) scheme for PBL parameterization and Kain-Fritsch 2 (KF2) scheme as the CPS give the best results in terms of intensity and track. A sensitivity study of the Orissa super cyclone by Rao and Prasad (2007) also indicates that a combination of the MY scheme from the PBL and KF2 from CPS gives better results in terms of cyclone track and intensity prediction.

Deshpande *et al.* (2010) however conclude that the prediction of cyclone track and intensity are highly sensitive to only convective parameterization schemes compared to other physical parameterization schemes based on their studies on cyclone Gonu using the MM5 model. Loh *et al.* (2010) also report that the PBL parameterization schemes do not significantly affect track and intensity prediction of near equatorial typhoons. Prater and Evans (2002) modeled the tropical cyclone Irene (1999) with various CPS and concluded that the Kain-Fritsch (KF) scheme in MM5 produces relatively accurate storm predictions compared to observations. Mandal *et al.* (2004) simulated two severe tropical cyclones in the Bay of Bengal using MM5 with various CPS, PBL and radiation schemes and inferred that the combination of Medium Range Forecast (MRF) scheme in PBL and Grell scheme in CPS with Community Climate Model Version 2 (CCM2) scheme in radiation gives better performance in so far as track and intensity predictions are concerned.

Yang and Ching (2005) also concluded that the MRF in PBL and Grell in CPS combined with the Goddard Graupel in cloud microphysics scheme give the best performance in the study of typhoon Toraji (2001). Based on a study of impact of cloud microphysics on hurricane Charley, Pattnaik and Krishnamurti (2007) reported that the microphysical parameterization schemes have strong impact on the intensity prediction of hurricane but have negligible impact on the track forecast. Krieger (2009) analyzed the sensitivity of Advanced Research WRF (ARW) v3.0 model on the Beaufort Sea region with the available physical parameterization schemes and concluded that the combination of KF scheme for

CPS, Pleim-Xu scheme for land surface and asymmetrical convective model 2 (ACM2) scheme for PBL produces better surface wind prediction agreement with both station observations and Quick Scatter meter (QuikSCAT) surface wind data. The above studies on regional weather models clearly indicate that the best combinations of physical parameterization schemes are very essential to predict a mesoscale weather system. Previous sensitivity studies on mesoscale models were mostly initiated with NCEP Final analysis (FNL) data as initial and boundary conditions. Very few studies have been initiated with the NCEP Global Forecast System (GFS) real time prediction. In this study, the sensitivity of a very recent tropical cyclone Mahasen to model physical parameterization is conducted with GFS real time predictions as the initial and boundary conditions. Use of GFS real time prediction is akin to running a real time forecast. Furthermore, most of the previous sensitivity studies have been done with only combinations of Cumulus, PBL and microphysics parameterizations and very few studies consider different radiation schemes are short wave radiation, long wave radiation and other physics options. In this study, all physical parameterizations available in the ARW v3.5.1 model are systematically evaluated.

1.2 Objectives and Scope of the Research Work

The objective of the present research is "Sensitivity of Tropical Cyclone Mahasen to Physical Parameterization Schemes using Weather Research & Forecasting (WRF) model."

The present study has been conducted with the following objectives:

- ◆ To investigate the performance of WRF model.
- ◆ To setup the model and using various physical parameters to study Sensitivity of Tropical Cyclone Mahasen.
- ◆ To investigate the Physics and dynamics related to prediction of the tracks, wind speed and central sea level pressure of Tropical Cyclone Mahasen using initial condition.

1.3 Social and Economic Benefit of the Research Work.

The economic activities of the country is not well. Besides, the tropical cyclones, tornadoes and other mesoscale directly impact arise economic losses or human injuries and loss of life. In the Asian and Pacific regions that have half of the world's population (3.1 billion people), approximately 900 million (30 percent) are poor and over 1.9 billion (60 percent) live in

rural areas. In addition to this, Bangladesh is supposed to become the worst victim of the impacts of global warming and associated climate change. When the tropical cyclones impact the poor, their livelihoods along with their ability to obtain food, shelter, and clothing can be significantly disrupted because they have fewer assets, reserves, or opportunities to fall back on. Some countries such as India and Bangladesh have lost thousands of people due to storm surges. High winds with flying debris have taken a tremendous toll in some areas. Tropical cyclone can neither be destroyed nor be prevented, but the damages can be minimized by proper management which includes preparedness, rescue operation and rehabilitation.

If we earlier, identify the impact of the tropical cyclone's event and declared the phenomena or predict the people of the cyclone formation, Land falling place and intensity. It can be benefited for the stricken area and economic losses or human injuries and loss of life will be saved the people such like as a coastal country of Bangladesh, India or Nepal.

So, this requires research on the Sensitivity of Tropical Cyclone Mahasen to Physical Parameterization Schemes using WRF model and this method will apply to another formation cyclone to save the valuable life and assets.

1.4 Structure of the Thesis

The thesis has been constructed with the following structure:

Abstract is the gist of the research work performed for this dissertation.

Chapter 1 contains general introduction. It describes the geographical settings of Bangladesh and adjacent land masses, climate and disaster of Bangladesh, objectives and scope of the study and explains how the research results will be of social and economic benefit.

Chapter 2 contains description of WRF models and condition and physics options.

Chapter 3 deals with model setup, initialization of WRF models.

Chapter 4 contains the results and discussions of the study of track, wind speed and central sea level pressure of selected tropical cyclone (Mahasen) over Bangladesh and Bay of Bengal based on WRF models results.

In Chapter 5, the conclusion of the research findings have been brought in with a few recommendations for future research in this subject.

CHAPTER II

Literature Review

2.1 Tropical Cyclone

Tropical cyclones are intense, cyclonically rotating, low-pressure weather systems that form over the tropical oceans. Intense means that near surface wind speeds exceed 17 ms^{-1} (60 km h^{-1} , 32 kn). Severe tropical cyclones with near surface sustained wind speeds equal to or exceeding 34 ms^{-1} (120 kmh^{-1} , 64 kn) are called hurricanes over the Atlantic Ocean, the East Pacific Ocean and the Caribbean Sea, and Typhoons over the Western North Pacific Ocean. Typically the strongest winds occur in a ring some tens of kilometers from the center and there is a calm region near the center, the eye, where winds are light, but for moving storms, the wind distribution may be asymmetric with the maximum winds in the forward right quadrant. The eye is so-called because it is normally free of cloud, except perhaps near the surface, but in a mature storm it is surrounded by a ring of deep convective cloud that slopes outwards with 16 km height. This is the so-called eye wall cloud. At larger radii from the center, storms usually show spiral bands of convective cloud. Figure 2.1 has been shown a satellite view of the eye and eye wall of a mature typhoon which marks the belt of strongest winds and heaviest rainfall.

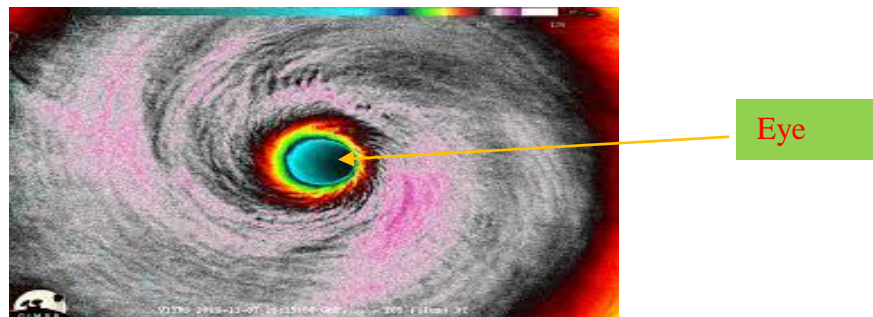


Figure 2.1: Satellite view eye and eye wall of TC

In addition to strong winds and rain, TCs are capable of generating high waves, damaging storm surge, and tornadoes. They typically weaken rapidly over land where they are cut off from their primary energy source. For this reason, coastal regions are particularly vulnerable to damage from a TC as compared to inland regions. Heavy rains, however, can cause significant flooding inland, and storm surges can produce extensive coastal flooding up to 40 kilometers from the coastline. Though their effects on human populations are often

devastating, TCs can relieve drought conditions. They also carry heat energy away from the tropics and transport it toward temperate latitudes, which may play an important role in modulating regional and global climate.

2.1.1 Classification of tropical cyclones

Tropical cyclones of different intensity are given different names. Tropical cyclones are classified in accordance with the World Meteorological Organization's recommendation by their maximum sustained wind speeds near the center. Cyclonic disturbances in the North Indian Ocean are classified according to their intensity. The following nomenclature is in use:

Sl no	Types of Disturbances	Km/hr	knots	m/s
1	Low (L)	≤31	≤17	≤8
2	Depression (D)	31-51	17-27	9-13
3	Deep depression (DD)	52-61	28-33	14-17
4	Cyclonic Storm (CS)	62-88	34-47	18-24
5	Severe Cyclonic Storm (SCS)	89-118	48-63	25-32
6	Very Severe Cyclonic Storm (VSCS)	119-221	64-119	33-61
7	Super Cyclonic Storm (SuCS)	≥222	≥120	≥62

2.1.2 Different Name of Tropical Cyclones

Most tropical cyclones are given a name using one of several lists of tropical cyclone names. Storms reaching tropical storm strength were initially given names to eliminate confusion when there are multiple systems in any individual basin at the same time, which assists in warning people of the coming storm. In most cases, a tropical cyclone retains its name throughout its life; however, under special circumstances, tropical cyclones may be renamed while active. These names are taken from lists that vary from region to region and are usually drafted a few years ahead of time. The lists are decided on, depending on the regions, either by committees of the World Meteorological Organization or by national weather offices involved in the forecasting of the storms. Table has been shown the list of North Indian Ocean cyclone names.

Table 2.1: Local name of tropical cyclones in different basin.

Area	Local Name
North Indian Ocean	Tropical Cyclone
North Atlantic Ocean	Hurricane
Northwest Pacific Ocean	Typhoon

2.1.3 Structure of Tropical Cyclone

A tropical cyclone is a large Structure, rotating system of clouds, wind, and thunderstorms around an area of low atmospheric pressure near the Earth’s surface having horizontal dimensions of around 500-1500 km (Ali, 1999). Tropical cyclones vertically extend up to upper troposphere. For a well-developed system it may extend up to tropopause. The system is characterized by a calm region at the center with diameter of around 5 to 50 km, which is known as the eye of the cyclone (Ali, 1999). In some cases this diameter may be double. The eye is more or less circular in shape. Around eye is the core region of the tropical cyclones which has very strong wind and is characterized by dense cloud overcast which is known as Central Dense Overcast (CDO). The CDO extends over a region of approximately 100-200 km radius from the center depending on. The overall size of the system. Away from the CDO is the outer periphery of the tropical clone. In the satellite pictures, the cloud distributions in the outer periphery are found to be banding features.

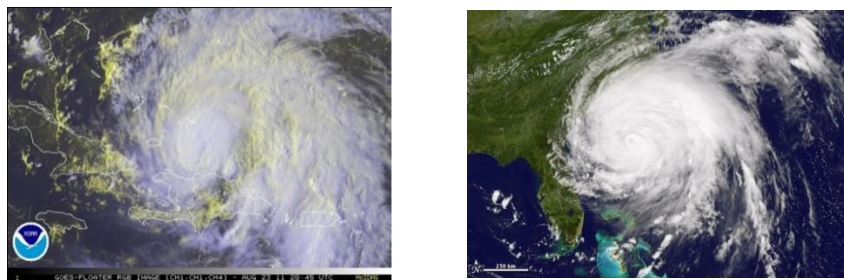


Figure 2.2: Structure of the tropical cyclone on the Satellite image.

The overall circulation feature of the tropical cyclone is shown in figures 2.2. The area of broken clouds at the center is its eye. Notice that the clouds align themselves into spiraling bands (called spiral rain bands) that swirl in toward the storm’s center, where they wrap themselves around the eye. Here rain bands are bands of showers and thunderstorms. Adjacent to the eye, an area about 16-80 km wide, is the eye wall, a ring of intense thunderstorms that whirl around the storm’s center and extend upward to almost 15 km above sea level.

2.2 Weather Research & Forecasting Model

The Weather Research and Forecasting (WRF) Model is a next-generation mesoscale numerical weather prediction system designed to serve both atmospheric research and operational forecasting needs. It features two dynamical cores, a data assimilation system, and a software architecture facilitating parallel computation and system extensibility. The model serves a wide range of meteorological applications across scales from tens of meters to thousands of kilometers. The effort to develop WRF began in the latter part of the 1990's and was a collaborative partnership principally among the NCAR, the National Oceanic and Atmospheric Administration (NOAA) represented by the National Centers for Environmental Prediction (NCEP) and the Forecast Systems Laboratory (FSL) the Air Force Weather Agency (AFWA), the Naval Research Laboratory, the University of Oklahoma, and the Federal Aviation Administration (FAA).

WRF offers two dynamical solvers for its computation of the atmospheric governing equations, and the variants of the model are known as WRF-ARW and WRF-NMM. The Advanced Research WRF (ARW) is supported to the community by the NCAR Mesoscale and Microscale Meteorology Division. The WRF-NMM solver variant was based on the Eta Model, and later Non hydrostatic Mesoscale Model, developed at NCEP. The WRF-NMM is supported to the community by the Developmental Test bed Center.

This section outlines the physics options available in the ARW. The WRF physics options fall into several categories, each contains several choices. The physics categories are (1) Cumulus parameterization, (2) PBL, (3) microphysics (MP), (4) land-surface model, and (5) radiation. The physics section is insulated from the rest of the dynamics solver by the use of physics drivers. These are between solver-dependent routines: a pre-physics preparation and post physics modifications of the tendencies. The physics preparation involves filling arrays with Physics required variables that include the temperature, pressure, heights, layer thicknesses, and other state variables in MKS units at half-level grid points and on full levels. The velocities are also de-staggered so that the physics part is independent of the dynamical solver's velocity staggering. Physics packages compute tendencies for the velocity components (un-staggered), potential temperature, and moisture fields. The solver-dependent post-physics step will restage these tendencies as necessary, couple tendencies with coordinate metrics, and convert to variables or units appropriate to the dynamics solver. In the first Runge-Kutta step, prior to the acoustic tendencies are computed for cumulus,

PBL, surface, and radiation physics. These tendencies are then held fixed through the Runge-Kutta steps. Microphysics is computed after the last Runge-Kutta step in order to maintain proper saturation conditions at the end of the time-step. The initialization of the physics is called prior to the first model step. This initialization may include reading in data files for physics tables or calculating look-up tables of functions. Each physics module includes an initialization routine for this purpose. Often physics packages will have many of their own constants that should also be included in their own module, while common physical constants are passed in from the physics drivers. Each physics option has many parameterization schemes. Descriptions of the parameterization schemes used for the present study are written as follows:

2.2.1 Map Projection Considerations

For ARW configurations using the Lambert conformal, polar stereographic, or Mercator projections, the time step constraints is determined by the smallest physical horizontal grid spacing, i.e. $\min(\frac{\Delta x}{m_x}, \frac{\Delta y}{m_y})$. For global applications, the grid distance used to determine the time step should be $\frac{\Delta x}{m_x}$ evaluated at the computational latitude at which the polar filters are activated.

2.2.2 Initial Conditions

The ARW may be run with user-defined initial conditions for idealized simulations, or it may be run using interpolated data from either an external analysis or forecast for real-data cases.

WRF Preprocessor System, referred to as WPS) that converts the large-scale GriB data into a format suitable for ingest by the ARW's real-data processor.

The programs that generate the specific initial conditions for the selected idealized or real data case function similarly. They provide the ARW with:

- Input data that is on the correct horizontal and vertical staggering;
- Hydrostatically balanced reference state and perturbation fields; and
- Metadata specifying such information as the date, grid physical characteristics, and projection details.

2.2.3 Cumulus parameterization

These schemes are responsible for the sub-grid-scale effects of convective and/or shallow clouds. The schemes are intended to represent vertical fluxes due to unresolved updrafts and downdrafts and compensating motion outside the clouds. They operate only on individual columns where the scheme is triggered and provide vertical heating and moistening profiles. Some schemes additionally provide cloud and precipitation field tendencies in the column, and future schemes may provide momentum tendencies due to convective transport of momentum. The schemes all provide the convective component of surface rainfall. Cumulus parameterizations are theoretically only valid for coarser grid sizes, (e.g., greater than 10km), where they are necessary to properly release latent heat on a realistic time scale in the convective columns. Cumulus Schemes options of this model are outlined below:

2.2.3.1 Kain-Fritsch scheme

The modified version of the Kain-Fritsch scheme (Kain, 2004) is based on Kain and Fritsch (1990) and Kain and Fritsch (1993), but has been modified based on testing within the Eta model. As with the original KF scheme, it utilizes a simple cloud model with moist updrafts and downdrafts, including the effects of detrainment, entrainment, and relatively simple microphysics. A minimum entrainment rate is imposed to suppress widespread convection in marginally unstable, relatively dry environments. Shallow (no precipitating) convection is allowed for any updraft that does not reach minimum cloud depth for precipitating clouds; this minimum depth varies as a function of cloud-base temperature. The entrainment rate is allowed to vary as a function of low-level convergence. Downdraft changes, Source layer is the entire 150-200 mb deep layer just above cloud base. Mass flux is specified as a fraction of updraft mass flux at cloud base. Fraction is a function of source layer RH rather than wind shear or other parameters, i.e., old precipitation efficiency relationship not used. Detrainment is specified to occur in updraft source layer and below.

2.2.3.2 Betts-Miller-Janjic scheme

The Betts-Miller-Janjic (BMJ) scheme (Janjic, 1994, 2000) was derived from the Betts-Miller (BM) convective adjustment scheme (Betts and Miller, 1986). However, the BMJ scheme differs from the Betts-Miller scheme in several important aspects. The deep convection profiles and the relaxation time are variable and depend on the cloud efficiency,

a non-dimensional parameter that characterizes the convective regime (Janjic, 1994). The cloud efficiency depends on the entropy change, precipitation, and mean temperature of the cloud. The shallow convection moisture profile is derived from the requirement that the entropy change be small and nonnegative (Janjic, 1994). The BMJ scheme has been optimized over years of operational application at NCEP, so that, in addition to the described conceptual differences, many details and/or parameter values differ from those recommended in Betts and Miller (1986). Recently, attempts have been made to refine the scheme for higher horizontal resolutions, primarily through modifications of the triggering mechanism. In particular, a floor value for the entropy change in the cloud is set up below which the deep convection is not triggered. In searching for the cloud top, the ascending particle mixes with the environment and the work of the buoyancy force on the ascending particle is required to exceed a prescribed positive threshold.

2.2.3.3 Grell–Freitas Scheme

Arakawa *et al.* (2011) build a unified convective parameterization for use at all horizontal scales, Grell and Freitas (2014) introduced a scale-aware approach into a pre-existing scheme based on a stochastic approach. Development and testing of the GF parameterization are partially supported by the National Weather Service Research to operations initiative. Interest in this scheme by Environmental Modeling Center (EMC) and the Next Generation Global Prediction System (NGGPS) Program Office has led to the implementation and testing for potential use in the NCEP operational global model. We implemented the GF parameterization in a developmental version of the NOAA Environmental Modeling System (NEMS)-based Global Spectral Model (GSM), and ran experimental retrospective forecasts using the NEMS-GSM over a warm (June, July and August 2015) and cool (December 2015, January, February 2016) season.

2.2.3.4 Old Simplified Arakawa-Schubert scheme (OSAS)

The Old Simplified Arakawa-Schubert scheme parameterizes the effect of deep convection on the environment (represented by the model state variables) in the following way. First, a simple cloud model is used to determine the change in model state variables due to one entraining/detraining cloud type, per unit cloud-base mass flux. Next, the total change in state variables is retrieved by determining the actual cloud base mass flux using the quasi-equilibrium assumption, whereby convection is assumed to be steady-state.

The SAS scheme uses the working concepts put forth in Arakawa and Schubert (1974) but includes modifications and simplifications from Grell (1993) such as saturated downdrafts and only one cloud type, rather than a spectrum based on cloud top heights or assumed entrainment rates. The scheme was implemented for the GFS in 1995 by Pan and Wu, with further modifications discussed in Han and Pan (2011), including the calculation of cloud top, a greater CFL-criterion-based maximum cloud base mass flux, updated cloud model entrainment and detrainment, improved convective transport of horizontal momentum, a more general triggering function and the inclusion of convective overshooting.

2.2.3.5 Grell-3 scheme

The Grell-3 scheme was first introduced in Version 3.0, and so is new, and not yet well tested in many situations. It shares a lot in common with the Grell-Devenyi in scheme, being based on an ensemble mean approach, but the quasi-equilibrium approach is no longer included among the ensemble members. The scheme is distinguished from other cumulus schemes by allowing subsidence effects to be spread to neighboring grid columns, making the method more suitable to grid sizes less than 10 km, while it can also be used at larger grid sizes where subsidence occurs within the same grid column as the updraft.

2.2.4 Planetary Boundary Layer

The PBL is responsible for vertical sub-grid-scale fluxes due to eddy transports in the whole atmospheric column, not just the boundary layer. Thus, when a PBL scheme is activated, explicit vertical diffusion is de-activated with the assumption. The most appropriate horizontal diffusion choices are those based on horizontal deformation or constant values where horizontal and vertical mixing are treated independently. The PBL schemes determine the flux profiles within the well-mixed boundary layer and the stable layer, and thus provide atmospheric tendencies of temperature, moisture (including clouds), and horizontal momentum in the entire atmospheric column. Most PBL schemes consider dry mixing, but can also include saturation effects in the vertical stability that determines the mixing. This assumption will become less clear at grid sizes below a few hundred meters, where boundary layer eddies may start to be resolved, and in these situations the scheme should be replaced by a fully three-dimensional local sub-grid turbulence scheme such as the TKE diffusion scheme. PBL Schemes options of this model are outlined below;

2.2.4.1 Yonsei University scheme

The Yonsei University PBL (Hong *et al.*, 2006) is the next generation of the MRF PBL, also using the counter gradient terms to represent fluxes due to non-local gradients. This adds to the MRF PBL (Hong and Pan, 1996) an explicit treatment of the entrainment layer at the PBL top. The entrainment is made proportional to the surface buoyancy flux in line with results from studies with large-eddy models (Noh *et al.*, 2003). A smaller magnitude of the counter-gradient mixing in the YSU PBL produces a well-mixed boundary-layer profile, whereas there is a pronounced over-stable structure in the upper part of the mixed layer in the case of the MRF PBL. Details are available in Hong *et al.* (2006), including the analysis of the interaction between the boundary layer and precipitation physics. In version 3.0, an enhanced stable boundary-layer diffusion algorithm (Hong, 2007) is also devised that allows deeper mixing in windier conditions.

2.2.4.2 Mellor-Yamada-Janjic scheme

This parameterization of turbulence in the PBL and in the free atmosphere (Janjic, 1990, 1996, 2002) represents a nonsingular implementation of the Mellor-Yamada Level 2.5 turbulence closure model (Mellor and Yamada, 1982) through the full range of atmospheric turbulent regimes. In this implementation, an upper limit is imposed on the master length scale. This upper limit depends on the TKE as well as the buoyancy and shear of the driving flow. In the unstable range, the functional form of the upper limit is derived from the requirement that the TKE production be nonsingular in the case of growing turbulence. In the stable range, the upper limit is derived from the requirement that the ratio of the variance of the vertical velocity deviation and TKE cannot be smaller than that corresponding to the regime of vanishing turbulence. The TKE production/dissipation differential equation is solved iteratively. The empirical constants have been revised as well (Janjic, 1996, 2002).

2.2.4.3 Grenier–Bretherton–Mc Caa scheme (GBM)

PBL model scheme is a heavily modified version from GBM parameterization, to improve its numerical stability for the use in climate models with longer time steps. To better resolve stratocumulus clouds, their inversion and the interaction between the turbulent diffusion and the vertical advection, the vertical grid is dynamically refined. The new grid is based on the reconstruction of the profiles of variables experiencing a sharp gradient (temperature, mixing

ratio) applying the method presented in Grenier and Bretherton (2001). In typical stratocumulus regions, an additional grid level is thus associated with the PBL top. In case a cloud can be formed, a new level is associated with the lifting condensation level as well. The regular grid plus the two additional levels define the new dynamical grid, which varies geographically and temporally.

2.2.4.4 The Mellor–Yamada–Nakanishi–Niino (MYNN) (Level 2 & 3)

The Mellor–Yamada–Nakanishi–Niino (MYNN) planetary boundary-layer (PBL) scheme is a second-order turbulence closure model that is an improved version of the Mellor–Yamada scheme based on large-eddy simulation data. It simulates PBL structure and evolution well, particularly over the ocean surface. However, when used with various underlying surfaces in China, the scheme overestimates the turbulent momentum flux and the sensible heat flux. To solve the problems of the Mellor–Yamada–Nakanishi–Niino (MYNN) model, we attempted to modify it by following the method proposed by Canuto *et al.* (2008) for the stable stratification case. In contrast to the original MYNN model, the modified model has no critical Richardson number and the effect of turbulent motions remains for all Richardson number values in the level 2 model. Furthermore, the modified model possesses an advantage even for the level 2.5 and level 3 models. The flux Richardson number is unbounded, and a lower limit of the turbulent kinetic energy must be imposed in the original MYNN model; these features do not appear in the modified model.

2.2.4.5 Asymmetrical Convective Model version 2

The ACM2 (Pleim, 2007) is a combination of the ACM, which is a simple transient model that was originally a modification of the Blackadar convective model, and an eddy diffusion model. Thus, in convective conditions the ACM2 can simulate rapid upward transport in buoyant plumes and local shear induced turbulent diffusion. The partitioning between the local and nonlocal transport components is derived from the fraction of non-local heat flux according to the model of Holtslag and Boville (1993). The algorithm transitions smoothly from eddy diffusion in stable conditions to the combined local and non-local transport in unstable conditions. The ACM2 is particularly well suited for consistent PBL transport of any atmospheric quantity including both meteorological (u , v , θ , qv) and chemical trace species.

2.2.4.6 Bougeault–Lacarrère scheme

This is the Bougeault–Lacarrère (BouLac) scheme (Bougeault and Lacarrere, 1989). The BouLac scheme is a one-and-a-half order, local closure scheme and has a TKE prediction option designed for use with the BEP (Building Environment Parameterization) multi-layer, urban canopy model (Martilli *et al.*, 2002). BouLac diagnoses PBLH as the height where the prognostic TKE reaches a sufficiently small value (in the current version of WRF is $0.005 \text{ m}^2 \text{ s}^{-2}$).

2.2.4.7 University of Washington scheme

MYJ is an implementation of the Mellor Yamada level 2.5 model (Mellor and Yamada, 1982). It applies a local approach to determine eddy diffusion coefficients from prognostic turbulent kinetic energy (TKE). Since the TKE is largest within the PBL, MYJ defines its top as the height where the TKE becomes negative or drops to a prescribed lower bound (Janjic, 2001). A similar approach is used in the recently added UW parameterization, but turbulent kinetic energy is diagnosed rather than prognoses for different regimes (stable or convective) and an explicit entrainment closure is used at the edge of the convective layers (Bretherton and Park, 2009). UW that use the Janjic Eta Monin–Obukhov surface layer scheme. Indeed, one possible cause of the biases can be related to the heat fluxes delivered by this scheme with respect to Monin–Obukhov surface layer scheme used with YSU, ACM2 and MRF. UW also verify the highest latent heat flux at the surface. UW parameterizations that use the Janjic Eta Monin–Obukhov surface layer scheme that was found of sensible and latent heat fluxes with respect to Monin–Obukhov surface layer scheme.

2.2.4.8 Total Energy–Mass Flux scheme

The Total Energy–Mass Flux (TEMF) scheme (Angevine *et al.*, 2010) is a one-and-a-half order, non-local closure scheme and has a sub-grid scale total energy prognostic variable, in addition to mass-flux-type shallow convection. TEMF uses eddy diffusivity and mass flux concepts to determine vertical mixing. PBLH is calculated through a Rib method with zero as a threshold value. In this study, there were minor stability issues with five simulation days using the TEMF scheme. All these days were characterized by low-level winds from the southwest. The stability issues are caused by a threshold of potential temperature over the desert regions in our parent domain. Decreasing the time between calls to the radiation physics scheme improved the stability for two of the five simulation days.

2.2.4.9 Medium Range Forecast Model

The scheme is described by Hong and Pan (1996). This PBL scheme employs a so-called counter-gradient flux for heat and moisture in unstable conditions. It uses enhanced vertical flux coefficients in the PBL, and the PBL height is determined from a critical bulk Richardson number. It handles vertical diffusion with an implicit local scheme, and it is based on local in the free atmosphere.

2.2.5 Microphysics schemes in WRF-ARW Model

Microphysics includes explicitly resolved water vapor, cloud, and precipitation processes. The model is general enough to accommodate any number of mass mixing-ratio variables, and other quantities such as number concentrations. Four-dimensional arrays with three spatial indices and one species index are used to carry such scalars. Memory, i.e., the size of the fourth dimension in these arrays, is allocated depending on the needs of the scheme chosen, and advection of the species also applies to all those required by the microphysics option. In the current version of the ARW, microphysics is carried out at the end of the time-step as an adjustment process, and so does not provide tendencies. The rationale for this is that condensation adjustment should be at the end of the time-step to guarantee that the final saturation balance is accurate for the updated temperature and moisture. However, it is also important to have the latent heating forcing for potential temperature during the dynamical sub-steps, and this is done by saving the microphysical heating as an approximation for the next time-step. The sedimentation process is accounted for inside the individual microphysics modules, and, to prevent instability in the calculation of the vertical flux of precipitation, a smaller time step is allowed. The saturation adjustment is also included inside the microphysics. In the future, however, it might be separated into an individual subroutine to enable the remaining microphysics to be called less frequently than the model's advection step for efficiency. The number of moisture variables, and whether ice-phase and mixed-phase processes are included. Mixed-phase processes are those that result from the interaction of ice and water particles, such as riming that produces graupel or hail. As a general rule, for grid sizes less than 10 km, where updrafts may be resolved, mixed-phase schemes should be used, particularly in convective or icing situations. For coarser grids the added expense of these schemes is not worth it because riming is not likely to be well resolved.

2.2.5.1 Kessler scheme

This scheme (Kessler, 1969), which was taken from the COMMAS model (Wicker and Wilhelmson, 1995), is a simple warm cloud scheme that includes water vapor, cloud water, and rain. The microphysical processes included are: the production, fall, and evaporation of rain; the accretion and auto conversion of cloud water; and the production of cloud water from condensation.

2.2.5.2 Purdue Lin scheme

Six classes of hydrometeors are included: water vapor, cloud water, rain, cloud ice, snow, and graupel. All parameterization production terms are based on Lin *et al.* (1983) and Rutledge and Hobbs (1984) with some modifications, including saturation adjustment following Tao *et al.* (1989) and ice sedimentation. This is a relatively sophisticated microphysics scheme in WRF, and it is most suitable for use in research studies. The scheme is taken from the Purdue cloud model, and the details can be found in Chen and Sun (2002).

2.2.5.3 WRF Single-Moment 3-class scheme

The WRF single-moment microphysics scheme follows Hong *et al.* (2004) including ice sedimentation and other new ice-phase parameterizations. A major difference from other approaches is that a diagnostic relation is used for ice number concentration that is based on ice mass content rather than temperature. The computational procedures are described in Hong and Lim (2006). As with WSM5 and WSM6, the freezing/melting processes are computed during the fall-term sub-steps to increase accuracy in the vertical heating profile of these processes. The order of the processes is also optimized to decrease the sensitivity of the scheme to the time step of the model. The WSM3 scheme predicts three categories of hydrometeors: vapor, cloud water/ice, and rain/snow, which is a so-called simple-ice scheme. It follows Dudhia (1989) in assuming cloud water and rain for temperatures above freezing, and cloud ice and snow for temperatures below freezing. This scheme is computationally efficient for the inclusion of ice processes, but lacks super cooled water and gradual melting rates.

2.2.5.4 WRF Single-Moment 5-class scheme

This scheme is similar to the WSM3 simple ice scheme. However, vapor, rain, snow, cloud ice, and cloud water are held in five different arrays. Thus, it allows super cooled water to

exist, and a gradual melting of snow falling below the melting layer. Details can be found in Hong *et al.* (2004), and Hong and Lim (2006). As with WSM6, the saturation adjustment follows Dudhia (1989) and Hong *et al.* (1998) in separately treating ice and water saturation processes, rather than a combined saturation such as the Purdue Lin (above) and Goddard (Tao *et al.*, 1989) schemes. This scheme is efficient in intermediate grids between the mesoscale and cloud-resolving grids.

2.2.5.5 WRF Single-Moment 6-class scheme

The six-class scheme extends the WSM5 scheme to include graupel and its associated processes. Some of the graupel-related terms follow Lin *et al.* (1983), but its ice-phase behavior is much different due to the changes of Hong *et al.* (2004). A new method for representing mixed-phase particle fall speeds for the snow and graupel particles by assigning a single fall speed to both that is weighted by the mixing ratios, and applying that fall speed to both sedimentation and accretion processes is introduced (Dudhia *et al.*, 2008). The behavior of the WSM3, WSM5, and WSM6 schemes differ little for coarser mesoscale grids, but they work much differently on cloud-resolving grids. Of the three WSM schemes, the WSM6 scheme is the most suitable for cloud-resolving grids, considering the efficiency and theoretical backgrounds (Hong and Lim, 2006).

2.2.5.6 Eta Grid-scale Cloud and Precipitation (2001) scheme

This is also known as EGCP01 or the Eta Ferrier scheme. The scheme predicts changes in water vapor and condensate in the forms of cloud water, rain, cloud ice, and precipitation ice (snow/graupel/sleet). The individual hydrometeor fields are combined into total condensate, and it is the water vapor and total condensate that are advocated in the model. Local storage arrays retain first-guess information that extract contributions of cloud water, rain, cloud ice, and precipitation ice of variable density in the form of snow, graupel, or sleet. The density of precipitation ice is estimated from a local array that stores information on the total growth of ice by vapor deposition and accretion of liquid water. Sedimentation is treated by partitioning the time averaged flux of precipitation into a grid box between local storage in the box and fall out through the bottom of the box. The mean size of precipitation ice is assumed to be a function of temperature following the observational results of Ryan (1996).

2.2.5.7 Thompson *et al.* scheme

A new bulk microphysical parameterization (BMP) has been developed for use with WRF or other mesoscale models. Unlike any other BMP, the assumed snow size distribution depends on both ice water content and temperature and is represented as a sum of exponential and gamma distributions. Furthermore, snow assumes a non-spherical shape with a bulk density that varies inversely with diameter as found in observations and in contrast to nearly all other BMPs that assume spherical snow with constant density. New features specific to this version of the bulk scheme compared to the Thompson *et al.* (2004) paper description include:

Generalized gamma distribution shape for each hydrometeor species, non-spherical, variable density snow, and size distribution matching observations, y-intercept of rain depends on rain mixing ratio and whether apparent source is melted ice, y-intercept of graupel depends on graupel mixing ratio, a more accurate saturation adjustment scheme, variable gamma distribution shape parameter for cloud water droplets based on observations, look-up table for freezing of water drops, look-up table for transferring cloud ice into snow category, improved vapor deposition/sublimation and evaporation, variable collection efficiency for rain, snow, and graupel collecting cloud droplets, improved rain collecting snow and graupel.

2.2.5.8 Morrison *et al.* 2-Moment scheme

The Morrison *et al.* (2008) scheme is based on the two-moment bulk microphysics scheme of Morrison *et al.* (2005) and Morrison and Pinto (2006). Six species of water are included: vapor, cloud droplets, cloud ice, rain, snow, and graupel/hail. The code has a user-specified switch to include either graupel or hail. Prognostic variables include number concentrations and mixing ratios of cloud ice, rain, snow, and graupel/hail, and mixing ratios of cloud droplets and water vapor (total of 10 variables). The prediction of two-moments (i.e., both number concentration and mixing ratio) allows for a more robust treatment of the particle size distributions, which are a key for calculating the microphysical process rates and cloud/precipitation evolution. Several liquid, ice, and mixed-phase processes are included. Particle size distributions are treated using gamma functions, with the associated intercept and slope parameters derived from the predicted mixing ratio and number concentration. The

scheme has been extensively tested and compared with both idealized and real case studies covering a wide range of conditions.

2.2.5.9 CAM 5.1 scheme

Version 5.1 of the Community Atmosphere Model (CAM) is the latest in a series of global atmosphere models originally developed at the NCAR. The current development of CAM is guided by the Atmosphere Model Working Group (AMWG) of the Community Earth System Model (CESM) project. CAM is used as both a standalone model and as the atmospheric component of the CESM. CAM has a long history of use as a standalone model by which we mean that the atmosphere is coupled to an active land model (CLM), a thermodynamic only sea ice model (CICE), and a data ocean model (DOCN). When one speaks of “doing CAM simulations” the implication is that it’s the standalone configuration that is being used. When CAM is coupled to active ocean and sea ice models then we refer to the model as CESM.

In versions of CAM before 4.0 the driver for the standalone configuration was completely separate code from what was used to couple the components of the CCSM. One of the most significant software changes in CAM-4.0 was a refactoring of how the land, ocean, and sea ice components are called which enabled the use of the CCSM coupler to act as the CAM standalone driver (this also depended on the complete rewriting of the CCSM coupler to support sequential execution of the components). Hence, for the CESM1 model, just as for CCSM4 before it, it is accurate to say that the CAM standalone configuration is nothing more than a special configuration of CESM in which the active ocean and sea ice components are replaced by Data Ocean and thermodynamic sea ice components.

Since the CAM standalone model is just a special configuration of CESM it can be run using the CESM scripts. This is done by using one of the “F” comp sets and is described in the CESM-1.0 User’s Guide³. The main advantage of running CAM via the CESM scripts is to leverage the high level of support that those scripts provide for doing production runs of predefined experiments on supported platforms. CAM is used in a lot of environments where the complexity of production ready scripts is not necessary. In either case though, the ability to customize a CAM build or runtime configuration depends on being able to use the utilities described in this document. Any build configuration can be set up via appropriate command line arguments to CAM’s configure utility, and any runtime configuration can be set up with

appropriate arguments to CAM's build-name list utility. Issues that are specific to running CAM from the CESM scripts will not be discussed in this guide. Rather we focus on issues that are independent of which scripts are used to run CAM, although there is some attention given in this guide to the construction of simple scripts designed for running CAM in its standalone mode.

2.2.5.10 SBU-Ylin scheme

The new State University of New York at Stony Brook BMP scheme (hereafter referred to as SBU-YLIN, but labeled as SUNY in all the figures) was developed using the Purdue-Lin scheme (Lin *et al.*, 1983; Chen and Sun 2002) as a starting point, which includes the super saturation adjustment from Tao *et al.* (1989). The SBU-YLIN scheme includes five prognostic mixing ratios: water vapor, cloud ice, precipitating ice (PI), cloud liquid water, and rain. Dry snow, rimed snow, and graupel are included in the PI category through the introduction of a varying riming intensity parameter. Since snow and graupel share the same category in this new scheme, they also share the same processes (deposition/sublimation and collision with other hydrometeors).

2.2.5.11 The WRF Double Moment 5-class scheme

The WSM5 scheme is the more complex version of WSM3 including 5 classes (cloud water, cloud ice, rain, snow, vapor). Because the different states of cloud water and precipitation are stored separately the scheme allows for super cooled water to exist and snow can gradually melt when falling. Both WSM schemes follow Hong *et al.* (2004). The third scheme (WDM5) is a version of WSM5 that includes double moment prediction for warm rain (Lim and Hong 2010).

2.2.5.12 WRF double-moment 6-Class (WDM6) scheme

The purpose of this study is to develop a new double-moment bulk microphysics parameterization of clouds and precipitation to be applicable in mesoscale and general circulation models. The new scheme is called the WRF double-moment 6-class (WDM6) microphysics scheme because only double-moment warm-rain microphysics, which predicts the number concentration of cloud and rainwater, are added into the corresponding single-moment scheme that is the WRF single-moment 6-class (WSM6) scheme (Hong *et al.*, 2004; Hong and Lim 2006). The ice-phase microphysics of Hong *et al.* (2004) are identical for

both the WDM6 and WSM6 schemes. Recognizing the importance of cloud–aerosol interaction in cloud microphysics and radiative properties (Ramanathan *et al.*, 2001; Wang 2005; Khain *et al.*, 2008), a prognostic treatment of CCN particles is introduced for the new scheme to activate cloud waters. An idealized 2D storm test bed is designed to differentiate the simulated storm morphology using the WDM6 and WSM6 schemes along with the intrinsic differences between the two schemes. In addition, CCN the effects on the cloud/raindrop properties and surface precipitation are investigated.

2.2.5.13 NSSL 2-moment scheme

This is a two-moment scheme for cloud droplets, rain drops, ice crystals, snow, graupel, and hail. It also predicts average graupel particle density, which allows graupel to span the range from frozen drops to low-density graupel. There is an additional option to predict cloud condensation nuclei (CCN, option 18) concentration (intended for idealized simulations). The scheme is intended for cloud-resolving simulations ($dx = 2\text{km}$) in research applications.

2.2.6 Land-Surface Model

The land-surface models (LSMs) use atmospheric information from the surface layer scheme, radiative forcing from the radiation scheme, and precipitation forcing from the microphysics and convective schemes, together with internal information on the land's state variables and land-surface properties, to provide heat and moisture fluxes over land points and sea-ice points. These fluxes provide a lower boundary condition for the vertical transport done in the PBL schemes (or the vertical diffusion scheme in the case where a PBL scheme is not run, such as in large-eddy mode). The land-surface models have various degrees of sophistication in dealing with thermal and moisture fluxes in multiple layers of the soil and also may handle vegetation, root, and canopy effects and surface snow-cover prediction. The land surface model provides no tendencies, but does update the land's state variables which include the ground (skin) temperature, soil temperature profile, soil moisture profile, snow cover, and possibly canopy properties. There is no horizontal interaction between neighboring points in the LSM, so it can be regarded as a one-dimensional column model for each WRF land grid-point, and many LSMs can be run in a stand-alone mode.

2.2.6.1 5-layer Thermal Diffusion Scheme

This simple LSM is based on the MM5 5-layer soil temperature model. Layers are 1, 2, 4, 8, and 16 cm thick. Below these layers, the temperature is fixed at a deep-layer average. The

energy budget includes radiation, sensible, and latent heat flux. It also allows for a snow-cover flag, but the snow cover is fixed in time. Soil moisture is also fixed with a land use- and season-dependent constant value, and there are no explicit vegetation effects.

2.2.6.2 Noah Land Surface (NLS) Model

The Noah LSM is the successor to the OSU LSM described by Chen and Dudhia (2001). The scheme was developed jointly by NCAR and NCEP, and is a unified code for research and operational purposes, being almost identical to the code used in the NCEP North American Mesoscale Model (NAM). This is a 4-layer soil temperature and moisture model with canopy moisture and snow cover prediction. The layer thickness are 10, 30, 60 and 100 cm (adding to 2 meters) from the top down. It includes root zone, evapotranspiration, soil drainage, and runoff, taking into account vegetation categories, monthly vegetation fraction, and soil texture. The scheme provides sensible and latent heat fluxes to the boundary-layer scheme. The Noah LSM additionally predicts soil ice, and fractional snow cover effects, has an improved urban treatment, and considers surface emissivity properties, which are all new since the OSU scheme.

2.2.6.3 Rapid Update Cycle (RUC) Model

The RUC LSM has a multi-level soil model (6 levels is default, could be 9 or more) with higher resolution in the top part of soil domain (0, 5, 20, 40, 160, 300 cm is default). The soil model solves heat diffusion and Richards's moisture transfer equations, and in the cold season takes into account phase changes of soil water (Smirnova *et al.*, 1997, 2000). The RUC LSM also has a multi-layer snow model with changing snow density, refreezing liquid water percolating through the snow pack, snow depth and temperature dependent albedo, melting algorithms applied at both snow-atmosphere interface and snow-soil interface, and simple parameterization of fractional snow cover with possibility of grid averaged skin temperature going above freezing. It also includes vegetation effects and canopy water. The RUC LSM has a layer approach to the solution of energy and moisture budgets. The layer spans the ground surface and includes half of the first atmospheric layer and half of the top soil layer with the corresponding properties (density, heat capacity, etc.) The residual of the incoming fluxes modify the heat storage of this layer. An implicit technique is applied to the solution of these equations. Prognostic variables include soil temperature, volumetric liquid, frozen and total soil moisture contents, surface and sub-surface runoff, canopy moisture,

evapotranspiration, latent, sensible and soil heat fluxes, heat of snow-water phase change, skin temperature, snow depth and density, and snow temperature.

2.2.6.4 Pleim-Xiu Scheme (PXS)

The PX LSM (Pleim and Xiu, 1995; Xiu and Pleim, 2001), originally based on the ISBA model Noilhan and Planton (1989), includes a 2-layer force-restore soil temperature and moisture model. The top layer is taken to be 1 cm thick, and the lower layer is 99 cm. The PX LSM features three pathways for moisture fluxes: evapotranspiration, soil evaporation, and evaporation from wet canopies. Evapotranspiration is controlled by bulk stomata resistance that is dependent on root zone soil moisture, photo synthetically active radiation, air temperature, and the relative humidity at the leaf surface. Grid aggregate vegetation and soil parameters are derived from fractional cover ages of land use categories and soil texture types. There are two indirect nudging schemes that correct biases in 2-m air temperature and RH by dynamic adjustment of soil moisture (Pleim and Xiu, 2003) and deep soil temperature (Pleim and Gilliam, 2008). Note that a small utility program (ipxwrf) can be used to propagate soil moisture and temperature between consecutive runs to create a continuous simulation of these quantities.

2.2.6.5 Community Land Model (CLM4)

The Community Land Model is the land model for the Community Earth System Model (CESM) and the CAM. It is a collaborative project between scientists in the Terrestrial Sciences Section (TSS) and the Climate and Global Dynamics Division (CGD) at the NCAR and the CESM Land Model Working Group. The model formalizes and quantifies concepts of ecological climatology. Ecological climatology is an interdisciplinary framework to understand how natural and human changes in vegetation affect climate. The central theme is that terrestrial ecosystems, through their cycling of energy, water, chemical elements, and trace gases, are important determinants of climate. Model components consist of: biogeophysics, hydrologic cycle, biogeochemistry and dynamic vegetation.

The land surface is represented by 5 primary sub-grid land cover types (glacier, lake, wetland, urban, vegetated) in each grid cell. The vegetated portion of a grid cell is further divided into patches of plant functional types, each with its own leaf and stem area index

and canopy height. Each sub grid land cover type and PFT patch is a separate column for energy and water calculations. The current version of the Community Land Model is CLM4.

2.2.6.6 Unified Noah land surface (UNLS) model

Unified land model (ULM), which is a merger of the Noah and Sac models. The motivation for this merger is to incorporate a hydro logically realistic structure within a model construct that can be used in coupled land–atmosphere applications. Because Noah is used operationally at NCEP for offline hydrologic simulations and is coupled with a suite of atmospheric models, the implications of improving its soil moisture run off generation scheme would be widespread. Conversely, the Sac model is used operationally for flood forecasting at over 3000 forecast points across the United States, and it would benefit from Noah’s more physically based vegetation and ET algorithms. We follow with a brief description of the heritage and components of each model, the nature of the approach we used to merge key parameterizations from each, and an assessment of ULM performance.

2.2.7 Shortwave Radiation

Shortwave radiation is radiant energy with wavelengths in the visible, ultraviolet, and near-infrared spectra. There is no standard cut-off for the near-infrared range; therefore, the shortwave radiation range is also variously defined. It may be broadly defined to include all radiation with a wavelength between 0.1 and 5.0 μm or narrowly defined so as to include only radiation between 0.2 μm and 3.0 μm . There is little radiation flux to the Earth’s surface below 0.2 μm or above 3.0 μm , although photon flux remains significant as far as 6.0 μm , compared to shorter wavelength fluxes. Shortwave Radiation Schemes are bellow

2.2.7.1 MM5 Shortwave

It has a simple downward integration of solar flux, accounting for clear-air scattering, water vapor absorption (Lacis and Hansen, 1974), and cloud albedo and absorption. It uses look-up tables for clouds from Stephens (1978). In Version 3, the scheme has an option to account for terrain slope and shadowing effects on the surface solar flux.

2.2.7.2 Goddard and New Goddard (shortwave and long wave)

Goddard and New Goddard are two schemes based on the same publications: Chou and Suarez (1999) and Chou *et al.* (2001). Goddard was included in 2000 and New Goddard in

2011, divergences between both schemes were fully described in Shi *et al.* (2011). This scheme was originally proposed by the NASA Goddard Space Flight Center (GSFC) for being used in global models such as the Goddard Earth Observing System (GEOS) General Circulation Model (GCM), GEOS-GCM, and in limited area models such as the Fifth-Generation Penn State/NCAR MM5. The scheme can deal with shortwave and long wave spectral regions but, in this document, we only will detail the parameterization for solar radiation. Although the set of approximations are fully detailed in Chou and Suarez (1999) and Chou *et al.* (2001), both schemes include some modifications with respect to the original publications that will be discussed in the following sections.

2.2.7.3 CAM Shortwave

A spectral-band scheme used in the NCAR CAM 3.0 for climate simulations. It has the ability to handle optical properties of several aerosol types and trace gases. It uses cloud fractions and overlap assumptions in unsaturated regions, and has a monthly zonal ozone climatology. It is documented fully by Collins *et al.* (2004). The CAM radiation scheme is especially suited for regional climate simulations by having a ozone distribution that varies during the simulation according to monthly zonal-mean climatological data.

2.2.7.4 Radiative and Rapped Transfer Model Gu/Gas (RRTMG) shortwave

The parameterization has been tested using the Rapid Radiative Transfer Model for climate and weather models (RRTMG) SW scheme of the Weather Research and Forecasting (WRF) NWP model for data over the continental US. In principle, it can be adapted to any other shortwave radiative transfer band model. It has been verified against a control experiment and using data from five radiometric stations in the contiguous US. The control experiment consisted of a clear-sky evaluation of the RRTMG solar radiation estimates obtained in WRF when RRTMG is driven with ground-observed aerosol optical properties. Overall, the verification has shown satisfactory results for both broadband shortwave surface direct and diffuse irradiances. The parameterization has proven effective in significantly reducing the prediction error and constraining the seasonal bias in clear sky conditions to within the typical observational error expected in well maintained radiometers.

2.2.7.5 Fu-Liou-Gu Radiative Transfer Model (shortwave and long wave)

The atmospheric radiative transfer calculations are performed using the Fu-Liou-Gu (FLG) radiative transfer mode (RTM), which is a modified and improved version based on the original Fu-Liou scheme. A combination of the delta four-stream approximation for solar flux calculations (Liou *et al.*, 1988) and delta-two/four-stream approximation for Infrared (IR) flux calculations (Fu *et al.*, 1997) is employed in the model to assure both accuracy and efficiency. The incorporation of non-gray gaseous absorption in multiple scattering atmospheres is based on the correlated k distribution method developed by Fu and Liou (1992). Parameterization of the single-scattering properties for cloud particles is implemented by following the procedure developed by Fu and Liou (1993). The scheme works within shortwave and long wave regions of the electromagnetic spectrum. However, only the solar case is analyzed.

2.2.8 Long Wave Radiation

All surfaces above absolute zero emit radiation. The temperatures of building surfaces are sufficiently low that they emit energy as longwave radiation. This radiation lies within the wavelengths 3-100 μm with a maximum occurring at approximately 10 μm . Long Wave Radiation schemes are below:

2.2.8.1 Rapid Radiative Transfer Model Long wave

This RRTM, which is taken from MM5, is based on Mlawer *et al.* (1997) and is a spectral-band scheme using the correlated-k method. It uses pre-set tables to accurately represent long wave processes due to water vapor, ozone, CO₂, and trace gases (if present), as well as accounting for cloud optical depth.

2.2.8.2 CAM Long wave

A spectral-band scheme used in the NCAR CAM 3.0 for climate simulations. It has the potential to handle several trace gases. It interacts with resolved clouds and cloud fractions, and is documented fully by Collins *et al.* (2004).

2.2.8.3 Radiation and Radiative Transfer Model Gu/ Gas (RRTMG) long wave

We are developing radiation codes known as “Psrad” which are modeled on the RRTMG parameterization (Mlawer *et al.*, 1997; Iacono *et al.*, 2008). We make use of the RRTMG

description of gas optics, which is among the most accurate parameterizations available (Oreopoulos *et al.*, 2012) and initially make many of the same algorithmic decisions, including the choice to neglect long wave scattering. Our codes are intended as a drop-in replacement for RRTMG (which has already been implemented in NOGAPS) but we have implemented it almost entirely from scratch. The most important technical difference lies in the organization: each of our subroutines is designed to operate on many columns at a time, a choice that increases computational efficiency on a wide range of platforms. Operational centers such as the European Centre for Medium-Range Weather Forecasts have often modified RRTMG in this way (Morcrette *et al.*, 2008).

2.2.8.4 Held-Suarez scheme

The atmosphere model can best be described as combining the numeric of Hendon and Hartmann with the physics of Held and Suarez with some modifications to both. The result is a 2-level, global, spectral transform, primitive equation model with reasonably complete physics which runs with acceptable speed at T21 (triangular-21) truncation on a workstation for long integrations¹. This model is intended for mechanistic studies. The many idealizations involved in formulating the physics and dynamics can be seen as assets because they simplify interpretation, even though they may reduce the fidelity of the model output to the climatology of the atmosphere. The model was originally coded to include an arbitrary distribution of land and ocean with zonally asymmetric physics, lower-level moisture advection and a simple precipitation parameterization, as in Semtner's (1984) version of the HS model. The current study only uses a "dry" version of this model in which there is no advection of moisture. Instead, latent heat is released immediately and locally, and the atmosphere is convectively adjusted to a moist-neutral profile.

CHAPTER III

Model Description and Methodology

In the present study the Weather Research and Forecast (WRF-ARW Version 3.5.1) model consists of fully compressible non-hydrostatic equations and different prognostic variables is utilized. The model vertical coordinate is terrain following hydrostatic pressure and the horizontal grid is Arakawa C-grid staggering. Third-order Runge-Kutta time integration is used in the model. The model description and methodology are given below:

3.1 Model Description

The model is configured in single domain, 12 km horizontal grid spacing with 208×229 grids in the west-east and north-south directions and 19 vertical levels. The Cumulus schemes bring out the effect of sub-grid scale convection on the grid-resolved thermodynamic variables. At first, five numerical experiments have been conduct the cumulus parameterization schemes with a combination of various physics options are KF, BMJ, Grell–Freitas (GF), Old Simplified Arakawa-Schubert (OSAS) and Grell-3 scheme. The other physics schemes held fixed. The PBL schemes provide the atmospheric ‘tendencies’ of temperature, moisture (including clouds) and horizontal momentum in the entire atmospheric column (Skamarock 2008). Ten numerical experiments have been conducted with a combination of five surface layer schemes, the best result from the cumulus scheme parameterization experiments and the other fixed physical parameterization schemes. The ten PBL schemes are Yonsei University (YSU), Mellor-Yamada-Janjic (MYJ), Grenier–Bretherton–McCaa (GBM), The Mellor–Yamada–Nakanishi–Niino Level 3 (MYNN3), ACM2, Mellor–Yamada–Nakanishi–Niino Level 2.5 (MYNN2), BouLac, University of Washington (UW), TEMF and MRF scheme and the five surface layer schemes are Moin-Obukhov (MON), Moin-Obukhov(Janjik Eta), NCEP GFS (NMM only), QNSE and 10 number scheme. The microphysics (MP) parameterizations explicitly handle water vapor, cloud, precipitation processes, melting of snow, graupel, hydrometeors and suppression of falling rain by evaporation. In this set of experiments, sixteen different MP schemes have been considered along with the best result of the cumulus, the PBL and with the surface layer parameterization and other physics are kept fixed. Various microphysics options are WRF Single-Moment 6-class (WSM6), Kessler, Purdue Lin, WRF Single-Moment 3-class

(WSM3), WRF Single-Moment 5-class (WSM5), Eta Grid-scale Cloud and Precipitation (2001) (Eta), Thompson *et al.* (Thompson), Morrison *et al.* 2-Moment (Morrison 2-mom), Community Atmosphere Model Version 5.1 (CAM5.1), SBU-Ylin, The WRF Double Moment 5-class (WDM5), The WRF Double Moment 6-class (WDM6), NSSL 2-moment (NSSL 2-mom), NSSL 2-moment w/CCN Prediction (NSSL 2-mom-CCN), NSSL 1-moment (NSSL 1-mom) and NSSL 1-momentlfo(NSSL 1-momlfo) scheme. The land-surface models (LSMs) are responsible for the thermal and moisture fluxes in multiple layers of the soil, vegetation, root, canopy effects, surface snow-cover, heat fluxes and moisture over the land points, sea-ice points and also give the lower boundary condition fluxes to the PBL schemes (Skamarock 2008). In this set of experiments, six different land-surface models have been considered along with the best result of the cumulus, the PBL and with the surface layer parameterization, the microphysics and other physics are kept fixed. Various land-surface models options are Unified Noah Land Surface model (UNLS), Thermal Diffusion Scheme (TDS), Rapid Update Cycle Model (RUC), Noah Land Surface Model (NLS), Community Land Model is the land model Version 4.0 (CLM4.0) and Pleim-Xiu LSM (PXS) scheme. The other physics options are kept fixed. The short wave radiation (SWR) schemes handle the process of absorption, reflection and scattering in the atmosphere and from the surface. In this set of experiments, six different short wave radiation schemes have been considered along with the best result of the cumulus, the PBL and with the surface layer parameterization, the microphysics, the land surface model and other physics are kept fixed. Various short wave radiation schemes options are MM5 Shortwave (Dudhia), GSFC ARW+Chem(τ), CAM Shortwave (CAM), Rapid Radiative Transfer Model Gu/Gas (RRTMG), New Goddard and Fu-Liou-Gu Radiative Transfer Model (FLG) scheme. The long wave radiation (LWR) schemes handle the process of absorption and emission of infrared or thermal radiation by gases and surfaces. In this set of experiments, six different long wave radiation schemes have been considered along with the best result of the cumulus, the PBL and with the surface layer parameterization, the microphysics, the land surface model, short wave radiation schemes and other physics are kept fixed. Various long wave radiation schemes options are Rapid Radiative Transfer Model (RRTM), CAM Long wave (CAM), Rapid Radiative Transfer Model Gu/Gas (RRTMG), New Goddard, Fu-Liou-Gu Radiative Transfer Model (FLG) and Held-Suarez scheme. The model domain is given in Fig. 3.1 The detail of the model and domain configuration is given in Table 3.1.

3.2 Model Domain and Configuration

In this study, the WRF–ARW model has been configured with single domain for the analysis of track, wind speed 10m height and central sea level pressure. The model domain region is 2.05-26.48° N & 73.96-97.04° E.

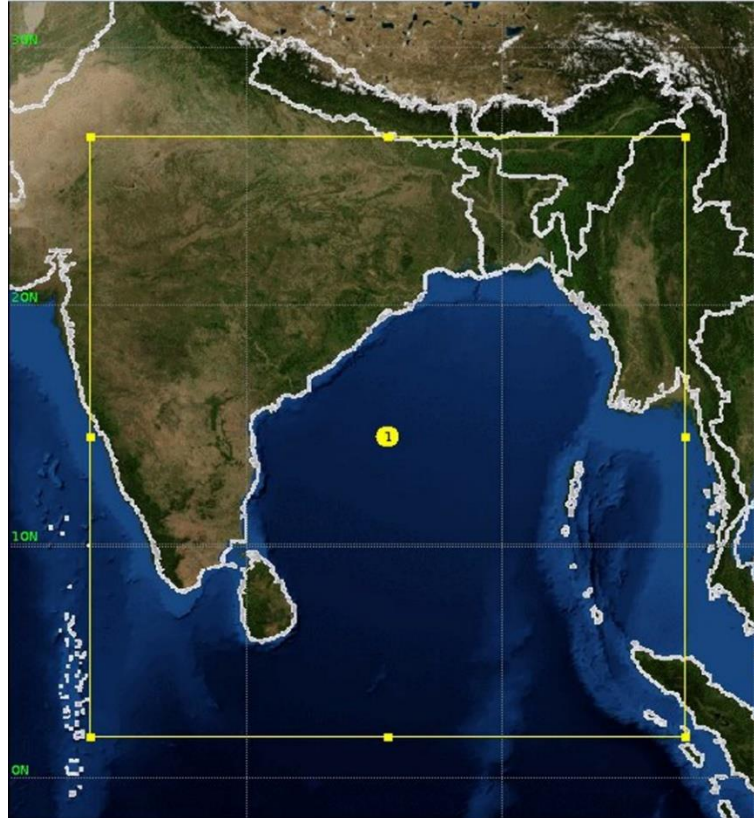


Figure. 3.1: The WRF–ARW domain set up for the study.

3.3 Data and Methodology

Final Reanalysis (FNL) data (1° x 1°) collected from National Centre for Environment Prediction (NCEP) is used as initial and lateral boundary conditions (LBCs) which is updated at six hours interval i.e. the model is initialized with 0000, 0600, 1200 and 1800 UTC initial field of corresponding date. The NCEP FNL data is interpolated to the model horizontal and vertical grids and the model was integrated for 96 h period for TC Mahasen.

Table 3.1: WRF Model and Domain Configurations.

Dynamics	Non-hydrostatic
Number of domain	1
Central points of the domain	Central Lat. : 14.6°N, Central Lon. : 85.5°E

Horizontal grid distance	12 km
Integration time step	60 s
Number of grid points	X-direction 209 points, Y-direction 230 points
Map projection	Mercator
Horizontal grid distribution	Arakawa C-grid
Nesting	One way
Vertical co-ordinate	Terrain-following hydrostatic-pressure co-ordinate (19 sigma levels up to 100 hPa)
Time integration	3 rd order Runge-Kutta
Spatial differencing scheme	6 th order centered differencing
Initial conditions	Three-dimensional real-data (FNL: 1° × 1°)
Lateral boundary condition	Specified options for real-data
Top boundary condition	Gravity wave absorbing
Bottom boundary condition	Physical or free-slip
Diffusion and Damping	Simple Diffusion
Cumulus parameterization	1) KF 2) BMJ 3) GF 4) OSAS and 5) Grell-3 schemes
Planetary Boundary Layer	1) YSU 2) MYJ 3) GBM 4) MYNN3 5) ACM2 6) MYNN2 7) BouLac 8) UW 9) TEMF and 10) MRF schemes.
Microphysics	1) WSM6 2) Kessler 3) Purdue Lin 4) WSM3 5) WSM5 6) Eta 7) Thompson 8) Morrison 2-mom 9) CAM5.1 10) SBU-Ylin 11) WDM5 12) WDM6, 13) NSSL 2-mom 14) NSSL 2-mom-CCN 15) NSSL 1-mom and 16) NSSL 1-momlfo schemes.
Land surface model	1) UNLS 2) TDS 3) RUC 4) NLS 5) CLM4.0 and 6) PXS schemes.
Short Wave Radiation	1) Dudhia 2) GSFC ARW+Chem(τ) 3) CAM 4) RRTMG 5) New Goddard and 6) FLG scheme.
Long Wave Radiation	1) RRTM 2) CAM Long wave (CAM) 3) RRTMG 4) New Goddard 5) FLG and 6) Held-Suarez schemes.

First set of experiment 48 and secondly 49 schemes have been conducted in this experiment with a initial condition. In this regard, the initial conditions of 2013-05-13_00:00:00 to 2013-05-17_00_00_00 (0000 UTC of 12 to 17 May 20130000 UTC) has been considered for Mahasen.

Table 3.2: Observed information of Simulated Tropical Cyclones in the Bay of Bengal

Name of TC	Country of landfall	Date of Formation	Date and Time of landfall UTC	Minimum SLP, hPa	MWS, km/h or m/s
Mahasen	Bangladesh	11 May	0800 UTC of 16 May 2013	990	84 or 23

3.4 Experimental procedure and scheme selection

The model simulated MSLP, maximum wind at 10 m level and track have been studied and analyzed for the cyclone. Simulated track and intensity have also been compared with the IMD and simulation observed results.

Calculated the Track, Wind speed and central sea level pressure (CSLP) of the cyclone Mahasen by using the software Grid Analysis and Display Systems (GrADS). The Grid Analysis and Display System (GrADS) is an interactive desktop tool that is used for easy access, manipulation, and visualization of earth science data. GrADS have two data models for handling gridded and station data. GrADS supports many data file formats, including binary (stream or sequential), GRIB (version 1 and 2), NetCDF, HDF (version 4 and 5), and BUFR (for station data). GrADS have been implemented worldwide on a variety of commonly used operating systems. GrADS use a 5-Dimensional data environment: the four conventional dimensions (longitude, latitude, vertical level, and time) plus an optional 5th dimension for grids that is generally implemented but designed to be used for ensembles. Data sets are placed within the 5-D space by use of a data descriptor file. GrADS handles grids that are regular, non-linearly spaced, Gaussian, or of variable resolution. Data from different data sets may be graphically overlaid, with correct spatial and time registration. Operations are executed interactively by entering FORTRAN-like expressions at the command line. Data may be displayed using a variety of graphical techniques: line and bar graphs, scatter plots, smoothed contours, shaded contours, streamlines, wind vectors, grid boxes, shaded grid boxes, and station model plots. Graphics may be output in PostScript or image formats. GrADS provides geo physically intuitive defaults, but the user has the option to control all aspects of graphics output. After getting txt data from grads we converted it into Excel sheet and plotted graph using Excel. We have plotted the data on Excel for observing the changing of Track error and Track RMS error, Wind speed 10 meter height,

error from observe and wind speed RMS error and CSLP, error from observe and RMS error for different sensitivity schemes studies. For the track experiments, the minimum CSLP (hPa) and corresponding latitude and longitude values have been obtained for every 6 and 3 hours from the ARW model output for all schemes in a particular physics parameterization. The model simulated tracks, wind speed and CSLP for the cyclone Mahasen have then been compared with the observation track, wind speed and CSLP obtained from IMD. Error is computed as given in equation (1), (3) and (5). The root mean square (RMS) error has also been calculated up to 90 hr for every 6hours, as given in equation (2), (4), (6).

$$T_{Err} = \sqrt{(lat_{simulation} - lat_{IMD})^2 + (lon_{simulation} - lon_{IMD})^2} \quad (1)$$

$$Track\ Err\ RMS = \sqrt{\frac{1}{n} \sum_{n=1}^n T_{Err}^2} \quad (2)$$

$$WS_{Err} = \sqrt{(WS_{simulation} - WS_{IMD})^2} \quad (3)$$

$$Wind\ Speed\ Err\ RMS = \sqrt{\frac{1}{n} \sum_{n=1}^n WS_{Err}^2} \quad (4)$$

$$CSLP_{Err} = \sqrt{(CSLP_{simulation} - CSLP_{IMD})^2} \quad (5)$$

$$CSLP\ Err\ RMS = \sqrt{\frac{1}{n} \sum_{n=1}^n CSLP_{Err}^2} \quad (6)$$

Where, at first T_{Err} (track error) is computed in degrees and finally calculated in km. WS_{Err} (Wind speed error) 10m height is computed in m/s and $CSLP_{Err}$ (central sea level pressure error) in hPa. N is the number of observations and simulations data. The best scheme has been chosen on the basis of both the propagation of simulated track and the RMS errors of the track, wind speed and central sea level pressure. Intensity experiments have also been conducted in a fashion analogous to the one described above and the maximum wind (m/s) at 10m height has been obtained from the model output. The best scheme is the one that gives the least RMS error. This Thesis has been written using Microsoft Word Document 2013.

3.5 Synoptic history of Mahasen

The TC Cyclone Mahasen was the fourth severe cyclonic storm of the north Indian Ocean in 2013. Mahasen developed from a low pressure area in the Bay of Bengal. Mahasen slowly developed. It became a depression on May 10 by almost remaining still. Gradually it gained

speed on May 13 and became a cyclonic storm. It was the first storm of the season. At first the system's ultimate direction was not clear, but moved closer to eastern India. On May 14, the circulation of Mahasen turned northeastward. Cyclone Mahasen struck Southern Bangladesh on 16 May 2013. The speed of the wind was about 84 kph. Gained energy from the warm waters and strengthened again as a category 1 storm on 13 May from 00 UTC to 17 May 00 UTC. The system weakened and became a deep depression after its landfall and made landfall 16 May 2013 Thursday northwest of Chittagong, Bangladesh, with peak winds near 24 m/s.

Table 3.3: Procedure for track prediction of 1st set

Exp. No.	Cumulus	PBL	Microphysics	Surface Physics	SWR	LWR	sf_sfclay _ physics
Cumulus parameterization schemes							
1	KF	YSU	WSM6	UNLS	Dudhia	RRTM	1
2	BMJ						
3	GF						
4	OSAS						
5	Grell-3						
Planetary boundary layer schemes							
6	BMJ	YSU	WSM6	UNLS	Dudhia	RRTM	1
7		MYJ					2
8		GBM					1
9		MYNN3					
10		ACM2					
11		MYNN2					
12		BouLac					
13		UW					10
14		TEMF					
15		MRF					
Microphysics schemes							
16	BMJ	MYNN2	WSM6	UNLS	Dudhia	RRTM	1
17			Kessler				
18			Lin (Purdue)				
19			WSM3				
20			WSM5				
21			Eta Ferrier				
22			Thompson				
23			Morrison2-mom				
24			CAM 5.1				

25			SBU-YL ln				
26			WDM5				
27			WDM6				
28			NSSL2-mom				
29			NSSL2-mom- CNN				
30			NSSL1-mom				
31			NSSL1-momlfo				
Land surface model							
32				UNLS			
33				TDS			
34	BMJ	MYNN2	WSM3	RUC	Dudhia	RRTM	1
35				NLS			
36				CLM4			
37				PXS			
Short wave radiation schemes							
38					Dudhia		
39					GSFC		
40					CAM		
41	BMJ	MYNN2	WSM3	UNLS	RRTMG	RRTM	1
42					New Goddard		
43					FLG		
Long wave radiation schemes							
44						RRTM	
45						RRTMG	
46	BMJ	MYNN2	WSM3	UNLS	FLG	New Goddard	1
47						FLG	
48						Held-Suarez	

Table 3.4: Experimental procedure for track prediction of second set.

Exp. No.	Cumulus	PBL	Microphysics	Surface Physics	SWR	LWR	sf_sfclay_physics
Microphysics schemes							
1	BMJ	MYNN2	WSM6	UNLS	Dudhia	RRTM	1
2			Kessler				
3			Lin (Purdue)				
4			WSM3				
5			WSM5				
6			Eta				
7			Thompson				
8			Morrison2-mom				
9			CAM 5.1				
10			SBU-YL ln				
11			WDM5				
12			WDM6				
13			NSSL2-mom				
14			NSSL2-mom-CNN				
15			NSSL1-mom				
16			NSSL1-momlfo				
Land surface model							
17	BMJ	MYNN2	WSM3	UNLS	Dudhia	RRTM	1
18				TDS			
19				RUC			
20				NLS			
21				CLM4			
22				PXS			

Short wave radiation schemes								
23	BMJ	MYNN2	WSM3	NLS		Dudhia	RRTM	1
24						GSFC		
25						CAM		
26						RRTMG		
27						New Goddard		
28						FLG		
Long wave radiation schemes								
29	BMJ	MYNN2	WSM3	NLS	FLG	RRTM	1	
30						CAM		
31						RRTMG		
32						New Goddard		
33						FLG		
34						Held-Suarez		

CHAPTER IV

Result and Discussion

4.0 Tropical Cyclone Mahasen

The model has simulated MSLP, maximum wind at 10m height and tracks have been studied and analyzed for the tropical cyclone Mahasen. Simulated track, wind speed and central sea level pressure have been compared with the IMD observed results. To get better result and comparing the performance of physical parameterization schemes it has been taken two sets. The results have been presented in the following sub sections.

4.1 Experiment with first set

Different experiments using Cumulus, PBL, MP, LSM, SWR and LWR have been discussed in below:

4.1.1 Cumulus parameterization

The Cumulus schemes bring out the effect of sub-grid scale convection on the grid-resolved thermodynamic variables. At first, five numerical experiments have been conducted with a combination of five cumulus parameterization schemes. Various cumulus physics options are KF, BMJ, GF, OSAS and Grell-3 schemes. The effect of cumulus physics on the simulations was studied. The other physics schemes are fixed as mentioned in Table 3.3.

4.1.1.1 Effect of Cumulus parameterization on track

The model simulated tracks from the five numerical experiments for different cumulus schemes with observed along with the Indian Meteorological Department (IMD) observation of TC Mahasen have been presented in figure 4.1.1.1(a). All tracks show North-Easterly movement of the cyclone.

Figure 4.1.1.1(b) has been shown the track error for all Cumulus compared with IMD observation data. Track errors at 24, 48, 72 hours are shown in figure 4.1.1.1(c) as a histogram plot and the as expected, for all the cases the track errors increase with forecast time and the RMS errors of track are obtained from 90 hr with 6 hr intervals those are 243,

212, 206, 287 and 267 km are obtained in the case of KF, BMJ, GF, OSAS and Grell-3 schemes respectively.

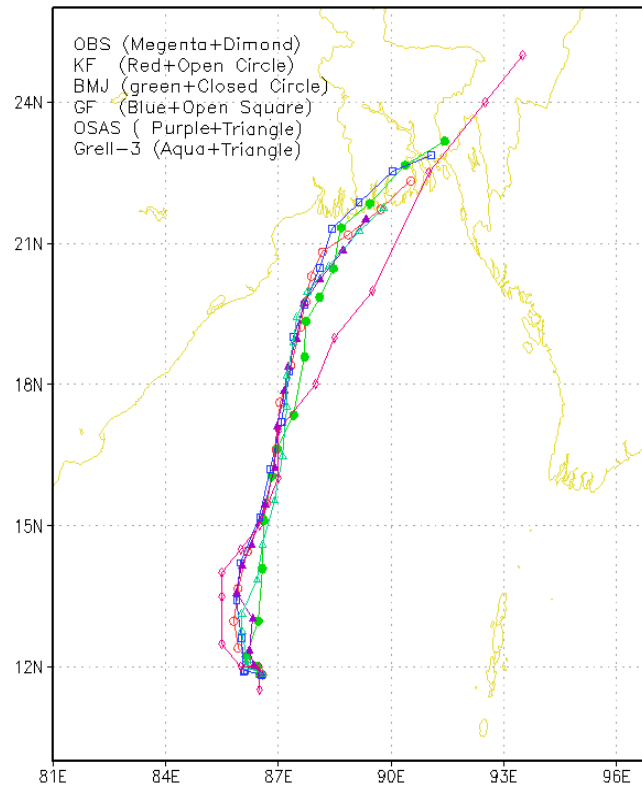


Figure 4.1.1.1(a): Model simulated track with IMD observed of TC Mahasen by using five different cumulus schemes.

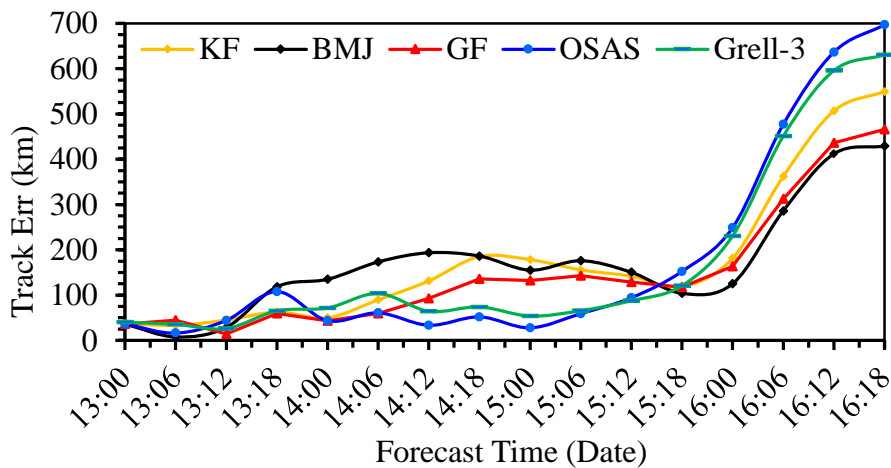


Figure 4.1.1.1(b): Model simulated track error of TC Mahasen by using five different cumulus schemes.

It has been observed from the above data that RMS track errors are obtained between 206 to 287 km and two cumulus schemes BMJ and GF give the less errors those are 212 and 206

km respectively whereas cumulus OSAS scheme gives the maximum track error 287 km with respect to IMD observation.

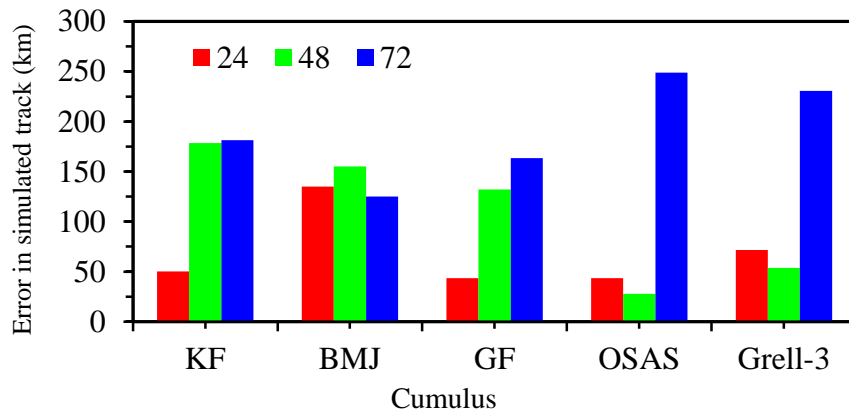


Figure 4.1.1.1(c) Model simulated track error in the 24, 48, and 72-hr forecasts with respect to IMD observed of TC Mahasen by using five different cumulus schemes.

Therefore, it may be concluded from the above discussion the combination of GF for the cumulus parameterizations gives least error 206 km with respect to IMD observation.

4.1.1.2 Effect of Cumulus parameterization on wind speed

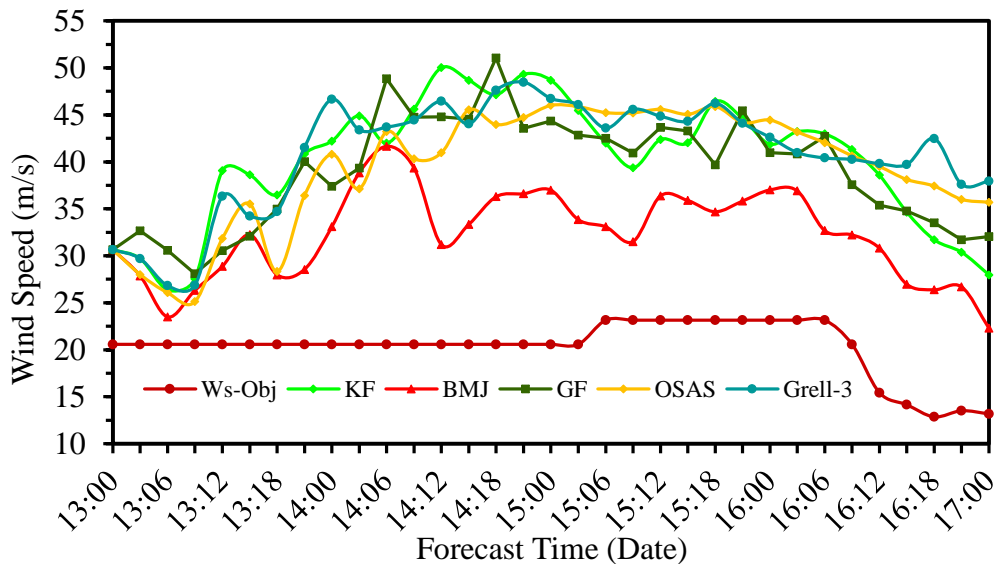


Figure 4.1.1.2(a): Model simulated wind speed with IMD observed of TC Mahasen by using five different cumulus schemes.

Figure 4.1.1.2(a) has been shown the wind speeds obtained from the five different simulations and the corresponding IMD wind data for every 6 hourly interval. From the

figure, it has been shown that initially all the simulations over-predict the wind speed with respect to IMD wind data.

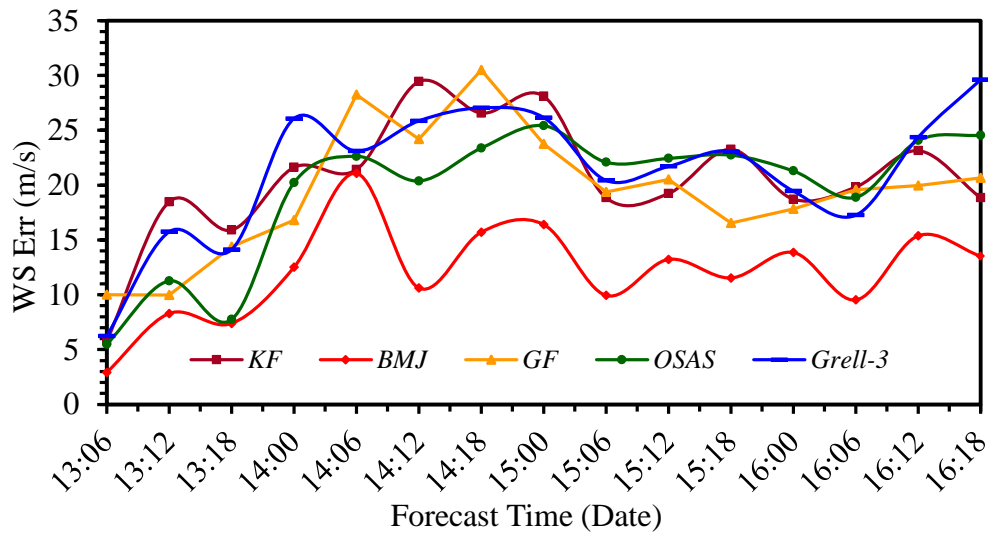


Figure 4.1.1.2(b): Model simulated wind speed error with respect to IMD observed of TC Mahasen by using five different cumulus schemes.

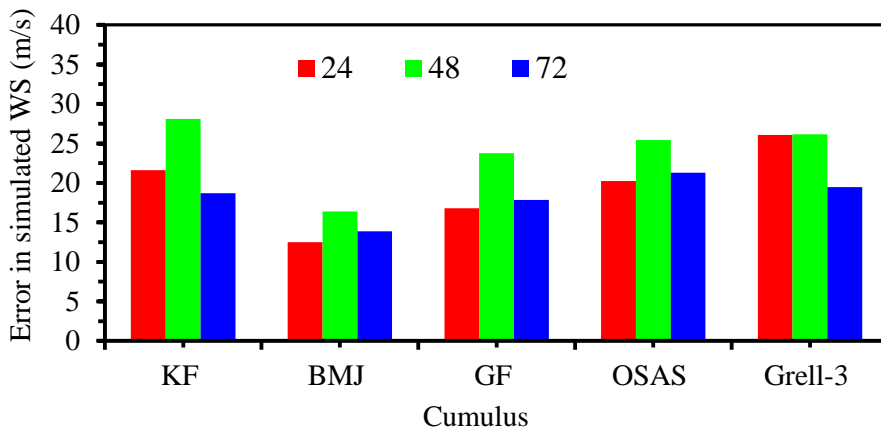


Figure 4.1.1.2(c): Model simulated wind speed error in the 24, 48, and 72-hr forecasts with respect to IMD observed of TC Mahasen by using five different cumulus schemes.

Figure 4.1.1.2(b) has been shown the wind speed error for all PBL compared with IMD observation data. Wind speed errors at 24, 48, 72 hours are shown in figure 4.1.1.2(c) as a histogram plot. This parameterizations also indicate that the model ‘produces’ a strong storm. All the cases produce a strong cyclone from the initial on 13 May from 00 UTC to 17 May 00 UTC. For all the cases the RMS errors of WS are obtained from 90 hr with 6 hourly intervals those are 21, 12, 19, 20 and 21 m/s in the case of KF, BMJ, GF, OSAS GRELL-3

schemes of Cumulus respectively. The IMD data is showing a maximum wind speed of 23 m/s at 06 UTC on 15 May to 06 UTC on 16 May 2013.

It has been observed from the above data that RMS maximum wind speed errors are obtained between 12 to 21 m/s and two cumulus schemes BMJ and GF give the less errors Those are 12 and 19 m/s respectively whereas cumulus GRELL-3 scheme gives the maximum wind speed error 21 m/s with respect to IMD observation. All the cases produce a strong cyclone. Therefore, it may be concluded from the above discussion the combination of BMJ for the cumulus parameterization gives least error 12 m/s with respect to IMD observation.

4.1.1.3 Effect of Cumulus parameterization on CSLP

The intensity of the cyclone from the point of CSLP is generally Over-predicted by all the schemes, as can be seen from the time series values which are too low for a category storm. The propagation of simulated cyclone CSLP for various combinations of cumulus schemes have been presented in figure 4.1.1.3(a). Figure 4.1.1.3(b) has been shown the CSLP error for all cumulus compared with IMD observation data. CSLP errors at 24, 48, 72 hours are shown in figure 4.1.1.3(c) as a histogram plot. This parameterizations also indicate that the model ‘produces’ a strong storms with CSLP in all cases at 00 UTC on 13 May to 00 UTC on 17 May, 2013.

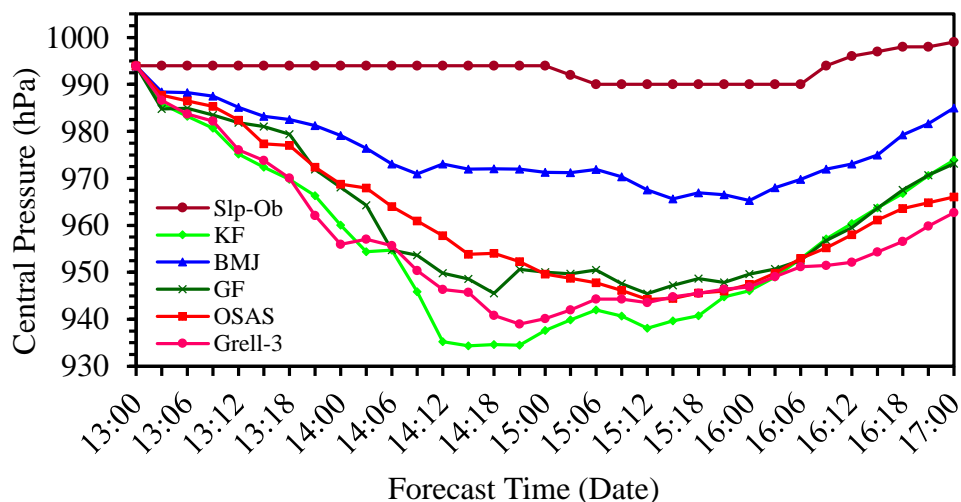


Figure 4.1.1.3(a): Model simulated CSLP with IMD observed of TC Mahasen by using five different cumulus schemes.

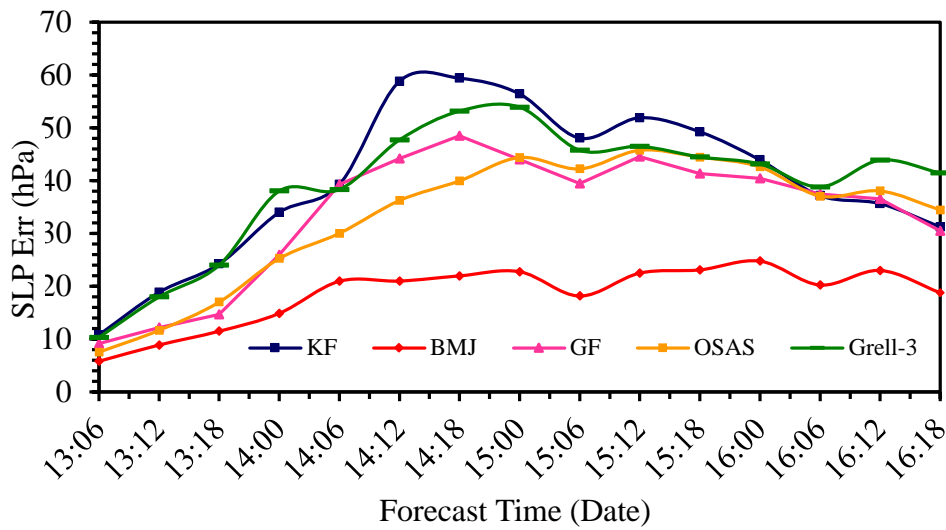


Figure 4.1.1.3(b): Model simulated CSLP error with respect to IMD observed of TC Mahasen by using five different cumulus schemes.

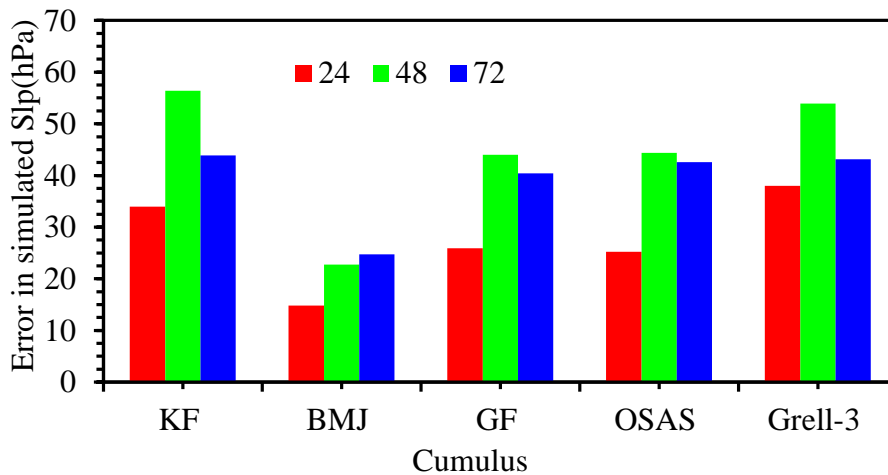


Figure 4.1.1.3(c): Model simulated CSLP error in the 24, 48, and 72-hr forecasts with respect to IMD observed of TC Mahasen by using five different cumulus schemes.

For all the cases the RMS errors of CSLP are obtained from 90 hr with 6 hourly intervals those are 40, 19, 34, 33 and 39 hPa for the case of the KF, BMJ, GF, OSAS Grell-3 schemes of Cu. It has been observed from the above data that RMS maximum CSLP errors are obtained between 19 to 40 hPa and two cumulus schemes BMJ and OSAS give the less errors those are 19 and 33 hPa respectively whereas cumulus KF scheme gives the maximum CSLP error 32 hPa with respect to IMD observation. All the cases produce a strong cyclone.

Therefore, it may be concluded from the above discussion the combination of BMJ for the cumulus Scheme gives least error 19 hPa with respect to IMD observation from the five numerical experiments.

From the five numerical experiments, it is clear that track propagation and RMS error among these five schemes have large variations, so the track prediction is indeed very sensitive to cumulus parameterization. There is few significant variation in the RMS error is 212 and 206 km between the BMJ and GF schemes and from the point of view of propagation of the track, GF scheme is good. However, it is instructive to mention here that the BMJ scheme over predicts the wind speed RMS as 12 m/s but GF scheme is 19 m/s with respect to the IMD wind speed data. On the another hand the BMJ scheme over predicts the CSLP RMS error is 19 hPa but GF scheme is 34 hPa with respect to the IMD CSLP data.

Finally from the RMS errors of track, wind and CSLP, the combination of BMJ for the cumulus Scheme gives least error with respect to IMD observation from the five numerical experiments.

4.1.2 Planetary boundary layer

The PBL is responsible for vertical sub-grid-scale fluxes due to eddy transports in the whole atmospheric column. While the surface layer schemes and land surface schemes provide the surface fluxes, the PBL schemes determine the flux profile within the well-mixed boundary layer and the stable layer. The PBL schemes provide the atmospheric ‘tendencies’ of temperature, moisture (including clouds) and horizontal momentum in the entire atmospheric column (Skamarock 2008). Nine numerical experiments have been conducted with a combination of nine PBL and five surface layer schemes. The best result from the cumulus scheme parameterization experiments namely the BMJ scheme and the other fixed physical parameterization schemes, as mentioned in table 3.3 are employed.

The ten PBL schemes are YSU, MYJ, GBM, MYNN3, ACM2, MYNN2, BouLac, UW, TEMF and MRF schemes.

4.1.2.1 Effect of PBL on Track

The propagation of simulated track for various combinations of PBL schemes and the surface layer scheme with observed of the cyclone have been presented in figure 4.1.2.1(a). All tracks show North-Easterly movement of the cyclone. Figure 4.1.2.1(b) has been shown the

track error for all PBL compared with IMD observation data. Track errors at 24, 48, 72 hours are shown in figure 4.1.2.1(c) as a histogram plot.

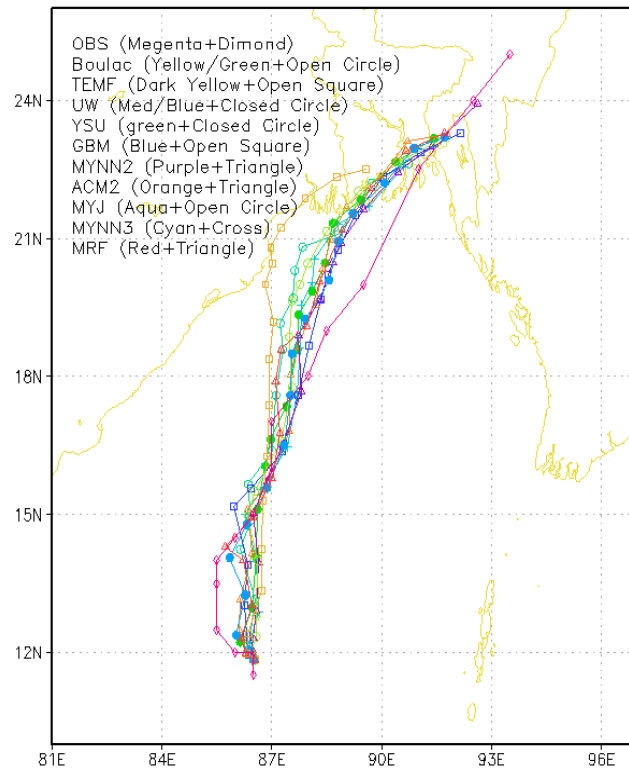


Figure 4.1.2.1(a): Model simulated track with IMD observed of TC Mahasen by using ten different PBL schemes.

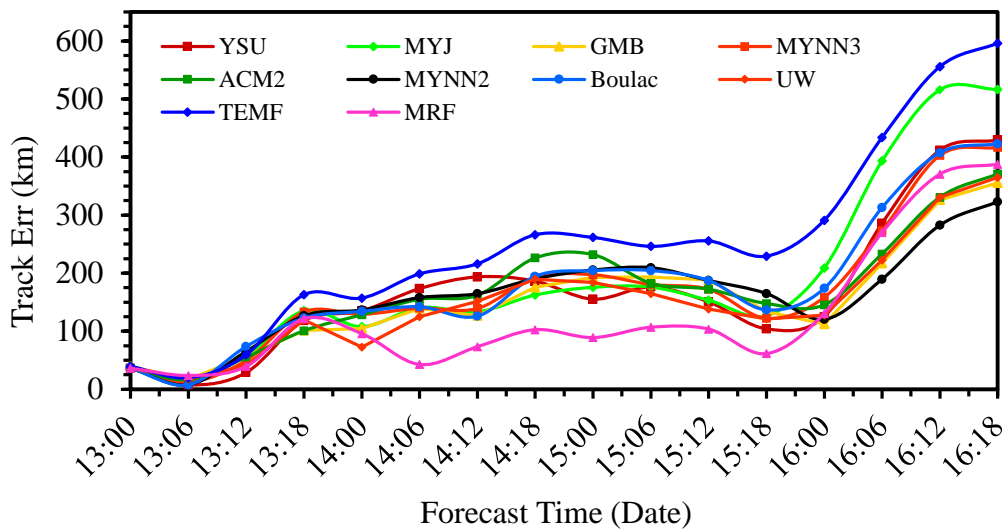


Figure 4.1.2.1(b): Model simulated track error with respect to IMD observed of TC Mahasen by using ten different PBL schemes.

As expected, for all the cases the track errors increase with forecast time and the RMS errors of track are obtained from 90 hr with 6 hr intervals those are 212, 249, 185, 210, 199, 184, 219, 182, 305 and 174 km are obtained in the case of YSU, MYJ, GMB, MYNN3, ACM2, MYNN2, Boulac, UW, TEMF and MRF PBL schemes respectively.

It has been observed from the above data that RMS track errors are obtained between 174 to 305 km and three PBL schemes MRF, UW and MYNN2 give the less errors those are 172, 182 and 184 km respectively where as PBL TEMF scheme gives the maximum track error 305km with respect to IMD observation.

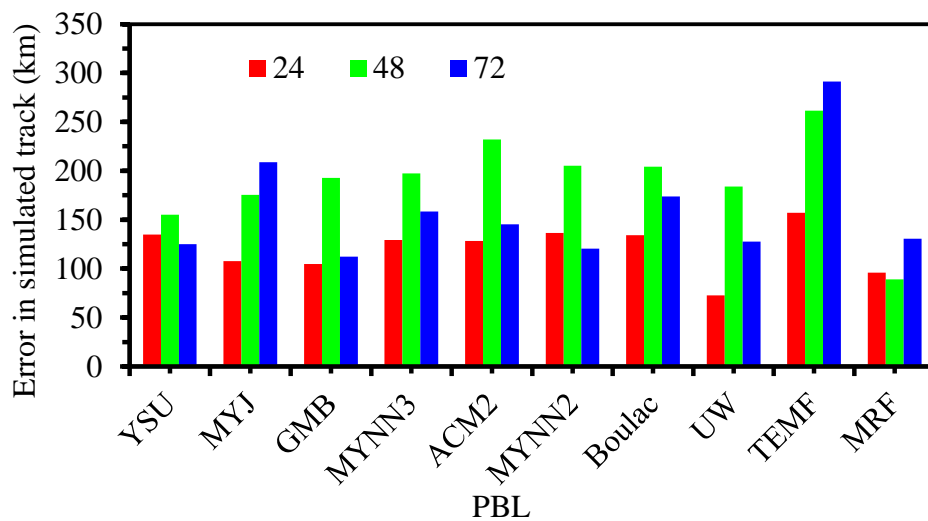


Figure 4.1.2.1(c): Model simulated track error in the 24, 48, and 72-hr forecasts with respect to IMD observed of TC Mahasen by using ten different PBL schemes.

Therefore, it may be concluded from the above discussion the combination of MRF for the PBL and MON Scheme for the surface layer parameterization gives least error 174 km with respect to IMD observation.

4.1.2.2 Effect of PBL on wind speed

The propagation of simulated wind speed and observed of the cyclone for various combinations of PBL schemes and the surface layer scheme have been presented in figure 4.1.2.2(a). Figure 4.1.2.2(b) has been shown the wind speed error for all PBL compared with IMD observation data. Wind speed errors at 24, 48, 72 hours are shown in figure 4.1.2.2(c). This parameterization also indicate that the model ‘produces’ a strong storm. All the cases produce a strong cyclone from the initial on 13 May from 00 UTC to 17 May 00 UTC.

For all the cases the RMS errors of WS are obtained from 90 hr with 6 hourly intervals those are 12.1, 10.9, 10.3, 10.7, 11.9, 10.1, 13.9, 12.6, 25.2 and 8.8 m/s in the case of the YSU, MYJ, GMB, MYNN3, ACM2, MYNN2, Boulac, UW, TEMF and MRF schemes of PBL respectively. The IMD data has been shown a maximum wind speed of 23 m/s at 06 UTC on 15 May to 06 UTC on 16 May 2013.

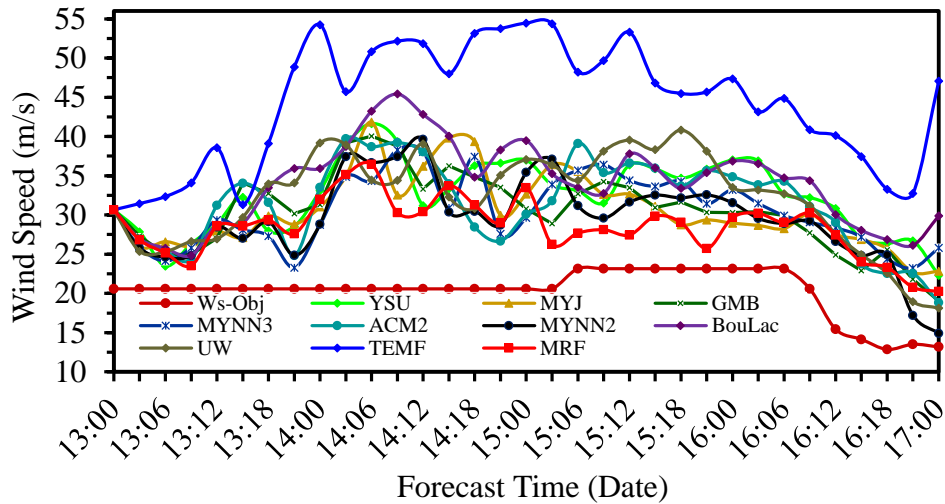


Figure 4.1.2.2(a): Model simulated wind speed with IMD observed of TC Mahasen by using ten different PBL schemes.

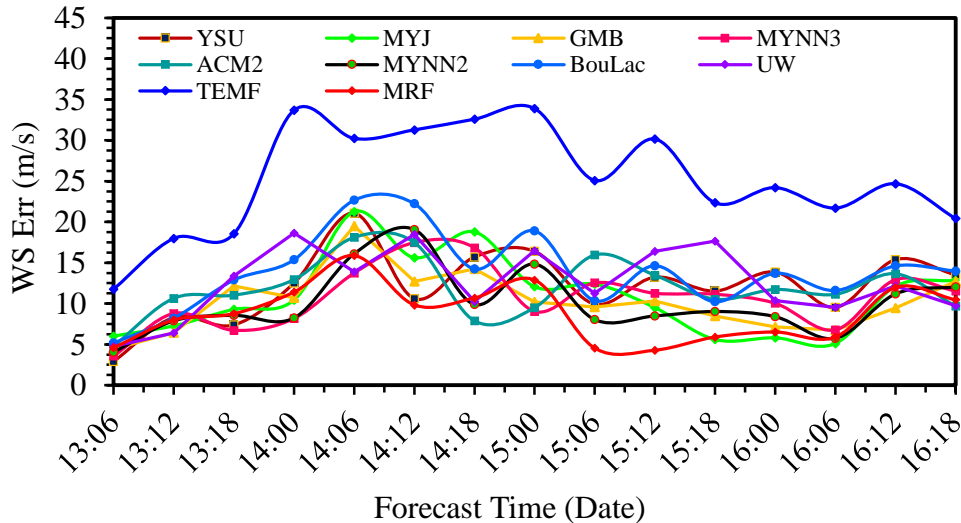


Figure 4.1.2.2(b): Model simulated wind speed error with respect to IMD observed of TC Mahasen by using ten different PBL schemes.

It has been observed from the above data that RMS maximum wind speed errors are obtained between 8.8 to 25.2 m/s and three PBL schemes MRF, MYNN2 and GMB give the less

errors those are 8.8, 10.1 and 10.3 m/s respectively where as PBL TEMF scheme gives the maximum wind speed error 25.2 m/s with respect to IMD observation. All the cases produce a strong cyclone.

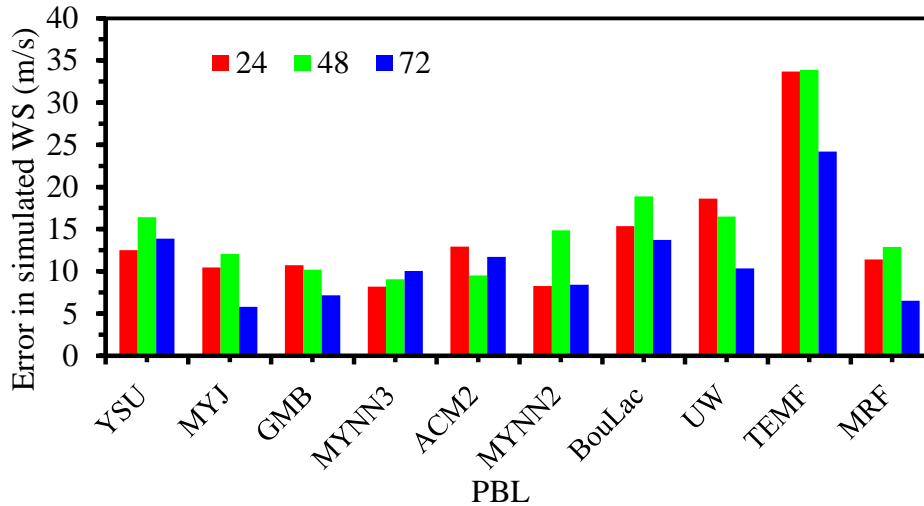


Figure 4.1.2.2(c): Model simulated wind speed error in the 24, 48, and 72-hr forecasts with respect to IMD observed of TC Mahasen by using ten different PBL schemes.

Therefore, it may be concluded from the above discussion the combination of MRF for the PBL and MON for the surface layer parameterization gives least error 8.8 m/s with respect to IMD observation.

4.1.2.3 Effect of PBL on CSLP

The propagation of simulated cyclone CSLP for various combinations of PBL scheme and the surface layer scheme have been presented in figure 4.1.2.3(a). Figure 4.1.2.3(b) has been shown the CSLP error for all PBL compared with IMD observation data. PBL errors at 24, 48, 72 hours are shown in figure 4.1.2.3(c). This parametrization also indicate that the model ‘produces’ a strong storm. All the cases produce a strong cyclone on 15 May from 06 UTC to 16 May 06 UTC.

For all the cases the RMS errors of CSLP are obtained from 90 hr with 6 hourly intervals those are 19, 15, 17, 18, 19, 16, 21, 20, 32 and 11 hPa in the case of YSU, MYJ, GMB, MYNN3, ACM2, MYNN2, Boulac, UW, TEMF and MRF schemes of PBL respectively.

It has been observed from the above data that RMS maximum CSLP errors are obtained between 11 to 32 hPa and three PBL schemes MRF, MYNN2 and MYJ give the less errors

those are 11, 16 and 15 hPa respectively where as PBL TEMF scheme gives the maximum CSLP error 32 hPa with respect to IMD observation. All the cases produce a strong cyclone.

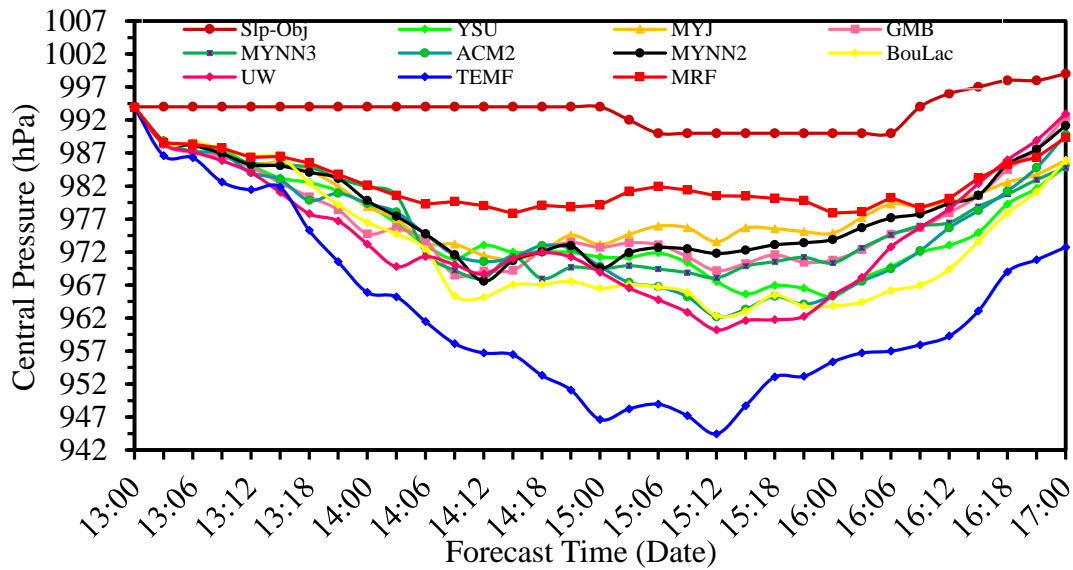


Figure 4.1.2.3(a): Model simulated CSLP with IMD observed of TC Mahasen by using ten different PBL schemes.

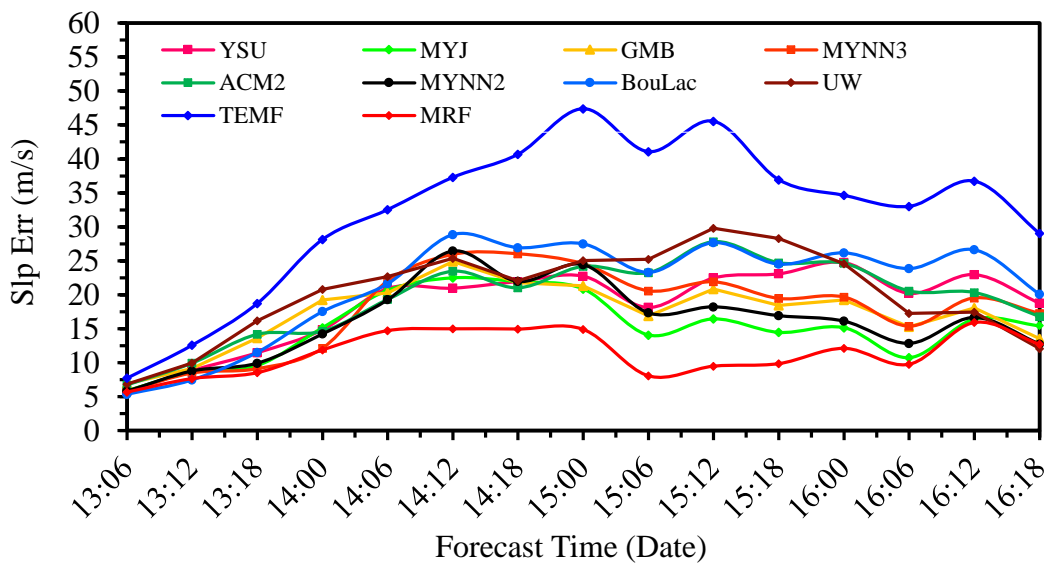


Figure 4.1.2.3(b): Model simulated CSLP error with respect to IMD observed of TC Mahasen by using ten different PBL schemes.

Therefore, it may be concluded from the above discussion the combination of MRF for the PBL and MON for the surface layer parameterization gives least error 11 hPa with respect to IMD observation from the ten numerical experiments.

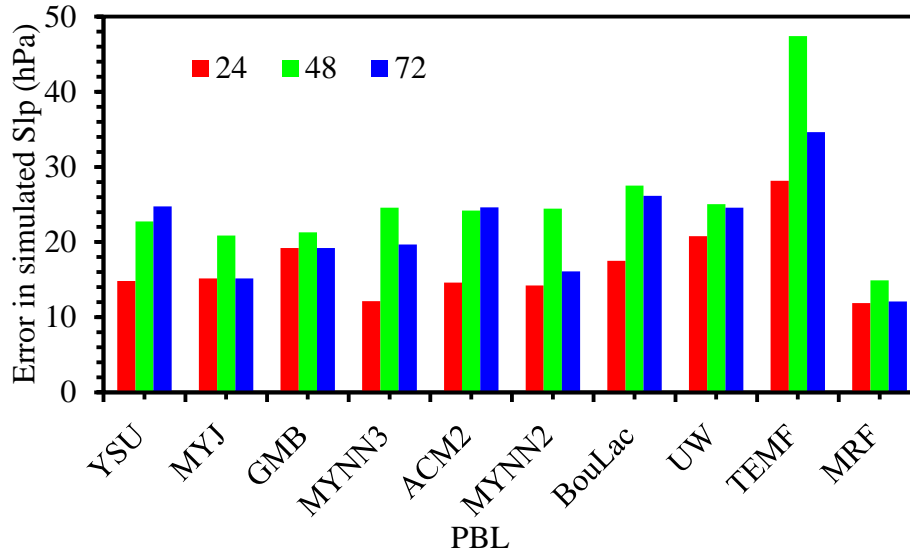


Figure 4.1.2.3(c): Model simulated CSLP error in the 24, 48, and 72-hr forecasts with respect to IMD observed of TC Mahasen by using ten different PBL schemes.

Finally from the RMS errors of track, wind and SLP, the combination of MRF for the PBL and MON for the surface layer parameterization gives least error with respect to IMD observation from the ten numerical experiments. So that MRF PBL has been taken for the next experiment.

4.1.3 Microphysics parameterization

The microphysics parameterizations explicitly handle water vapor, cloud and precipitation processes and also the microphysical processes of melting of snow, graupel and cloud ice hydrometeors, suppression of falling rain by evaporation. The MP parameterizations can also take into account the falling speed of snow and graupel hydrometeors. In this set of experiments, 16 different MP schemes have been considered along with the BMJ scheme for the cumulus parameterization and a combination of MRF for the PBL and MON for the surface layer parameterization. Various microphysics options are WSM6, KS, Lin Purdue, WSM3, WSM5, Eta, Thompson, Morrison, CAM5.1, SBU-YL, WDM5, WDM6, NSSL2, NSSL2-CCN), NSSL1 and NSSL1-lfo schemes. The other physics options are kept fixed, as shown in table 3.3.

4.1.3.1 Effect of Microphysics on track

The propagation of tracks are shown in figure 4.1.3.1(a). All tracks show North-Easterly movement of the cyclone. Figure 4.1.3.1(b) has been shown the track error for all

microphysics compared with IMD observation data. Track errors at 24, 48, 72 hours are shown in figure 4.1.3.1(c) as a histogram plot.

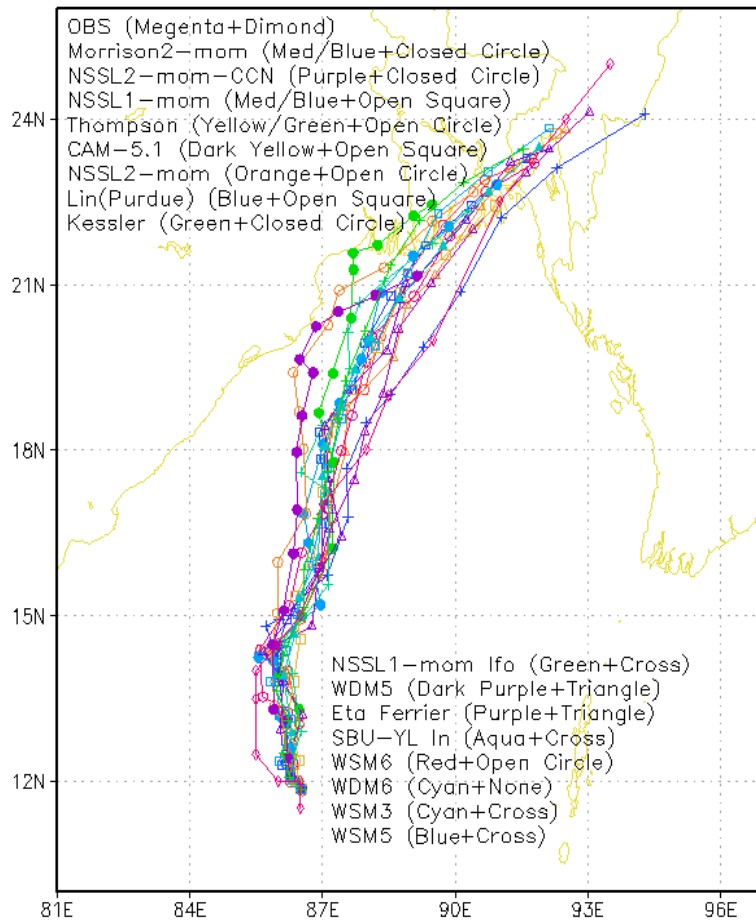


Figure 4.1.3.1(a): Model simulated track with IMD observed of TC Mahasen by using sixteen different MP schemes.

As expected, for all the cases the track errors increase with forecast time and the RMS errors of track are obtained from 90 hr with 6 hr intervals those are 174, 261, 200, 123, 148, 146, 178, 223, 193, 265, 163, 194, 259, 321, 171, and 192 km are obtained in the case of WSM6, Kessler, Lin Purdue, WSM3, WSM5, Eta Farrier, Thompson, Morrison2-mom, CAM5.1, SBU-YL In, WDM5, WDM6, NSSL2-mom, NSSL2-mom-CCN, NSSL1 and NSSL1-lfo schemes of MP respectively.

It has been observed from the above data that RMS track errors are obtained between 123 to 321 km and three microphysics schemes WSM3, WSM5 and Eta Farrier give the less errors those are 123, 1487 and 146 km respectively whereas microphysics NSSL2-mom-CCN scheme gives the maximum track error 321 km with respect to IMD observation.

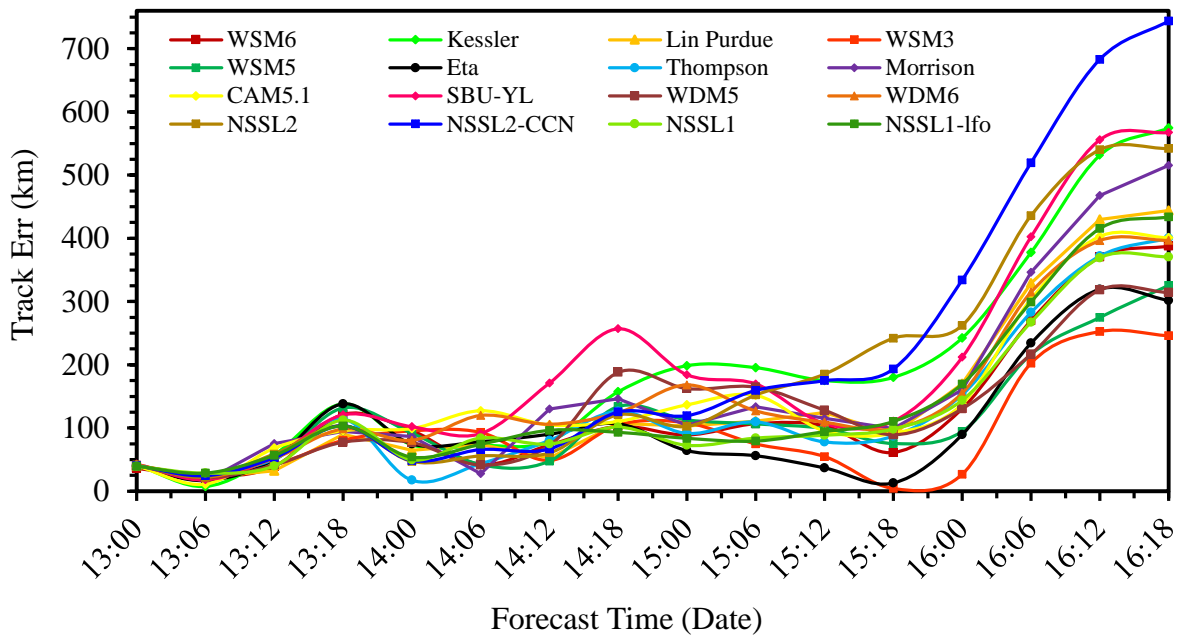


Figure 4.1.3.1(b): Model simulated track error with respect to IMD observed of TC Mahasen by using sixteen different MP schemes.

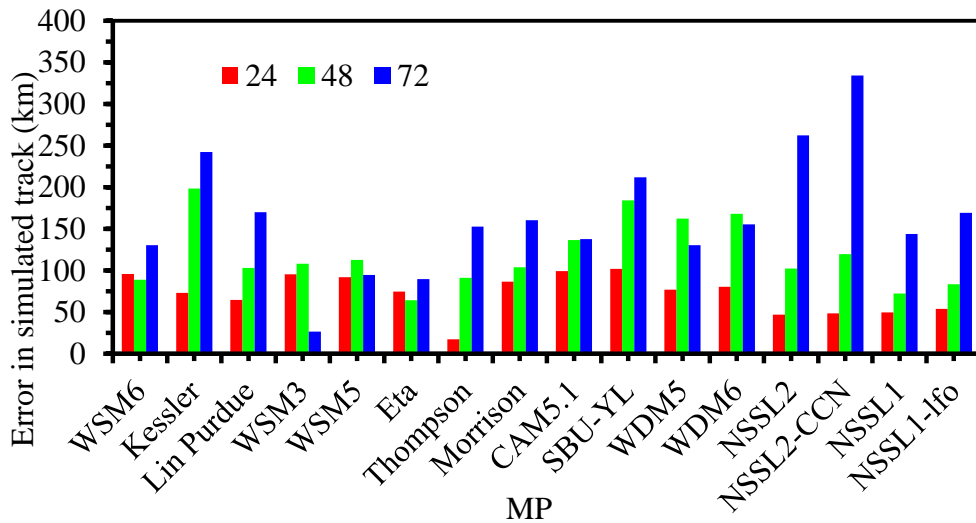


Figure 4.1.3.1(c): Model simulated track error in the 24, 48, and 72-hr forecasts with respect to IMD observed of TC Mahasen by using sixteen different MP schemes.

Therefore, it may be concluded from the above discussion the combination of WSM3 for the microphysics parameterization gives least error 123 km with respect to IMD observation.

4.1.3.2 Effect of Microphysics parameterization on wind speed

Figure 4.1.3.2(a) has been shown the wind speeds obtained from the sixteen different simulations and the corresponding IMD wind data for every 6 hourly interval. From the

figure, it has been shown that initially all the simulations over-predict the wind speed compared to IMD wind data. Figure 4.1.3.2(b) has been shown the wind speed error for all microphysics compared with IMD observation data. Wind speed errors at 24, 48, 72 hours are shown in figure 4.1.3.2(c) as a histogram plot. This parameterization also indicate that the model ‘produces’ a strong storm. All the cases produce a strong cyclone from the initial on 13 May from 00 UTC to 17 May 00 UTC.

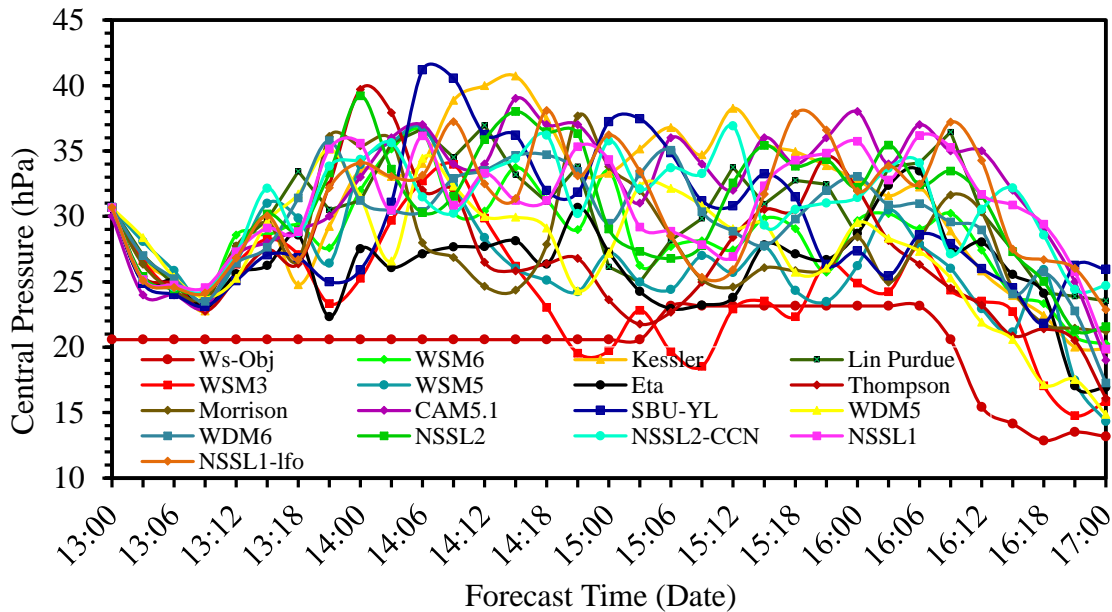


Figure 4.1.3.2(a): Model simulated wind speed with IMD observed of TC Mahasen by using sixteen different MP schemes.

For all the cases the RMS errors of WS are obtained from 90 hr with 6 hourly intervals those are 8.8, 11.3, 10.1, 4.6, 6.8, 6.3, 6.8, 7.2, 12.5, 9.4, 7.3, 9.4, 10.5, 11.2, 11.1 and 10.7 m/s in the case of WSM6, Kessler, Lin (Purdue), WSM3, WSM5, Eta, Thompson, Morrison2-mom, CAM 5.1, SBU-YL In, WDM5, WDM6, NSSL2-mom, NSSL2-mom-CNN, NSSL1-mom NSSL1-momlfo schemes of MP respectively. The IMD data is showing a maximum wind speed of 23 m/s at 06 UTC on 15 May to 06 UTC on 16 May 2013.

It has been observed from the above data that RMS maximum wind speed errors are obtained between 4.6 to 12.5 m/s and three microphysics schemes WSM3, Eta Farrier and Thompson scheme for the microphysics parameterization combined with the MON with the surface layer parameterization give the less errors those are 4.6, 6.3 and 6.8 m/s respectively whereas microphysics CAM 5.1 scheme gives the Maximum wind speed error 12.5 m/s with respect to IMD observation. All the cases produce a strong cyclone.

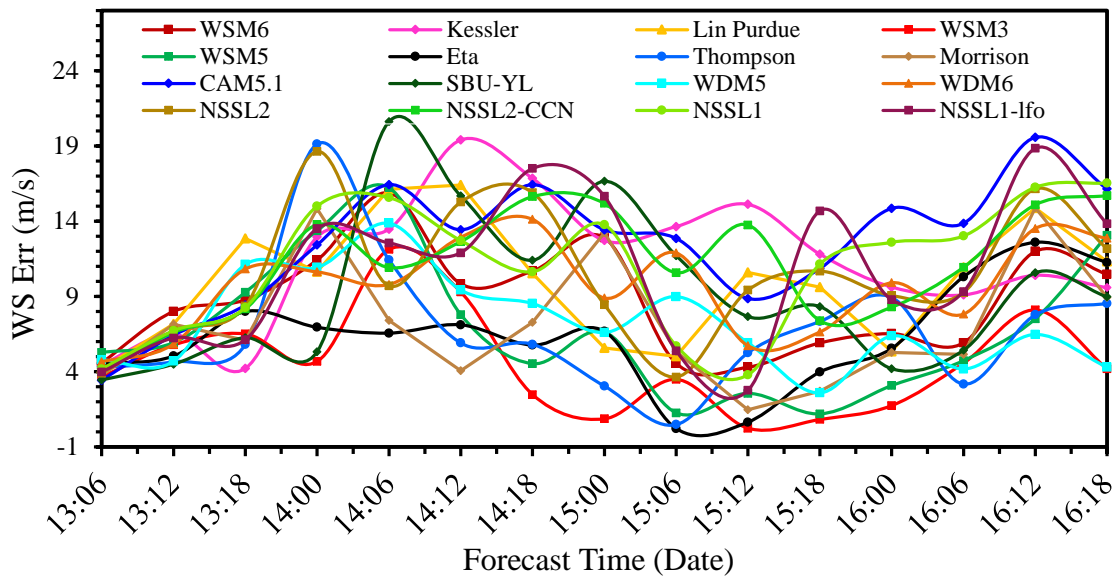


Figure 4.1.3.2(b): Model simulated wind speed error with respect to IMD observed of TC Mahasen by using sixteen different MP schemes.

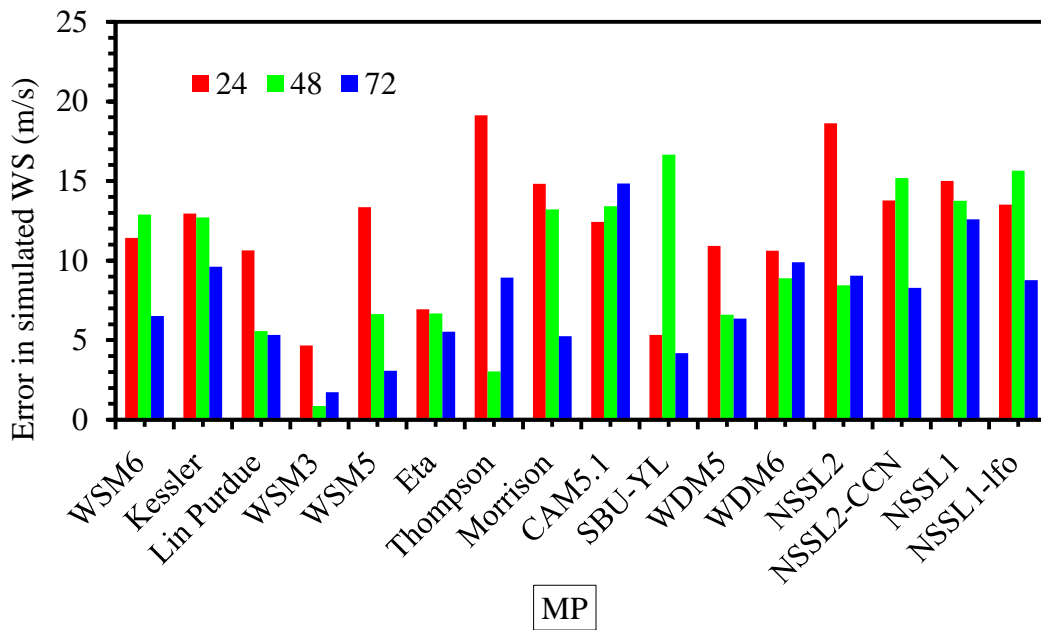


Figure 4.1.3.2(c): Model simulated wind speed error in the 24, 48, and 72-hr forecasts with respect to IMD observed of TC Mahasen by using sixteen different MP schemes.

Therefore, it may be concluded from the above discussion the combination of WSM3 for the microphysics scheme gives least error 4.6 m/s with respect to IMD observation.

4.1.3.3 Effect of Microphysics Parameterization on CSLP

The intensity of the cyclone from the point of CSLP is generally over-predicted by all the schemes, as can be seen from the time series values which are too low for a category storm. The propagation of simulated cyclone CSLP for various combinations of microphysics schemes have been presented in figure 4.1.3.3(a). Figure 4.1.3.3(b) has been shown the CSLP error for all microphysics schemes compared with IMD observation data. CSLP errors at 24, 48, 72 hours are shown in figure 4.1.3.3(c) as a histogram plot. This parameterization also indicate that the model ‘produces’ a strong storm. All the cases produce a strong cyclone from the initial on 13 May from 00 UTC to 17 May 00 UTC. For all the cases the RMS errors of CSLP are obtained from 90 hr with 6 hourly intervals those are 11.4, 20.9, 13.4, 6.6, 8.9, 9.6, 8.5, 10.3, 19.3, 17.0, 8.8, 11.5, 14.9, 14.8, 17.1 and 17.4 hPa for WSM6, Kessler, Purdue, WSM3, WSM5, Eta, Thompson, Morrison2-mom, CAM 5.1, SBU-YL In , WDM5, WDM6, NSSL2-mom, NSSL2-mom-CNN, NSSL1-mom and NSSL1-momlfo schemes respectively.

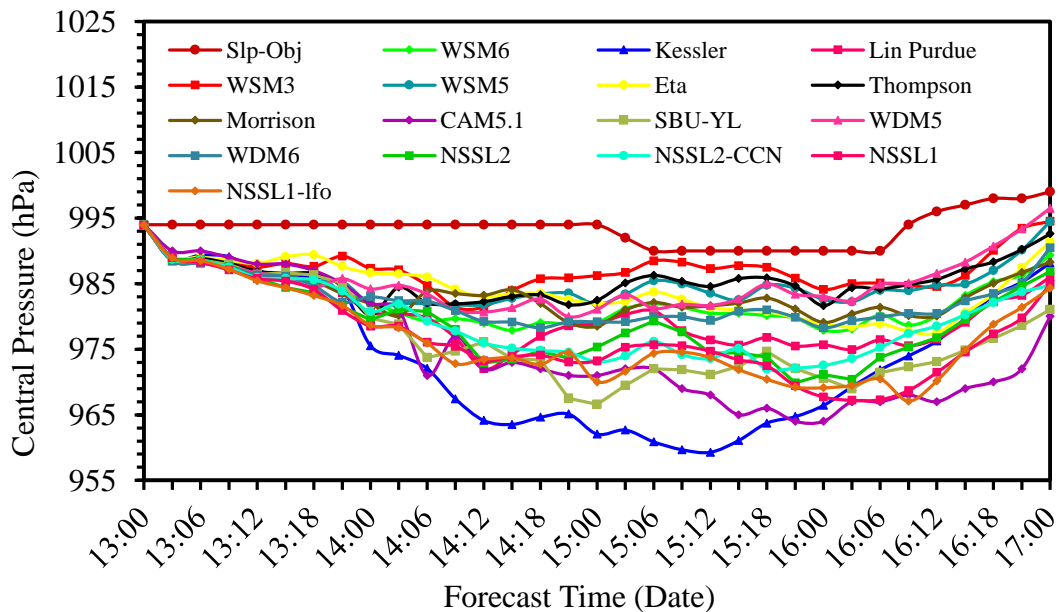


Figure 4.1.3.3(a): Model simulated CSLP with IMD observed of TC Mahasen by using sixteen different MP schemes.

It has been observed from the above data that RMS maximum CSLP errors are obtained between 6.6 to 20.9 hPa and three microphysics schemes WSM3, Thompson and WDM5 give the less errors those are 6.6, 8.5 and 8.8 hPa respectively whereas microphysics Kessler

scheme gives the maximum CSLP error 20.9 hPa with respect to IMD observation. All the cases produce a strong cyclone.

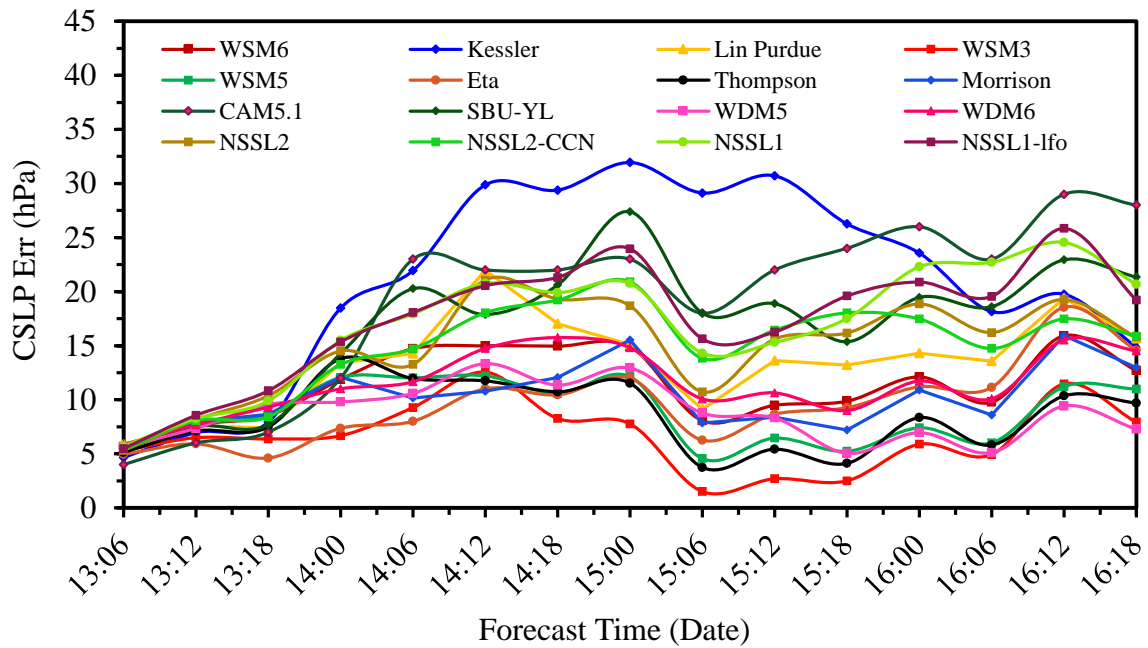


Figure 4.1.3.3(b): Model simulated CSLP error with respect to IMD observed of TC Mahasen by using sixteen different MP schemes.

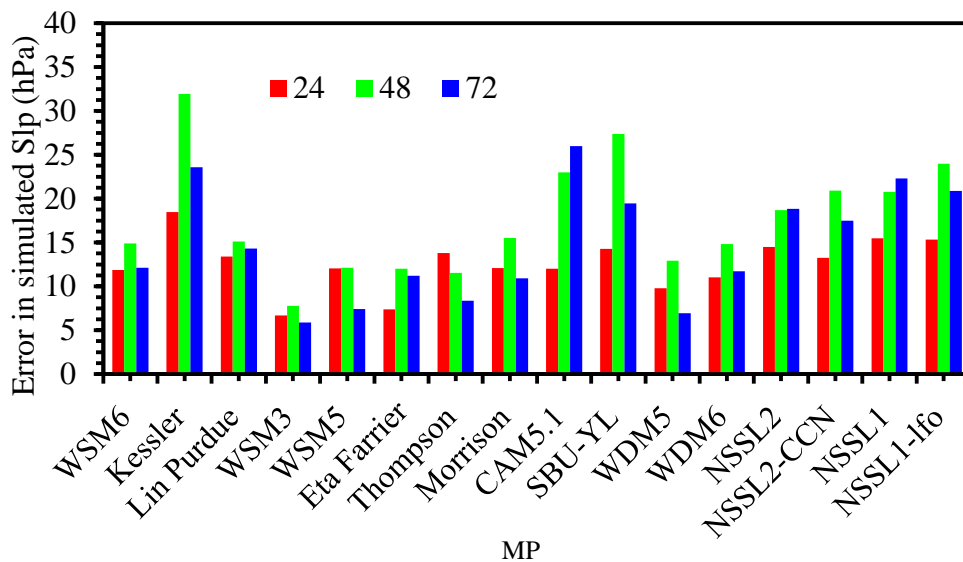


Figure 4.1.3.3(c): Model simulated CSLP error in the 24, 48, and 72-hr forecasts with respect to IMD observed of TC Mahasen by using sixteen different MP schemes.

Therefore, it may be concluded from the above discussion the combination of WSM3 for the microphysics Scheme gives least error 6.6 hPa with respect to IMD observation from the sixteen numerical experiments.

Finally from the RMS errors of track, wind and SLP, the combination of WSM3 for the microphysics parameterization gives least error with respect to IMD observation from the sixteen numerical experiments. So WSM3 scheme has been chosen the best scheme for the next experiment.

4.1.4 Land surface model (LSM)

The land-surface models (LSMs) are responsible for the thermal and moisture fluxes in multiple layers of the soil and also vegetation, root, canopy effects and surface snow-cover. These models use atmospheric information from the surface layer scheme, radiative forcing from the radiation scheme, and precipitation forcing from the microphysics and convective schemes. Along with above schemes, the LSMs provide heat fluxes and moisture over the land points and sea-ice points and also give the lower boundary condition fluxes to the PBL schemes (Skamarock 2008). In this study, numerical experiments were conducted with six different land surface models along with the best schemes from previous experiments. These six models distinguish land soil inherently. In this set of experiments, six different land-surface model schemes have been considered along with the BMJ scheme for the cumulus, a combination of MRF for the PBL and MON for the surface layer parameterization and WSM3 for the microphysics parameterization. Various land-surface models options are UNLS, TDS, RUC, NLS, CLM4.0 and PXS schemes. The other physics options are kept fixed, as shown in table 3.3.

4.1.4.1 Effect of land surface model on track

The propagation of tracks are shown in figure 4.1.4.1(a). All tracks show North-Easterly movement of the cyclone. Figure 4.1.4.1(b) has been shown the track error for all the land-surface models compared with IMD observation data. Track errors at 24, 48, 72 hours are shown in figure 4.1.4.1(c) as a histogram plot. As expected, for all the cases the track errors increase with forecast time and the RMS errors of track are obtained from 90 hr with 6 hr intervals those are 123, 125, 138, 135, 142 and 176 km are obtained in the case of UNLS, TDS, RUC, NLS, CLM4 and PXS schemes respectively. All tracks show North-Easterly movement of the cyclone.

It has been observed from the above data that RMS track errors are obtained between 123 to 176 km and three land surface model schemes UNLS, TDS and NLS give the less errors

those are 123, 125 and 135 km respectively whereas land surface model PXS scheme gives the maximum track error 176 km with respect to IMD observation.

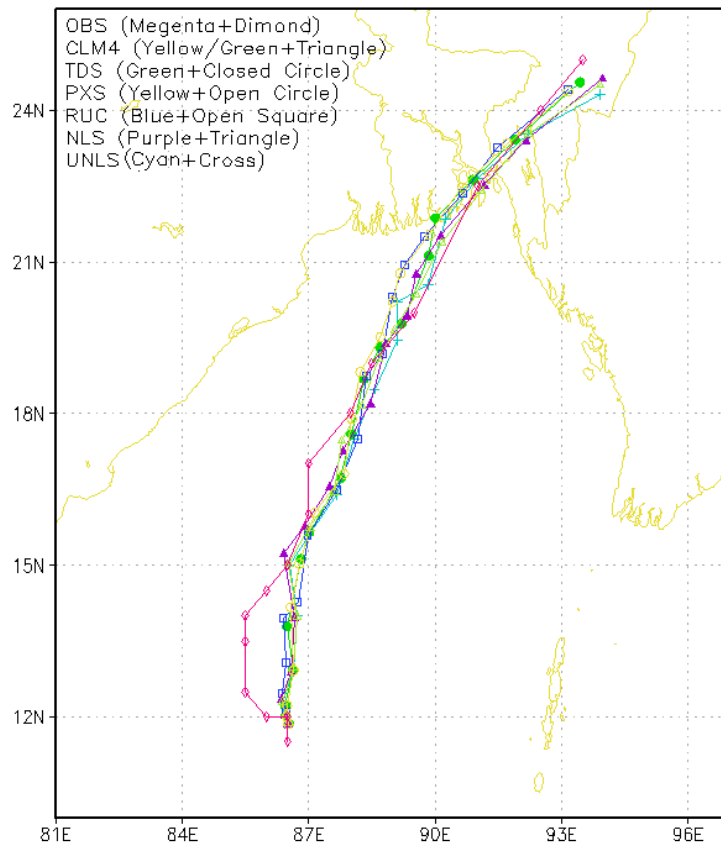


Figure 4.1.4.1(a): Model simulated track with IMD observed of TC Mahasen by using six different LSM schemes.

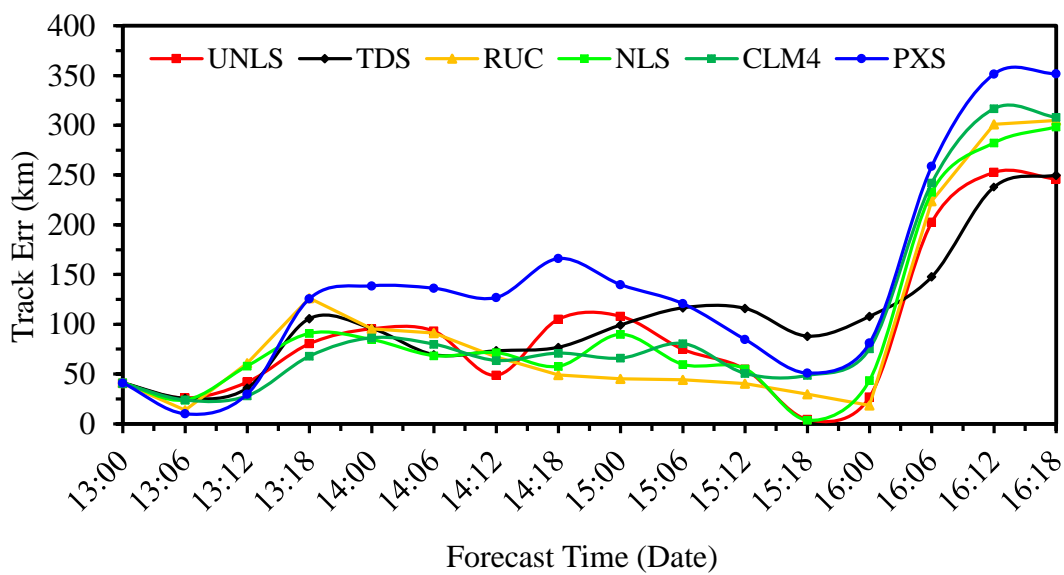


Figure 4.1.4.1(b): Model simulated track error with respect to IMD observed of TC Mahasen by using six different LSM schemes.

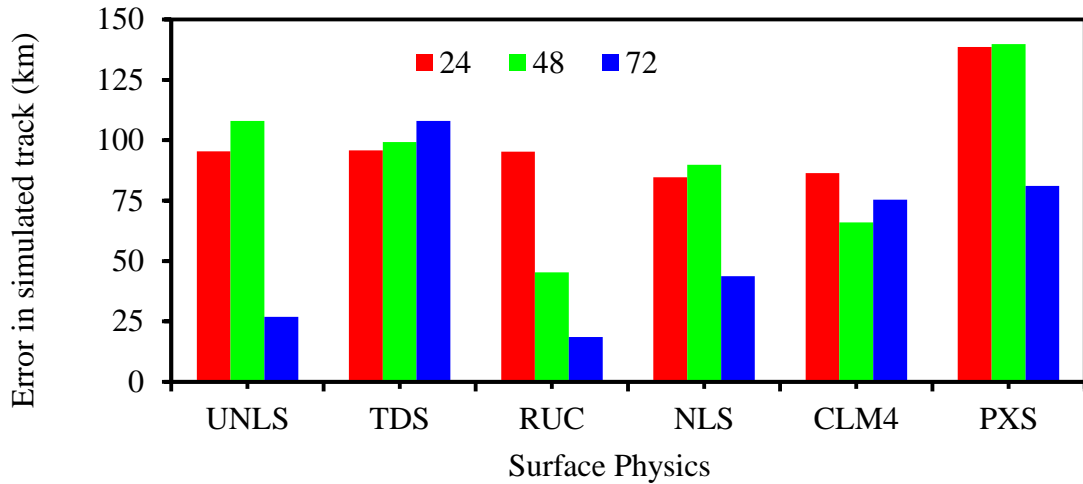


Figure 4.1.4.1(c): Model simulated track error in the 24, 48, and 72-hr forecasts with respect to IMD observed of TC Mahasen by using six different LSM schemes.

Therefore, it may be concluded from the above discussion the combination of UNLS for the land surface model schemes gives least error 123 km with respect to IMD observation.

4.1.4.2 Effect of land surface model on wind speed

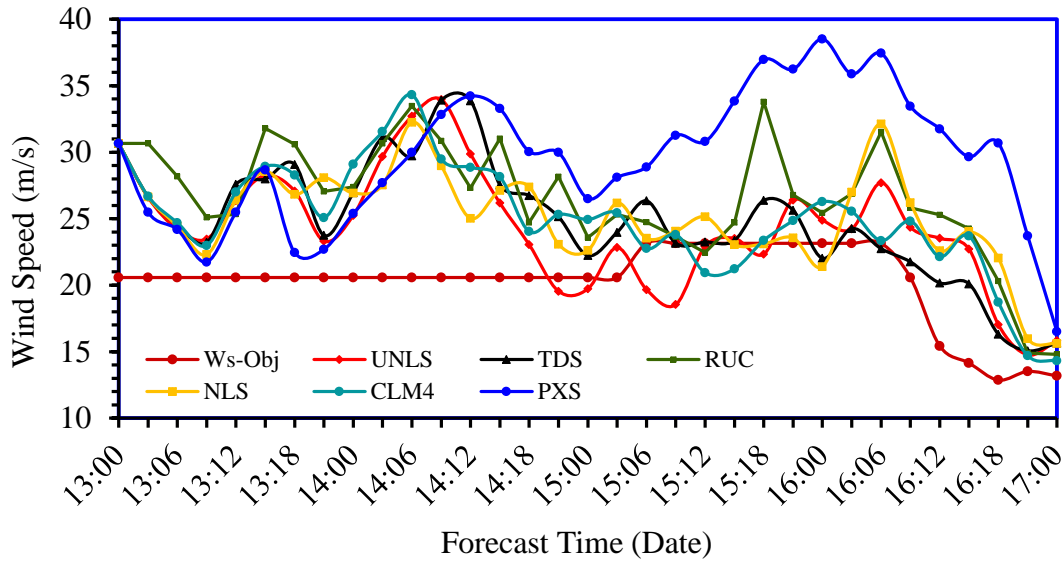


Figure 4.1.4.2(a): Model simulated wind speed with IMD observed of TC Mahasen by using six different LSM schemes.

Figure 4.1.4.2(a) has been shown the wind speeds obtained from the six different simulations and the corresponding IMD wind data for every 6 hourly interval. From the figure, it has been shown that initially all the simulations over-predict the wind speed compared to IMD wind data. Figure 4.1.4.2(b) has been shown the wind speed error for all LSM compared

with IMD observation data. Wind speed errors at 24, 48, 72 hours are shown in figure 4.1.4.2(c) as a histogram plot. This parameterization also indicate that the model ‘produces’ a strong storm. All the cases produce a strong cyclone from the initial on 13 May from 00 UTC to 17 May 00 UTC.

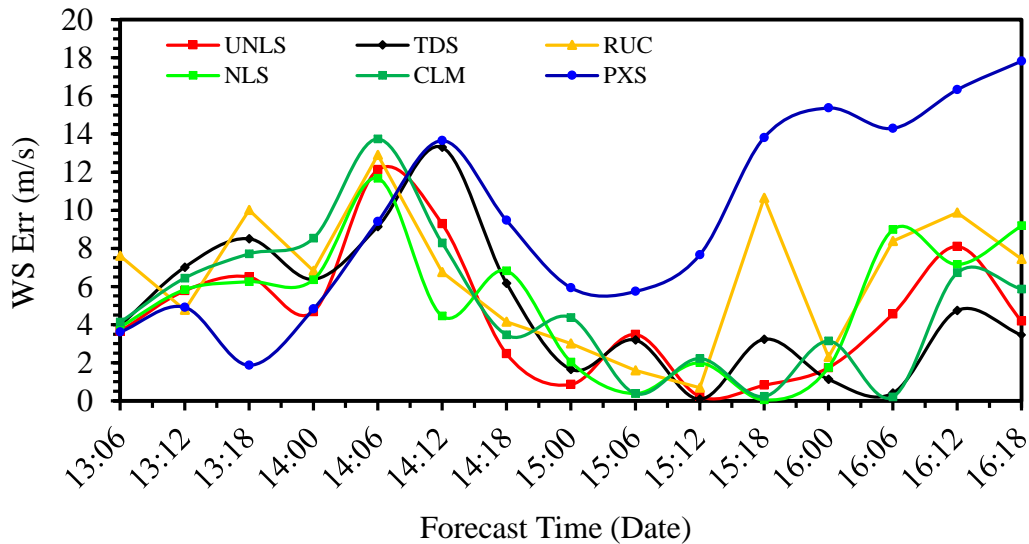


Figure 4.1.4.2(b): Model simulated wind speed error with respect to IMD observed of TC Mahasen by using six different LSM schemes.

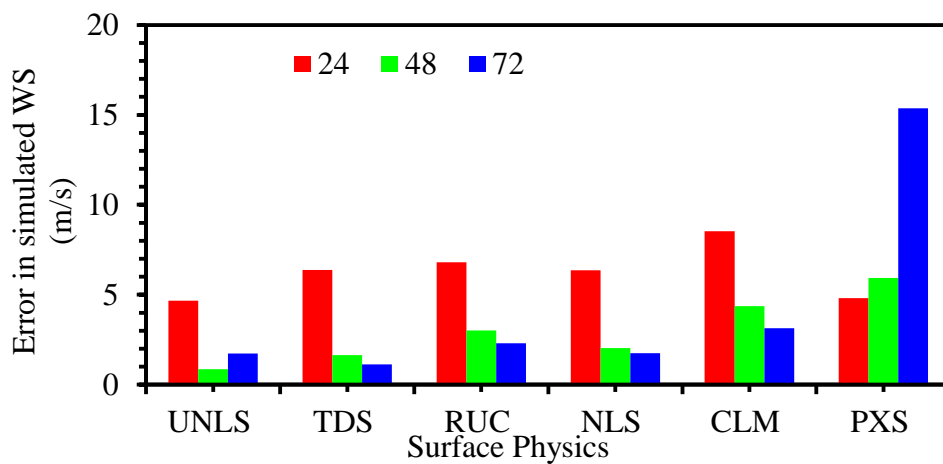


Figure 4.1.4.2(c): Model simulated wind speed error in the 24, 48, and 72-hr forecasts with respect to IMD observed of TC Mahasen by using six different LSM schemes.

For all the cases the RMS errors of WS are obtained from 90 hr with 6 hourly intervals those are 4.6, 4.8, 6.5, 5.1, 5.0 and 9.6 m/s in the case of the UNLS, TDS, RUC, NLS, CLM4 and PXS schemes of LSM respectively. The IMD data is showing a maximum wind speed of 23 m/s at 06 UTC on 15 May to 06 UTC on 16 May 2013.

It has been observed from the above data that RMS maximum wind speed errors are obtained between 4.6 to 9.6 m/s and three land surface model schemes UNLS, TDS and CLM4 give the less error those are 4.6, 4.8 and 5.0 m/s respectively whereas land surface model PXS scheme gives the maximum wind speed error 9.6 m/s with respect to IMD observation. All the cases produce a strong cyclone.

Therefore, it may be concluded from the above discussion the combination of UNLS for the land surface model gives least error 4.6 m/s with respect to IMD observation.

4.1.4.3 Effect of land surface model on CSLP

The intensity of the cyclone from the point of CSLP is generally over-predicted by all the schemes, as can be seen from the time series values which are too low for a category storm.

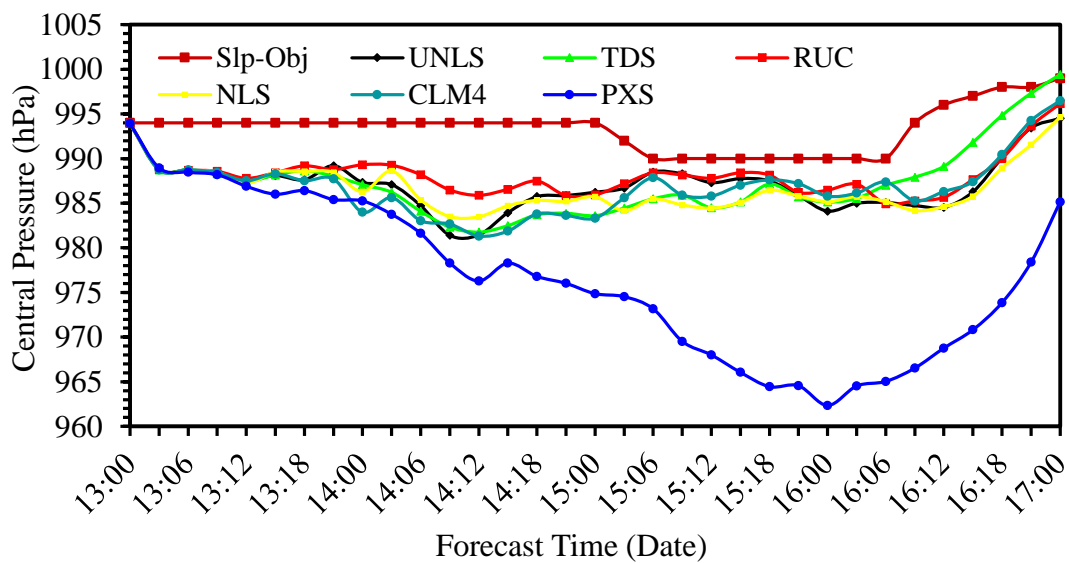


Figure 4.1.4.3(a): Model simulated CSLP with IMD observed of TC Mahasen by using six different LSM schemes.

The propagation of simulated cyclone CSLP for various combinations of land surface model have been presented in figure 4.1.4.3(a). Figure 4.1.4.3(b) has been shown the CSLP error for all LSM schemes compared with IMD observation data. CSLP errors at 24, 48, 72 hours are shown in figure 4.1.4.3(c) as a histogram plot. This parameterization also indicate that the model ‘produces’ a strong storm. All the cases produce a strong cyclone from the initial on 13 May from 00 UTC to 17 May 00 UTC. For all the cases the RMS errors of CSLP are

obtained from 90 hr with 6 hourly intervals those are 6.6, 6.5, 5.5, 7.0, 7.0 and 17.6 hPa in the case of PXS, UNLS, TDS, RUC, NLS and CLM4 schemes of LSM respectively.

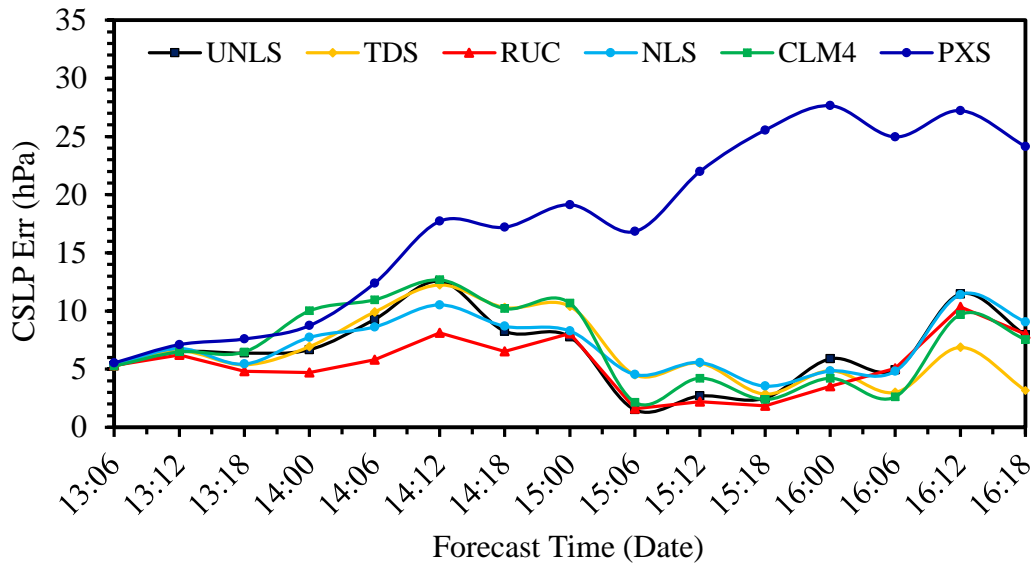


Figure 4.1.4.3(b): Model simulated CSLP error with respect to IMD observed of TC Mahasen by using six different LSM schemes.

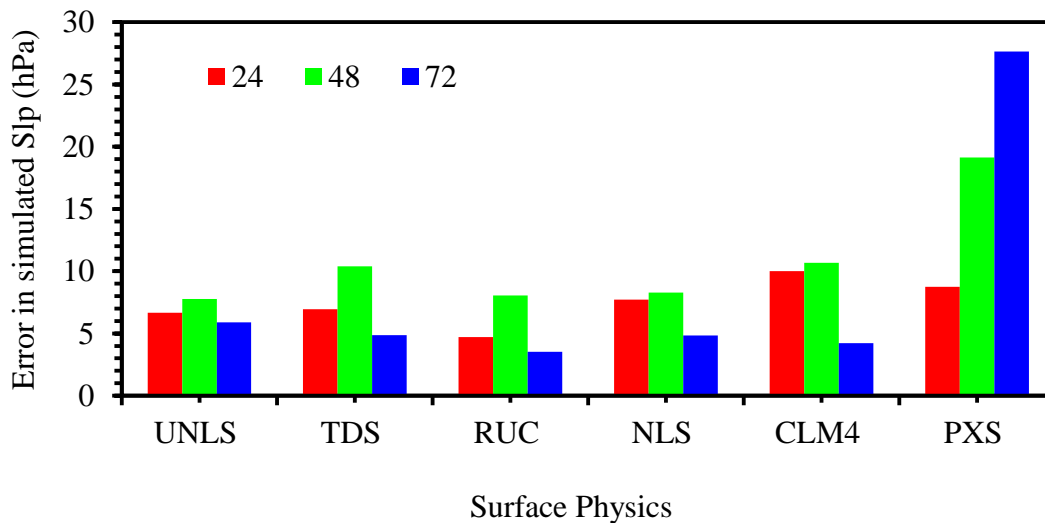


Figure 4.1.4.3(c): Model simulated CSLP error in the 24, 48, and 72-hr forecasts with respect to IMD observed of TC Mahasen by using six different LSM schemes.

It has been observed from the above data that RMS maximum CSLP errors are obtained between 6.6 to 17.6 hPa and three land surface model UNLS, TDS and RUC give the less errors those are 6.6, 6.5 and 5.5 hPa respectively whereas land surface model PXS scheme gives the maximum CSLP error 17.6 hPa with respect to IMD observation. All the cases produce a strong cyclone.

Therefore, it may be concluded from the above discussion the combination of RUC for the land surface model gives least error 5.5 hPa with respect to IMD observation from the six numerical experiments.

From the six numerical experiments, it is clear that track propagation and RMS error among these six schemes have small variations, so the track prediction is indeed very sensitive to land surface model. There is few significant variation in the RMS error is 123 and 125 km between the UNLS and TDS schemes and from the point of view propagation of the track, UNLS scheme is good. However, it is instructive to mention here that the UNLS scheme over predicts the wind speed RMS as 4.6 m/s but TDS scheme is 4.8 m/s with respect to the IMD wind speed data. On the another hand the RUC scheme over predicts the CSLP RMS error is 5.5 hPa but TDS scheme is 6.5 and UNLS scheme is 6.6 hPa with respect to the IMD CSLP data. They have small variation of those error.

Finally it is strongly recommending that considering from the RMS errors of track, wind and CSLP, the combination of UNLS for the land surface model gives least error with respect to IMD observation data from the six numerical experiments. So UNLS scheme has been chosen the best scheme for the next experiment.

4.1.5 Short wave radiation schemes

The radiation schemes in the model provide the atmospheric heating due to radiation flux from the Sun and the short wave radiation schemes handle the process of absorption, reflection and scattering in the atmosphere and from the surface. In this study, numerical experiments were conducted with six different short wave radiation schemes. In this set of experiments, six different short wave radiation schemes have been considered along with the BMJ scheme for the cumulus, a combination of MRF for the PBL and MON for the surface layer parameterization, WSM3 for the microphysics scheme and UNLS for the land surface model. Various short wave radiation schemes options are Dudhia, GSFC (ARW+Chem(τ)), CAM, RRTMG, New Goddard and FLG schemes. The other physics options are kept fixed, as shown in table 3.3.

4.1.5.1 Effect of the short wave radiation on track

The propagation of tracks and observed with respect to IMD are shown in figure 4.1.5.1(a). Figure 4.1.5.1(b) has been shown the track error for all the short wave radiation schemes

compared with IMD observation data. Track errors at 24, 48, 72 hours are shown in figure 4.1.5.1(c) as a histogram plot.

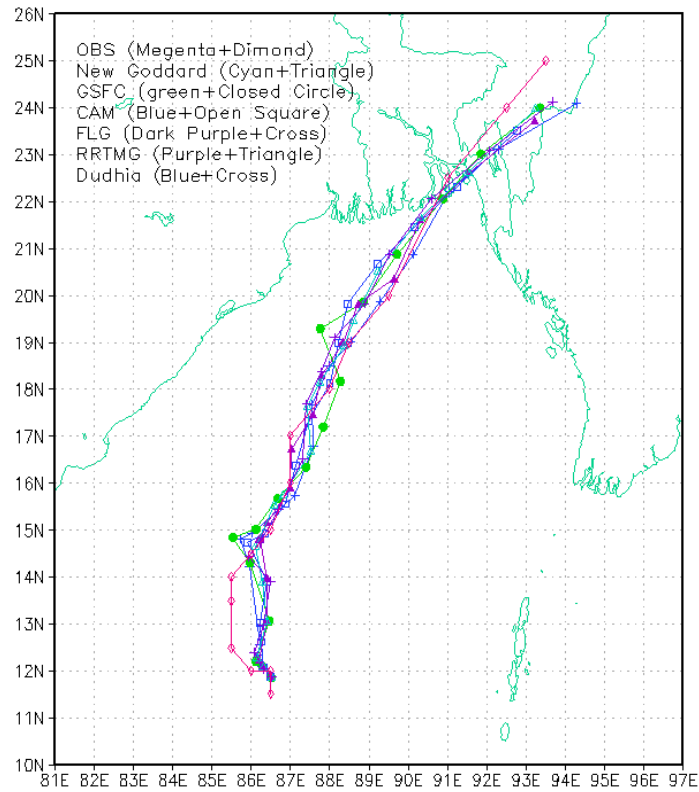


Figure 4.1.5.1(a): Model simulated track with IMD observed of TC Mahasen by using six different SWR schemes.

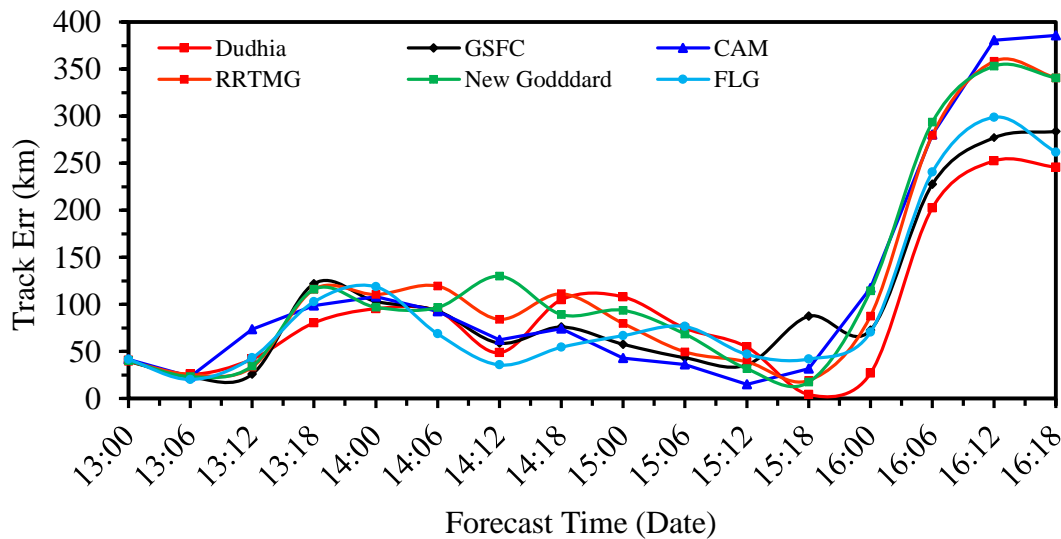


Figure 4.1.5.1(b): Model simulated track error with respect to IMD observed of TC Mahasen by using six different SWR schemes.

As expected, for all the cases the track errors increase with forecast time and the RMS errors of track are obtained from 90 hr with 6 hr intervals those are 123, 135, 171, 164, 167 and 134 km are obtained in the case of Dudhia, GSFC, CAM, RRTMG, New Goddard and FLG schemes respectively. All tracks show North-Easterly movement of the cyclone.

It has been observed from the above data that RMS track errors are obtained between 123 to 171 km and three short wave radiation schemes Dudhia, GSFC and FLG gives the less errors those are 123, 135 and 134 km respectively whereas short wave radiation scheme CAM scheme gives the maximum track error 171 km with respect to IMD observation.

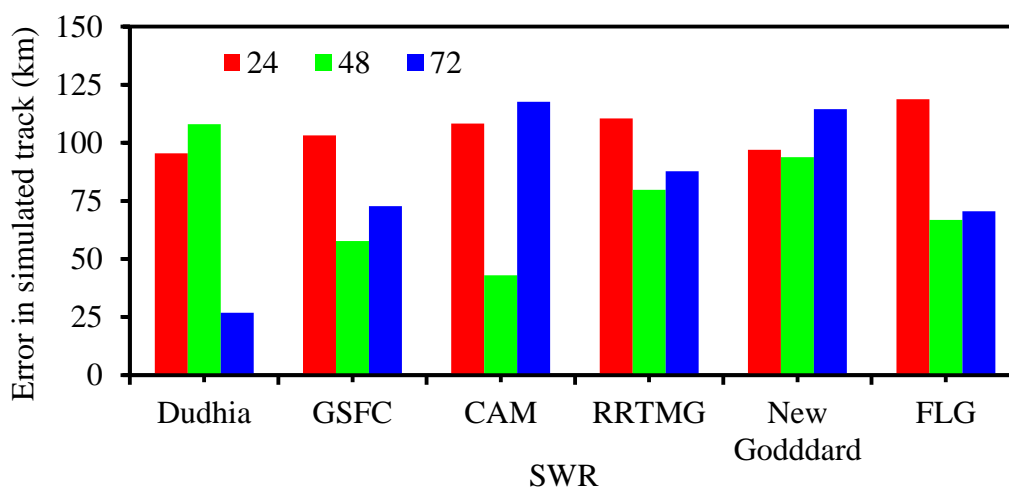


Figure 4.1.5.1(c): Model simulated track error in the 24, 48, and 72-hr forecasts with respect to IMD observed of TC Mahasen by using six different SWR schemes.

Therefore, it may be concluded from the above discussion the combination of Dudhia for the short wave radiation schemes gives least error 123 km with respect to IMD observation.

4.1.5.2 Effect of the short wave radiation schemes on wind speed

Figure 4.1.5.2(a) has been shown the wind speeds obtained from the six different simulations and the corresponding IMD wind data for every 6 hourly interval. From the figure, it has been shown that initially all the simulations over-predict except FLG the wind speed compared to IMD wind data.

Figure 4.1.5.2(b) has been shown the wind speed error for all short wave radiation schemes compared with IMD observation data. Wind speed errors at 24, 48, 72 hours are shown in figure 4.1.5.2(c) as a histogram plot. This parametrization also indicate that the model

‘produces’ a strong storm. All the cases produce a strong cyclone from the initial on 13 May from 00 UTC to 17 May 00 UTC.

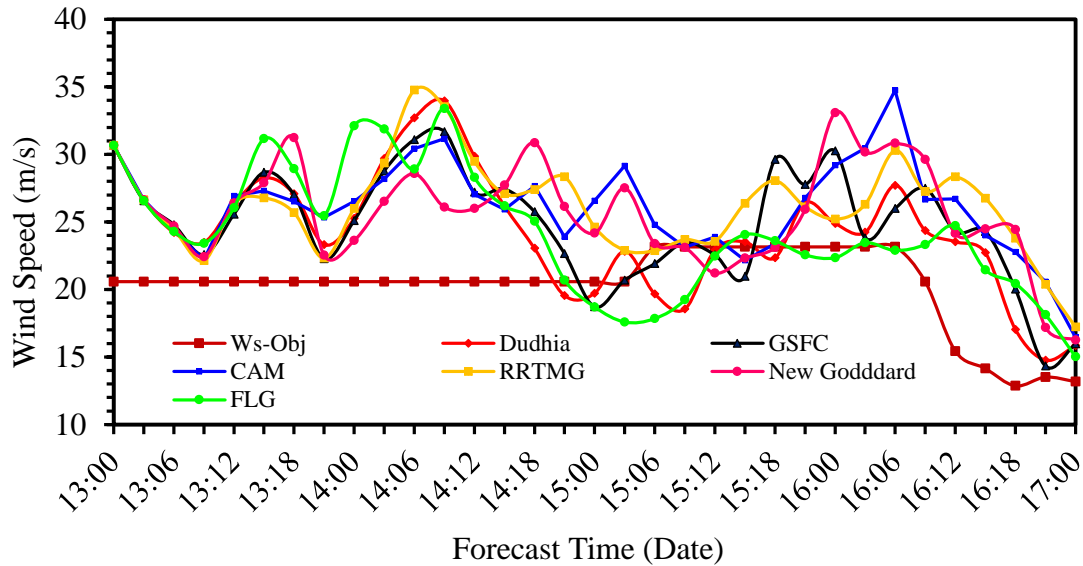


Figure 4.1.5.2(a): Model simulated wind speed with IMD observed of TC Mahasen by using six different SWR schemes.

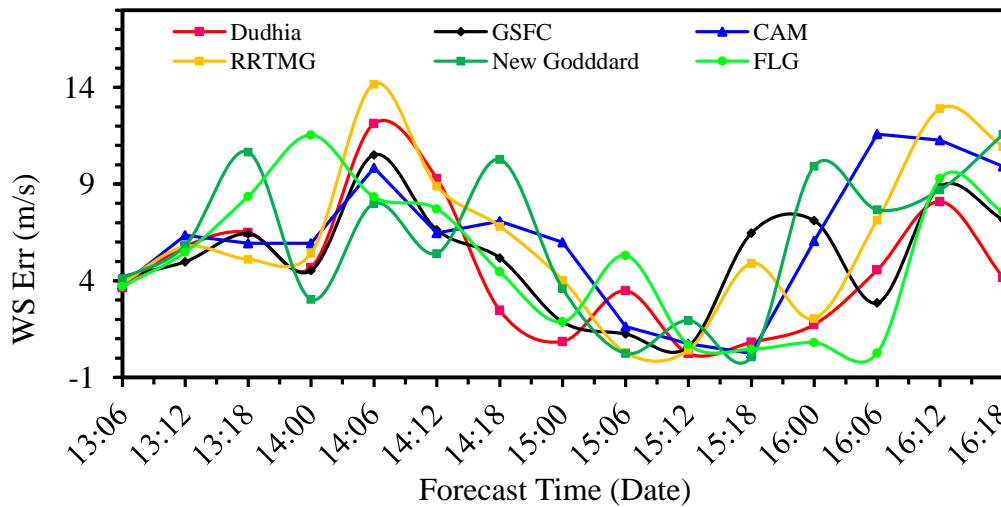


Figure 4.1.5.2(b): Model simulated wind speed error with respect to IMD observed of TC Mahasen by using six different SWR schemes.

For all the cases the RMS errors of WS are obtained from 90 hr with 6 hourly intervals those are 4.6, 5.2, 6.2, 6.2, 6.1 and 5.1 m/s in the case of Dudhia, GSFC, CAM, RRTMG, New Godddard FLG schemes of SWR respectively. The IMD data is showing a maximum wind speed of 23 m/s at 06 UTC on 15 May to 06 UTC on 16 May 2013.

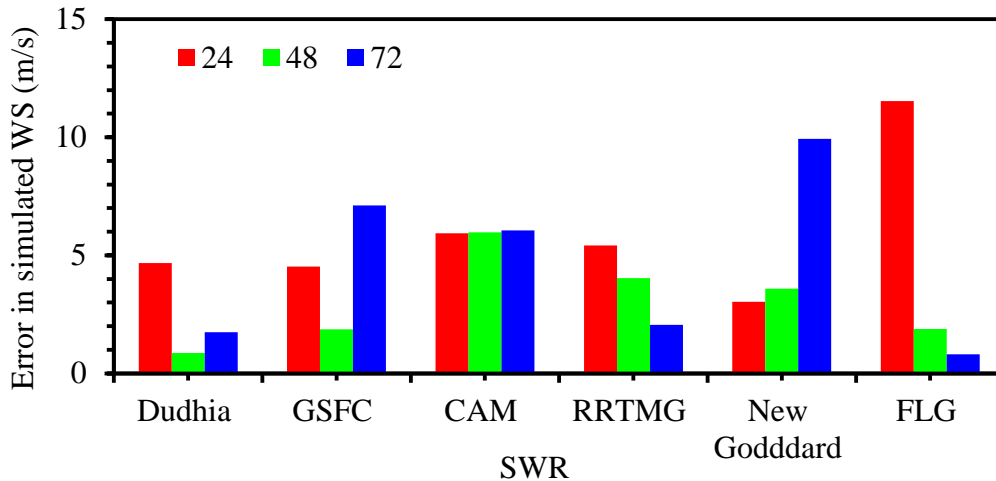


Figure 4.1.5.2(c): Model simulated wind speed error in the 24, 48, and 72-hr forecasts with respect to IMD observed of TC Mahasen by using six different SWR schemes.

It has been observed from the above data that RMS maximum wind speed errors are obtained between 4.6 to 6.2 m/s and three short wave radiation schemes Dudhia, GSFC and FLG scheme for the short wave radiation give the less errors those are 4.6, 5.2 and 5.1 m/s respectively whereas short wave radiation CAM scheme gives the maximum wind speed error 6.2 m/s with respect to IMD observation. All the cases produce a strong cyclone.

Therefore, it may be concluded from the above discussion the combination of Dudhia for the short wave radiation scheme gives least error 4.6 m/s with respect to IMD observation.

4.1.5.3 Effect of the short wave radiation schemes on CSLP

The intensity of the cyclone from the point of CSLP is generally over-predicted by all the schemes except FLG, as can be seen from the time series values which are too low for a category storm. The propagation of simulated cyclone CSLP for various combinations of short wave radiation schemes have been presented in figure 4.1.5.3(a). Figure 4.1.5.3(b) has been shown the CSLP error for all short wave radiation schemes compared with IMD observation data. CSLP errors at 24, 48, 72 hours are shown in figure 4.1.5.3(c) as a histogram plot. This parameterization also indicate that the model ‘produces’ a strong storm. All the cases produce a strong cyclone from the initial on 13 May from 00 UTC to 17 May 00 UTC.

For all the cases the RMS errors of CSLP are obtained from 90 hr with 6 hourly intervals those are 6.6, 6.8, 8.0, 9.0, 7.7 and 4.6 hPa in the case of Dudhia, GSFC, CAM, RRTMG, New Goddard and FLG schemes of SWR respectively.

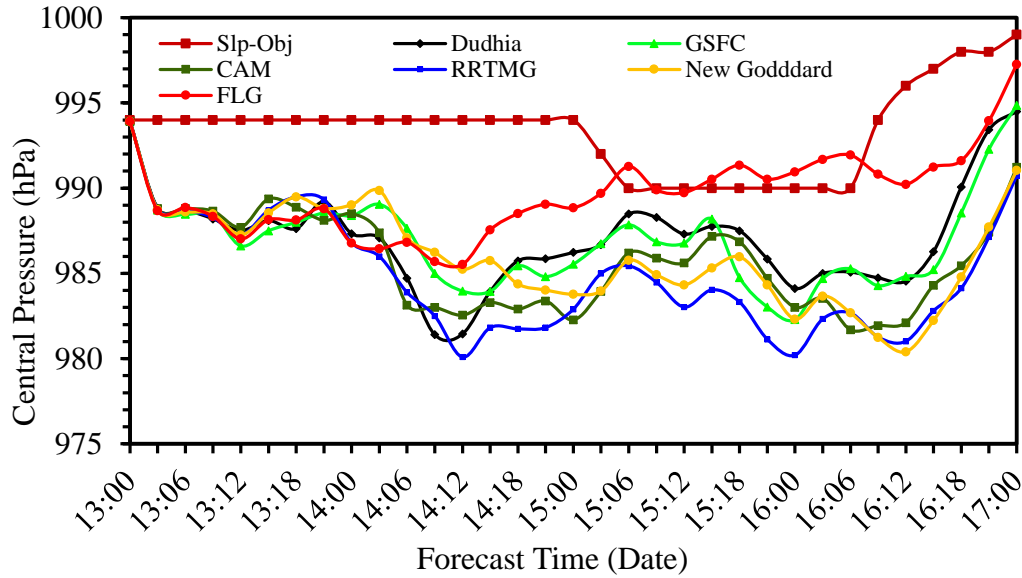


Figure 4.1.5.3(a): Model simulated CSLP with IMD observed of TC Mahasen by using six different SWR schemes.

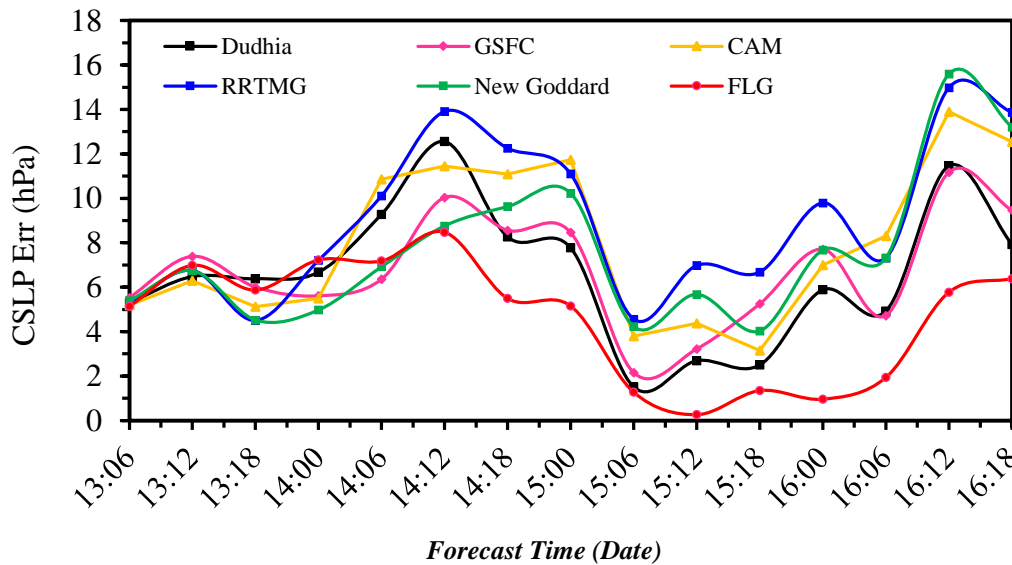


Figure 4.1.5.3(b): Model simulated CSLP error with respect to IMD observed of TC Mahasen by using six different SWR schemes.

It has been observed from the above data that RMS maximum CSLP errors are obtained between 4.6 to 9.02 hPa and three short wave radiation scheme FLG, Dudhia and GSFC

give the less errors those are 4.6, 6.6 and 6.8 hPa respectively whereas short wave radiation RRTMG scheme gives the maximum CSLP error 9.0 hPa with respect to IMD observation. All the cases produce a strong cyclone.

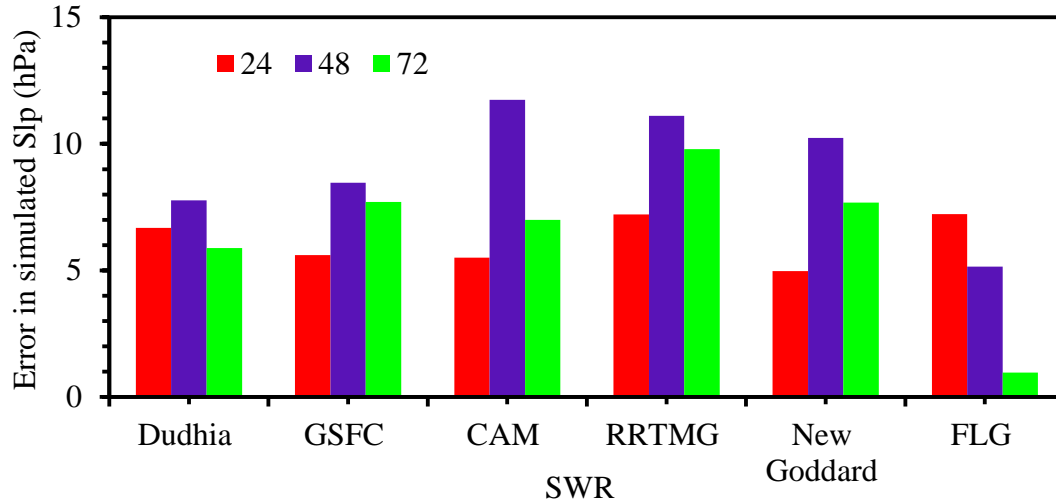


Figure 4.1.5.3(c): Model simulated CSLP error in the 24, 48, and 72-hr forecasts with respect to IMD observed of TC Mahasen by using six different SWR schemes.

Therefore, it may be concluded from the above discussion the combination of FLG for the short wave radiation scheme gives least error 4.6 hPa with respect to IMD observation from the six numerical experiments.

From the six numerical experiments, it is clear that track propagation and RMS error among these six schemes have small variations, so the track prediction is indeed very sensitive to short wave radiation schemes. There is few significant variation in the RMS error is 123 and 134 km between the Dudhia and FLG schemes and from the point of view propagation of the track, Dudhia scheme is good. However, it is instructive to mention here that the Dudhia scheme over predicts the wind speed RMS as 4.6 m/s but FLG scheme is 5.05 m/s with respect to the IMD wind speed data. On the another hand the FLG scheme over predicts the CSLP RMS error is 4.6 hPa but Dudhia scheme is 6.6 hPa with respect to the IMD CSLP data and they have small variation of those errors.

Finally it is strongly recommending that considering from the RMS errors of track, wind and CSLP, the combination of Dudhia for the short wave radiation schemes gives least error with respect to IMD observation from the six numerical experiments. So Dudhia scheme has been chosen the best scheme for the next experiment.

4.1.6 Long wave radiation (LWR) schemes

The long wave radiation (LWR) schemes handle the process of absorption and emission of infrared or thermal radiation by gases and surfaces. Simulations are carried out for five different long wave radiation (LWR) scheme along with the best schemes determined from previous numerical experiments. In this study, numerical experiments were conducted with five different long wave radiation (LWR) schemes. In this set of experiments, Five different long wave radiation schemes have been considered along with the BMJ scheme for the cumulus, a combination of MRF for the PBL and MON for the surface layer parameterization, WSM3 for the microphysics scheme, UNLS for the land surface model and Dudhaia scheme for the short wave radiation schemes. Various long wave radiation schemes options are RRTM, RRTMG, New Goddard, FLG and Held-Suarez schemes. The other physics options are kept fixed, as shown in table 3.3.

4.1.6.1 Effect of the long wave radiation on track

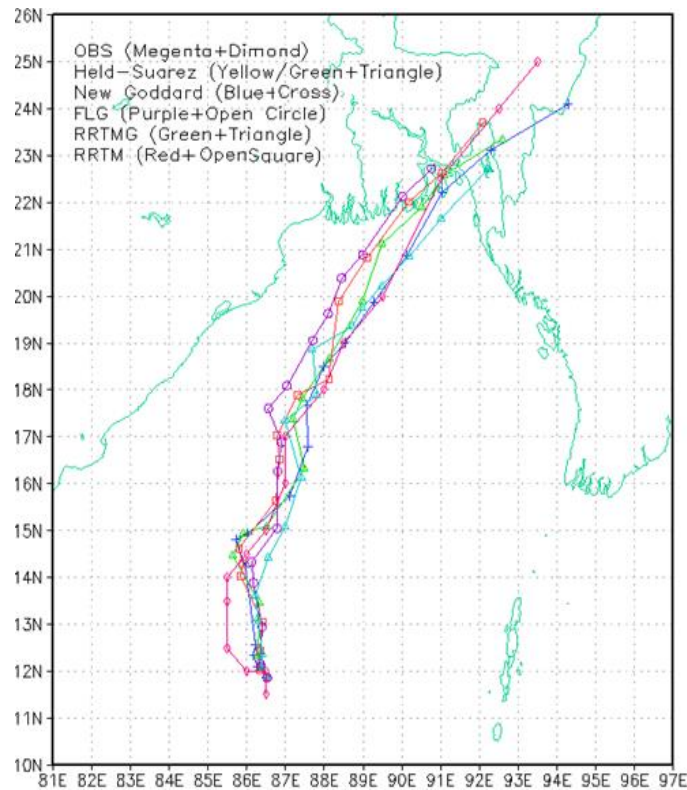


Figure 4.1.6.1(a): Model simulated track with IMD observed of TC Mahasen by using five different LWR schemes.

The propagation of tracks are shown in figure 4.1.6.1(a) and it has been shown that the propagation of simulated tracks closely follows the IMD observations. It is also showing the

results for the track propagation and it has been shown that all the schemes produce a good match with the IMD observation track with IMD observation data.

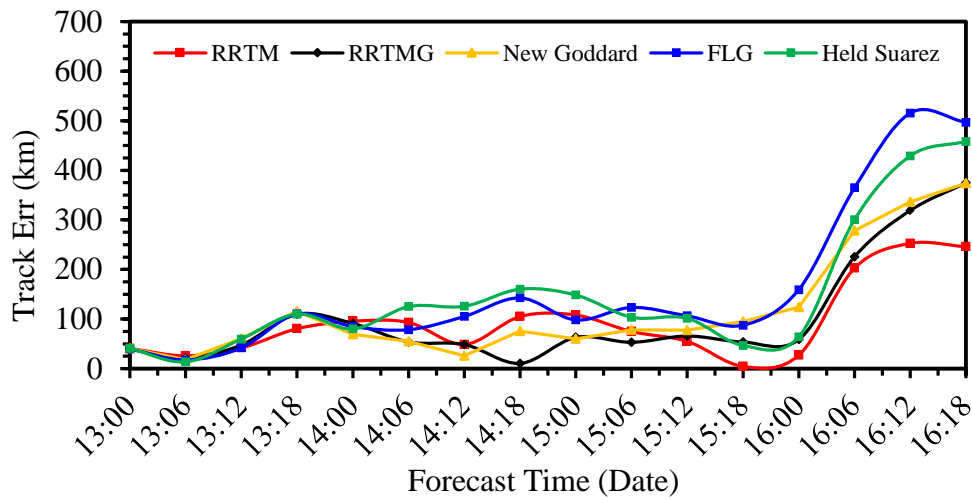


Figure 4.1.6.1(b): Model simulated track error with respect to IMD observed of TC Mahasen by using five different LWR schemes.

Figure 4.1.6.1(b) has been shown the track error for all the long wave radiation schemes compared with IMD observation data. Track errors at 24, 48, 72 hours are shown in figure 4.1.6.1(c) as a histogram plot. As expected, for all the cases the track errors increase with forecast time and the RMS errors of track are obtained from 90 hr with 6 hr intervals those are 123, 150, 164, 227 and 202 km are obtained in the case of RRTM, RRTMG, New Goddard, FLG and Held-Suarez schemes respectively. All tracks show North-Easterly movement of the cyclone.

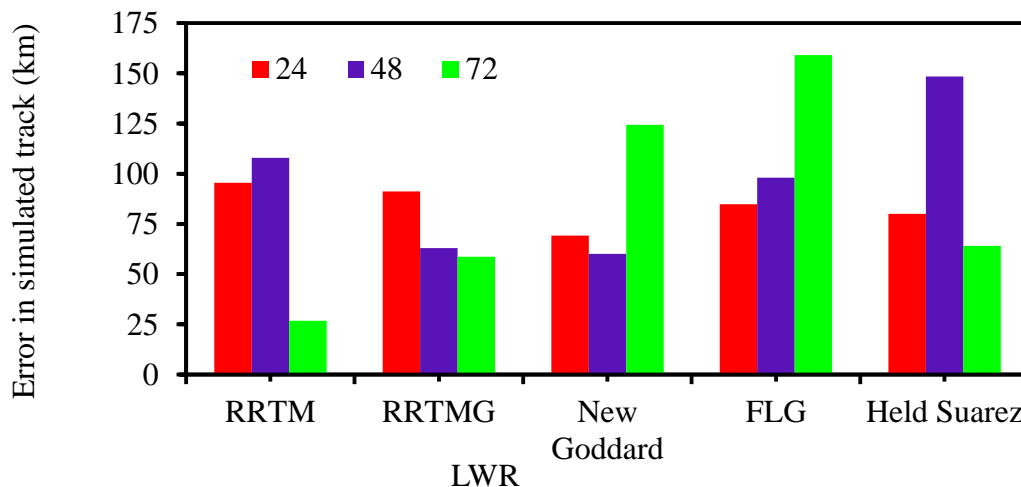


Figure 4.1.6.1(c): Model simulated track error in the 24, 48, and 72-hr forecasts with respect to IMD observed of TC Mahasen by using five different LWR schemes.

It has been observed from the above data that RMS track errors are obtained between 123 to 227 km and two long wave radiation schemes RRTM and RRTMG give the less errors those are 123 and 150 km respectively whereas long wave radiation scheme FLG gives the maximum track error 227 km with respect to IMD observation.

Therefore, it may be concluded from the above discussion the combination of RRTM for the long wave radiation schemes gives least error 123 km with respect to IMD observation.

4.1.6.2 Effect of the long wave radiation schemes on wind speed

Figure 4.1.6.2(a) has been shown the wind speeds obtained from the six different simulations and the corresponding IMD wind data for every 6 hourly interval. From the figure, it has been shown that initially FLG and Held-Suarez the simulations over-predict but RRTMG, RRTM and New Goddard are Predict the wind speed compared to IMD wind data. Figure 4.1.6.2(b) has been shown the wind speed error for all long wave radiation schemes compared with IMD observation data. Wind speed errors at 24, 48, 72 hours are shown in figure 4.1.6.2(c) as a histogram plot.

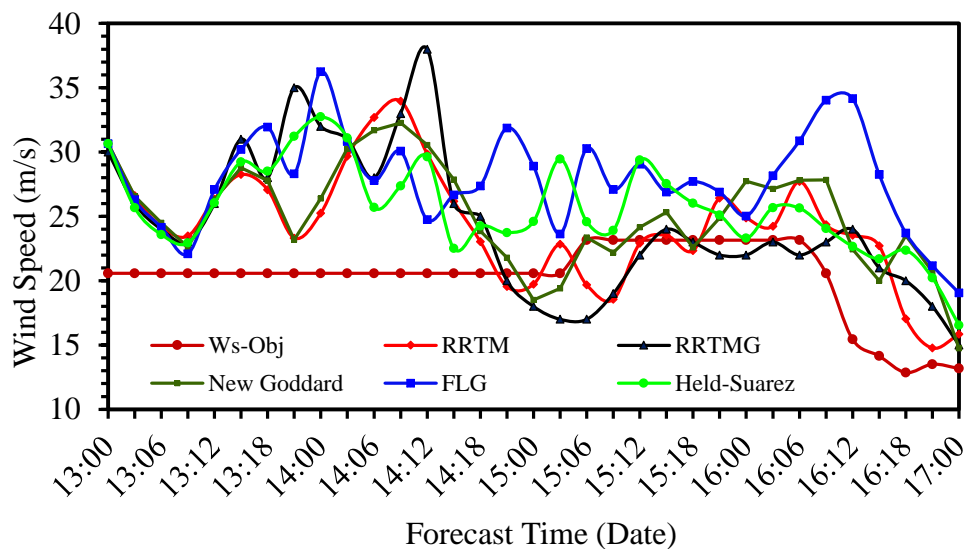


Figure 4.1.6.2(a): Model simulated wind speed with IMD observed of TC Mahasen by using five different LWR schemes.

This parameterization also indicate that the model ‘produces’ a strong storm. All the cases produce a strong cyclone from the initial on 13 May from 00 UTC to 17 May 00 UTC. For all the cases the RMS errors of WS are obtained from 90 hr with 6 hourly intervals those are 4.6, 5.7, 5.2, 8.0 and 5.4 m/s in the case of RRTM, RRTMG, New Goddard, FLG and Held

Suarez schemes of LWR respectively. The IMD data is showing a maximum wind speed of 23 m/s at 06 UTC on 15 May to 06 UTC on 16 May 2013.

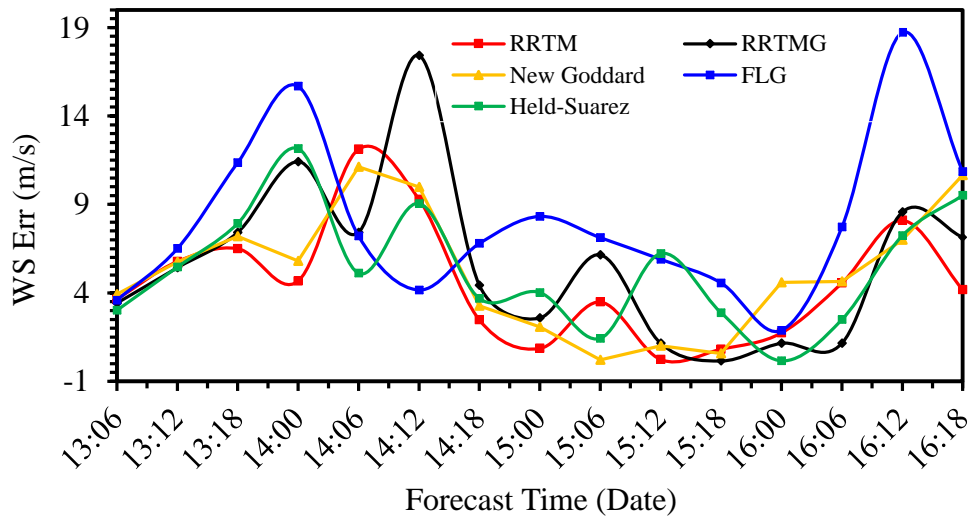


Figure 4.1.6.2(b): Model simulated wind speed error with respect to IMD observed of TC Mahasen by using five different LWR schemes.

It has been observed from the above data that RMS maximum wind speed errors are obtained between 4.6 to 8.0 m/s and two long wave radiation schemes RRTM and New Goddard scheme for the long wave radiation give the less errors those are 4.6 and 5.2 m/s respectively whereas long wave radiation FLG scheme gives the maximum wind speed error 8.0 m/s with respect to IMD observation. All the cases produce a strong cyclone.

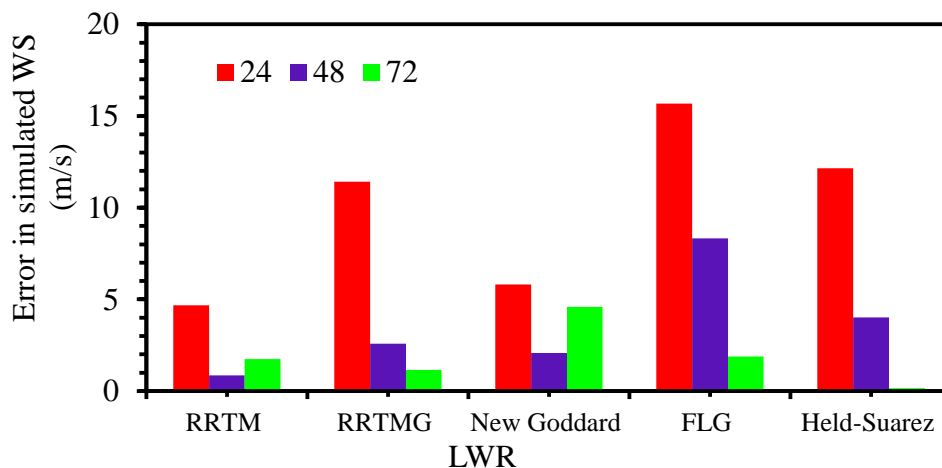


Figure 4.1.6.2(c): Model simulated wind speed error in the 24, 48, and 72-hr forecasts with respect to IMD observed of TC Mahasen by using five different LWR schemes.

Therefore, it may be concluded from the above discussion the combination of RRTM for the long wave radiation scheme gives least error 4.6 m/s with respect to IMD observation.

4.1.6.3 Effect of the long wave radiation schemes on CSLP

The intensity of the cyclone from the point of CSLP is generally over-predicted by all the schemes except RRTMG, as can be seen from the time series values which are too low for a category storm. The propagation of simulated cyclone CSLP for various combinations of long wave radiation schemes have been presented in figure 4.1.6.3(a). Figure 4.1.6.3(b) has been shown the CSLP error for all long wave radiation schemes compared with IMD observation data. CSLP errors at 24, 48, 72 hours are shown in figure 4.1.6.3(c) as a histogram plot. This parametrization also indicate that the model ‘produces’ a strong storm. All the cases produce a strong cyclone from the initial on 13 May from 00 UTC to 17 May 00 UTC.

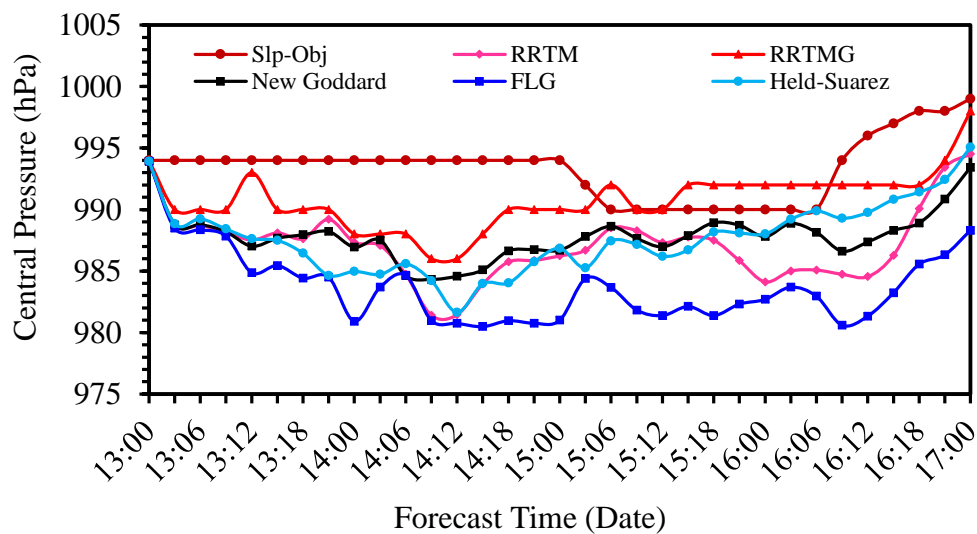


Figure 4.1.6.3(a): Model simulated CSLP with IMD observed of TC Mahasen by using five different LWR schemes.

For all the cases the RMS errors of CSLP are obtained from 90 hr with 6 hourly intervals those are 6.6, 3.7, 5.7, 10.1 and 5.9 hPa in the case of RRTM, RRTMG, New Goddard, FLG and Held-Suarez schemes of LWR respectively. It has been observed from the above data that RMS maximum CSLP errors are obtained between 3.7 to 10.1 hPa and two long wave radiation scheme RRTMG and New Goddard give the less errors those are 3.7 and 5.7 hPa

respectively whereas long wave radiation FLG scheme gives the maximum CSLP error 10.1 hPa with respect to IMD observation. All the cases produce a strong cyclone.

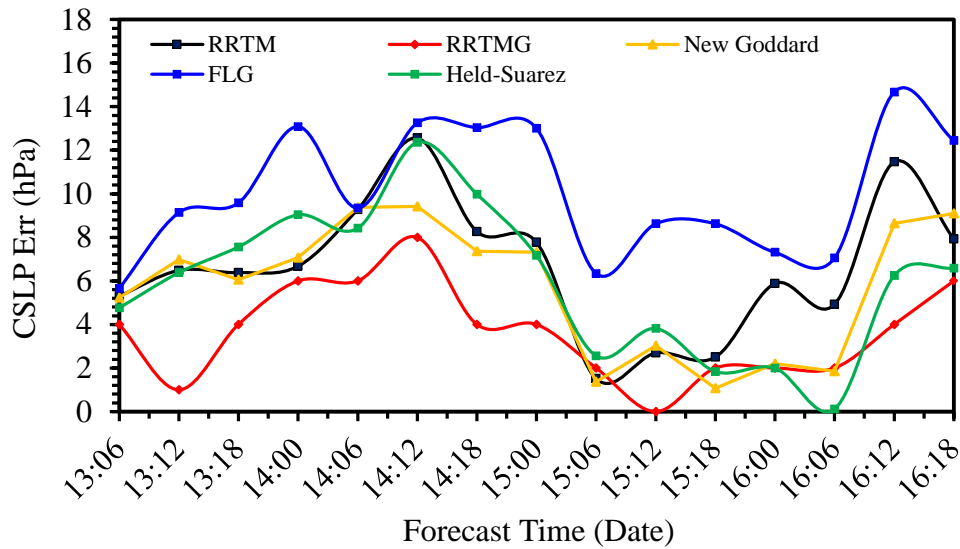


Figure 4.1.6.3(b): Model simulated CSLP error with respect to IMD observed of TC Mahasen by using five different LWR schemes.

Therefore it may be concluded from the above discussion the combination of RRTMG for the long wave radiation scheme gives least error 3.7 hPa with respect to IMD observation from the six numerical experiments.

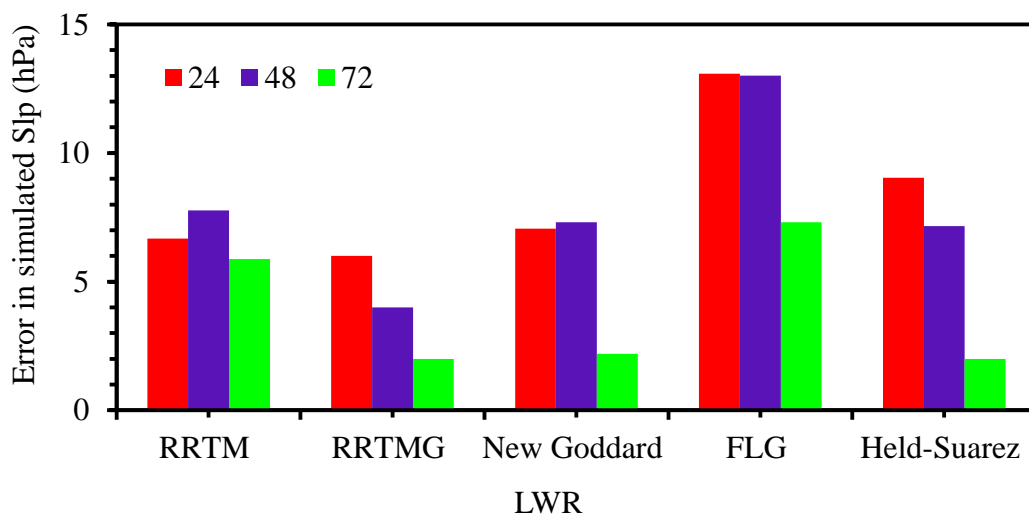


Figure 4.1.6.3(c): Model simulated CSLP error in the 24, 48, and 72-hr forecasts with respect to IMD observed of TC Mahasen by using five different LWR schemes.

From the five numerical experiments, it is clear that track propagation and RMS error among these five schemes have small variations, so the track prediction is indeed very sensitive to

long wave radiation schemes. There is few significant variation in the RMS error is 123 and 150 km between the RRTM and RRTMG schemes and from the point of view propagation of the track, RRTM scheme is good. However, it is instructive to mention here that the RRTM scheme over predicts the wind speed RMS as 4.6 m/s but RRTMG scheme is 5.05 m/s with respect to the IMD wind speed data. On the another hand the RRTMG scheme over predicts the CSLP RMS error is 3.7 hPa but New Goddard scheme is 5.7 hPa and RRTM 6.6 hPa with respect to the IMD CSLP data and they have small variation of those errors to each other.

Finally it is strongly recommending that considering from the RMS errors of track, wind and CSLP, the combination of RRTM for the long wave radiation schemes gives least error with respect to IMD observation from the five numerical experiments.

Table 4.1.1 Final result of these experiments

Name of Phy.	Cumulus	PBL	Microphysics	LSM	SWR	LWR
Subject/Parameter	BMJ	MRF	WSM3	UNLS	Dudhia	RRTM
Track err rms	212	184	123	123	123	123
WS err rms	12.1	10.1	4.6	4.6	4.6	4.6
CSLP err rms	18.5	16.1	6.6	6.6	6.6	6.6

4.2 Discussion experiment with 2nd set of Tropical Cyclone Mahasen

Have to get better result and comparing the performance of different physical parameterization schemes have been taken another set from MYNN2 in the PBL schemes because there RMS errors of track, WS and CSLP are closed to MRF scheme. Details result has been discussed below:

Different experiments have been used MP, LSM, SWR and LWR schemes.

4.2.1 Microphysics parameterization

The microphysics (MP) parameterizations explicitly handle water vapor, cloud and precipitation processes and also the microphysical processes of melting of snow, graupel and cloud ice hydrometeors, suppression of falling rain by evaporation. The MP

parameterizations can also take into account the falling speed of snow and graupel hydrometeors. In this set of experiments, 16 different MP schemes have been considered along with the BMJ scheme for the cumulus parameterization and a combination of MYNN2 for the PBL and MON for the surface layer parameterization. Various microphysics options are WSM6, Kessler, Purdue Lin, WSM3, WSM5, Eta, Thompson, Morrison 2-mom, CAM5.1, SBU-Ylin, WDM5, WDM6, NSSL 2-mom, NSSL 2-mom-CCN, NSSL 1-mom and NSSL 1-momlfo schemes. The other physics options are kept fixed, as shown in table 3.4.

4.2.1.1 Effect of the microphysics on track

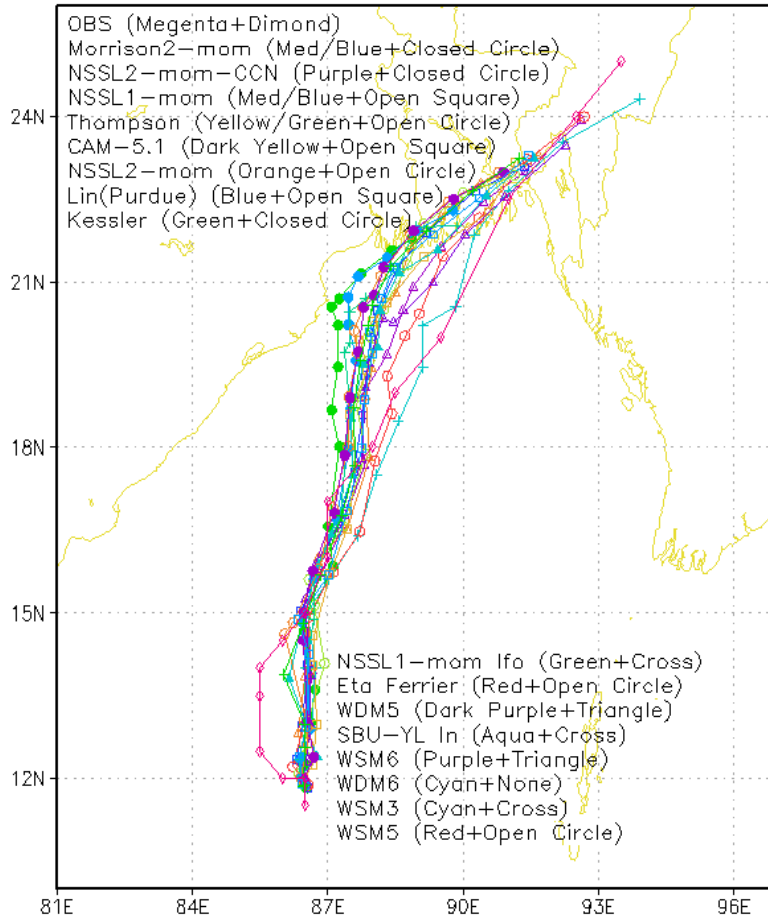


Figure 4.2.1.1(a): Model simulated track with IMD observed of TC Mahasen by using sixteen different MP schemes.

The propagation of tracks and observed with respect to IMD are shown in figure 4.2.1.1(a). All tracks show North-Easterly movement of the cyclone. Figure 4.2.1.1(b) has been shown the track error for all microphysics compared with IMD observation data. Track errors at 24,

48, 72 hours are shown in figure 4.2.1.1(c): as a histogram plot. As expected, for all the cases the track errors increase with forecast time and the RMS errors of track are obtained from 90 hr with 6 hr intervals those are 184, 305, 219, 161, 212, 181, 228, 276, 233, 274, 209, 215, 248, 244, 229, and 225 km are obtained in the case of WSM6, Kessler, Lin Purdue, WSM3, WSM5, Eta, Thompson, Morrison, CAM5.1, SBU-YL, WDM5, WDM6, NSSL2, NSSL2-CNN, NSSL1 and NSSL1-lfo schemes respectively.

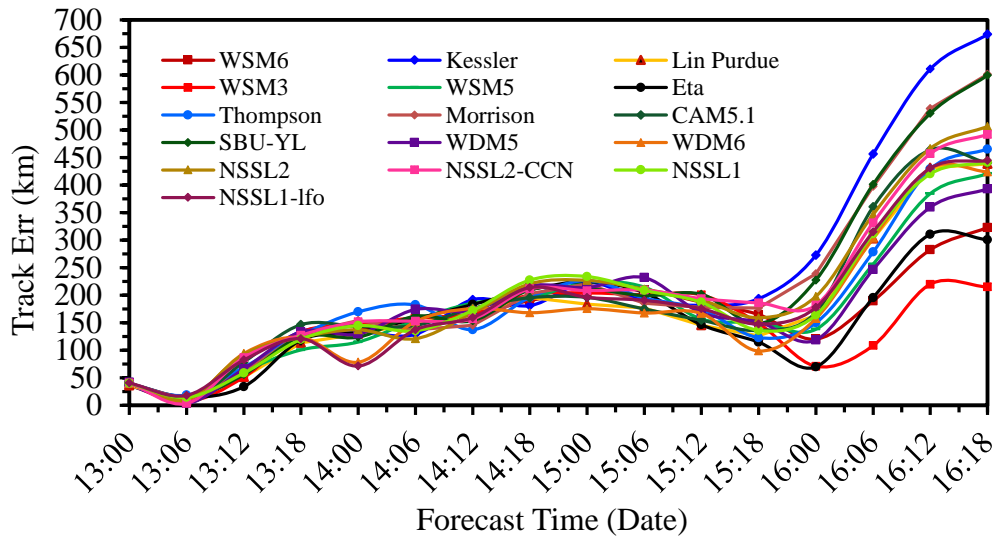


Figure 4.2.1.1(b): Model simulated track error with respect to IMD observed of TC Mahasen by using sixteen different MP schemes.

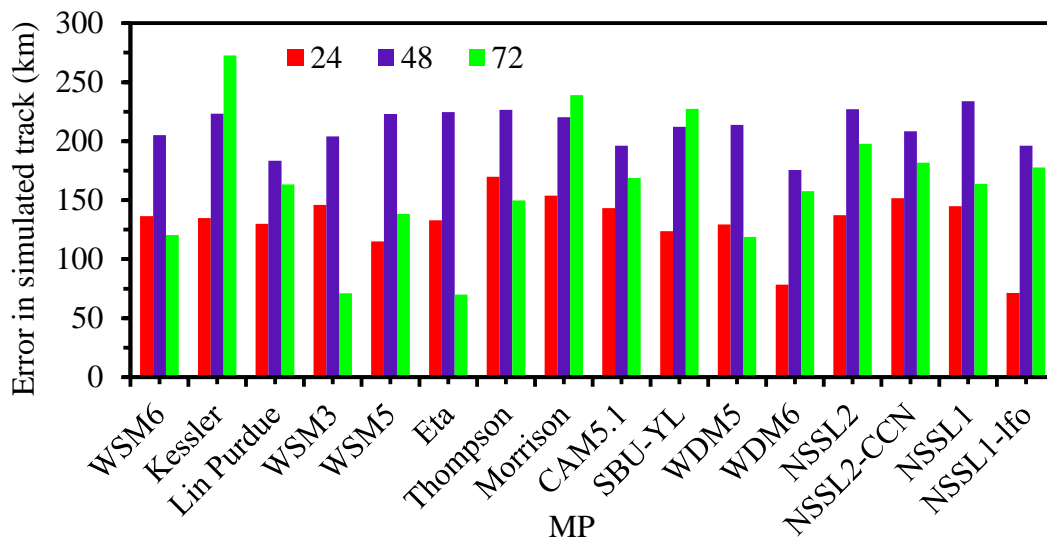


Figure 4.2.1.1(c): Model simulated track error in the 24, 48, and 72-hr forecasts with respect to IMD observed of TC Mahasen by using sixteen different MP schemes.

It has been observed from the above data that RMS track errors are obtained between 161 to 305 km and three microphysics schemes WSM6, WSM3 and Eta give the less errors those

are 184, 161 and 181 km respectively whereas microphysics Kessler scheme gives the maximum track error 305 km with respect to IMD observation.

Therefore, it may be concluded from the above discussion the combination of WSM3 for the microphysics parameterization gives least error 161 km with respect to IMD observation.

4.2.1.2 Effect of the microphysics schemes on wind speed

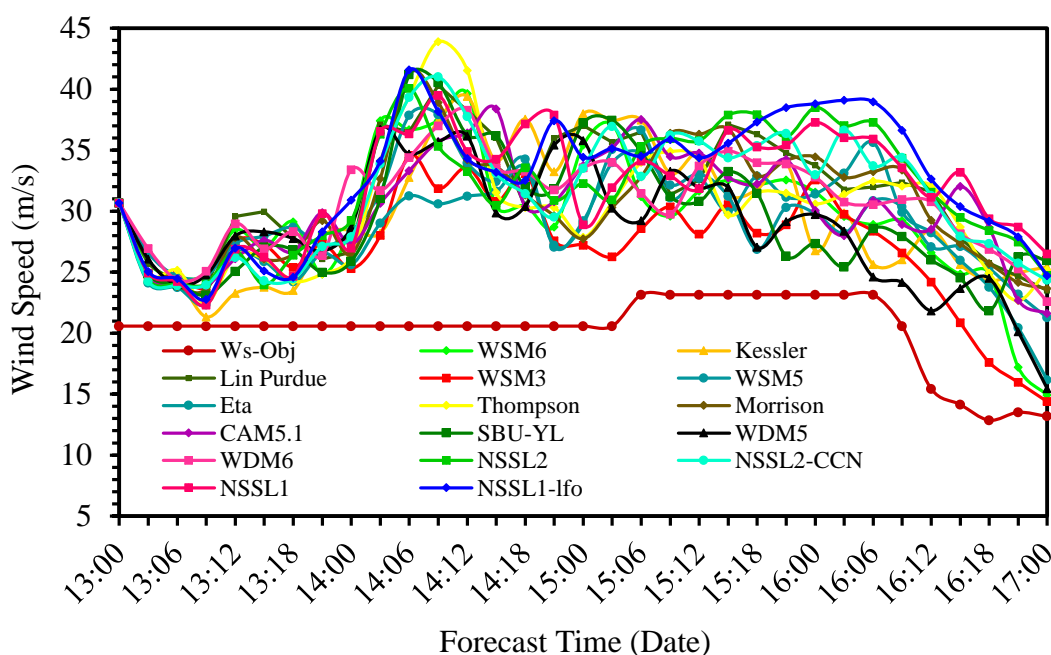


Figure 4.2.1.2(a): Model simulated wind speed with IMD observed of TC Mahasen by using sixteen different MP schemes.

Figure 4.2.1.2(a) has been shown the wind speeds obtained from the sixteen different simulations and the corresponding IMD wind data for every 6 hourly interval. From the figure, it has been shown that initially all the simulations over-predict the wind speed compared to IMD wind data. Figure 4.2.1.2(b) has been shown the wind speed error for all microphysics compared with IMD observation data. Wind speed errors at 24, 48, 72 hours are shown in figure 4.2.1.2(c) as a histogram plot. This parametrization also indicate that the model ‘produces’ a strong storm. All the cases produce a strong cyclone from the initial on 13 May from 00 UTC to 17 May 00 UTC.

For all the cases the RMS errors of WS are obtained from 90 hr with 6 hourly intervals those are 10.1, 9.9, 11.3, 7.4, 9.6, 9.2, 10.2, 10.4, 10.1, 9.4, 8.4, 11.1, 12.1, 11.0, 11.1 and 12.5 m/s in the case of WSM6, Kessler, Lin (Purdue), WSM3, WSM5, Eta, Thompson, Morrison2-

mom, CAM 5.1, SBU-YL In, WDM5, WDM6, NSSL2-mom, NSSL2-mom-CNN, NSSL1-mom and NSSL1-momlfo schemes of MP respectively. The IMD data is showing a maximum wind speed of 23 m/s at 06 UTC on 15 May to 06 UTC on 16 May 2013.

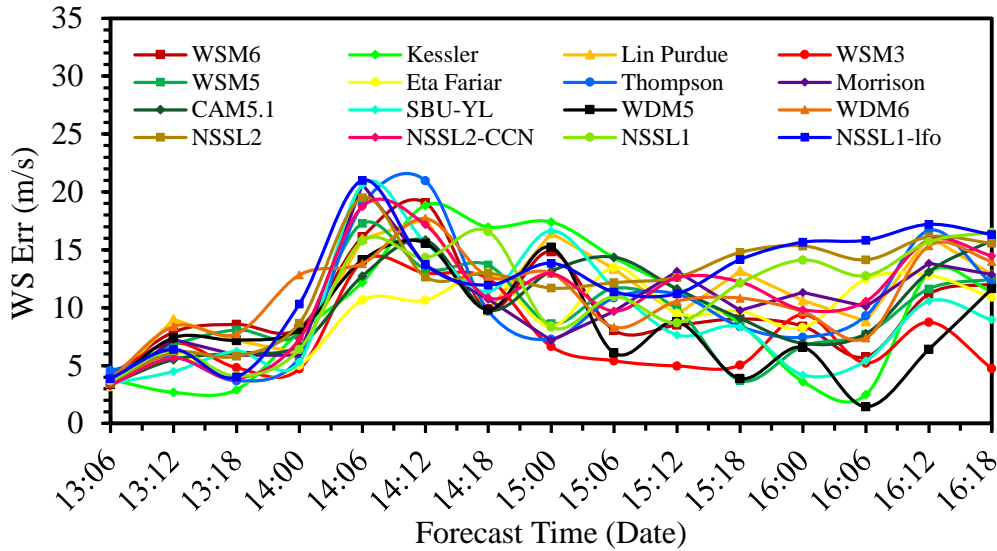


Figure 4.2.1.2(b): Model simulated wind speed error with respect to IMD observed of TC Mahasen by using sixteen different MP schemes.

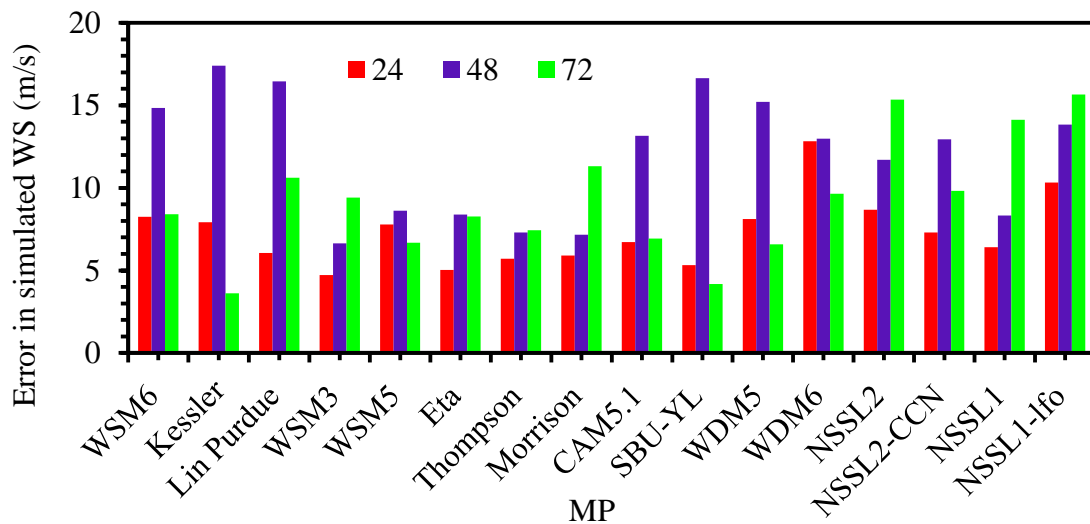


Figure 4.2.1.2(c): Model simulated wind speed error in the 24, 48, and 72-hr forecasts with respect to IMD observed of TC Mahasen by using sixteen different MP schemes.

It has been observed from the above data that RMS maximum wind speed errors are obtained between 7.4 to 23 m/s and three microphysics schemes WSM3, Eta and WDM5 scheme for the microphysics parameterization combined with the MON for the surface layer parameterization give the less errors those are 7.4, 9.2 and 8.4 m/s respectively whereas

microphysics NSSL1-momlfo scheme gives the maximum wind speed error 12.5 m/s with respect to IMD observation. All the cases produce a strong cyclone.

Therefore, it may be concluded from the above discussion the combination of WSM3 for the microphysics Scheme gives least error 7.4 m/s with respect to IMD observation.

4.2.1.3 Effect of the microphysics schemes on CSLP

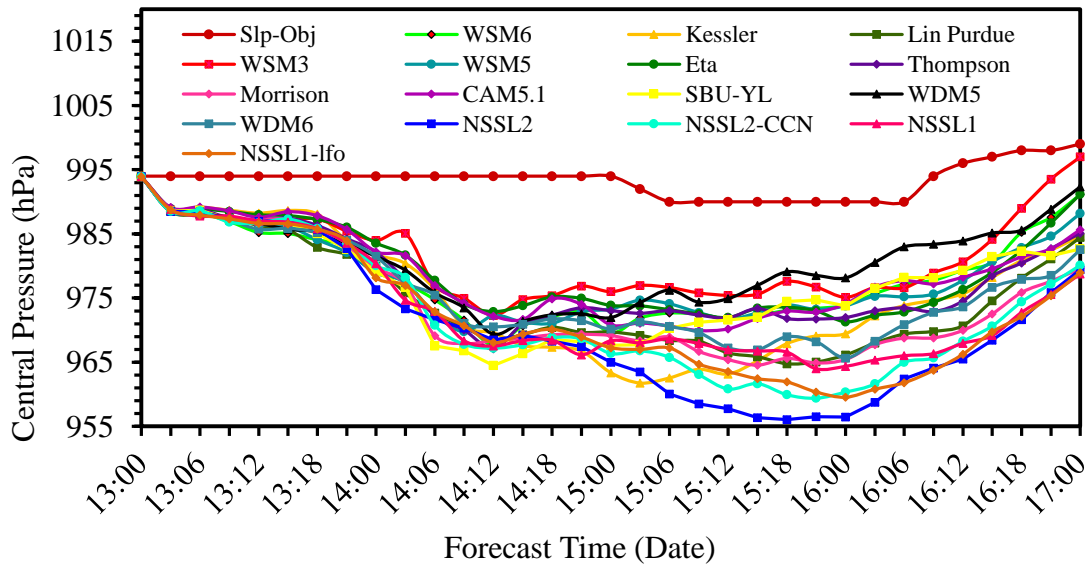


Figure 4.2.1.3(a): Model simulated CSLP with IMD observed of TC Mahasen by using sixteen different MP schemes.

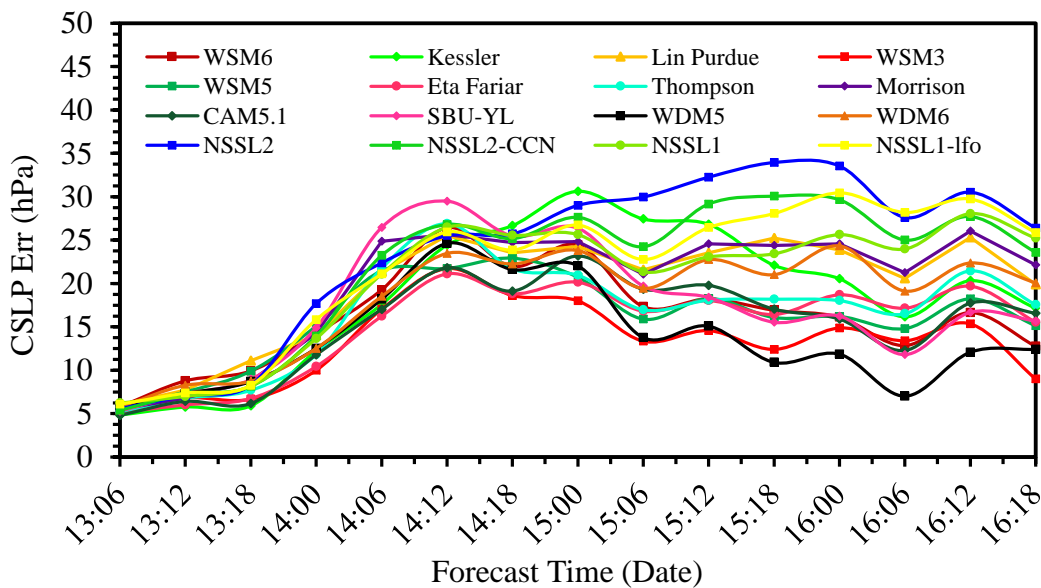


Figure 4.2.1.3(b): Model simulated CSLP error with respect to IMD observed of TC Mahasen by using sixteen different MP schemes

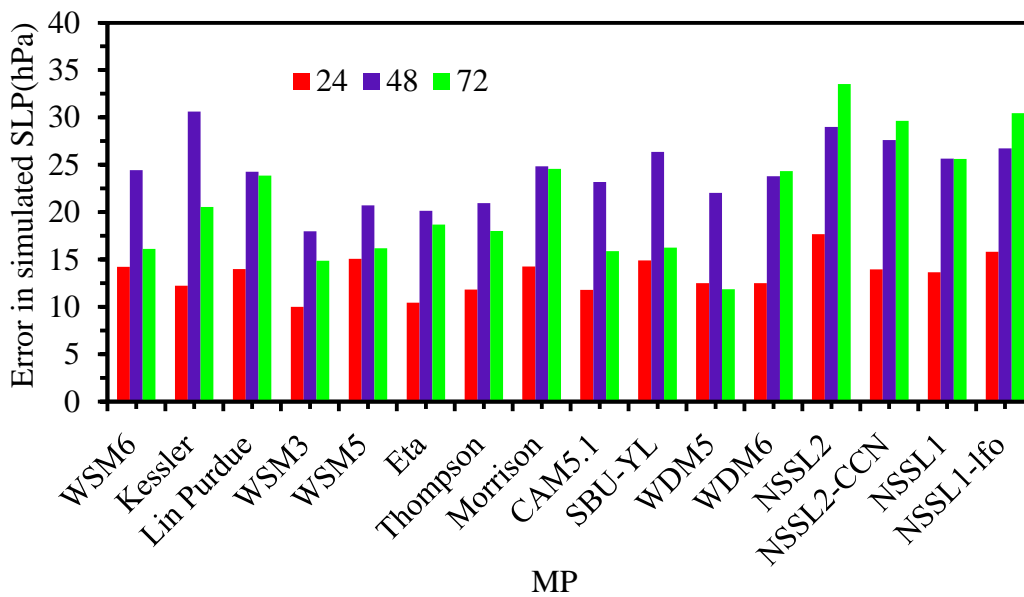


Figure 4.2.1.3(c): Model simulated CSLP error in the 24, 48, and 72-hr forecasts with respect to IMD observed of TC Mahasen by using sixteen different MP schemes.

For all the cases the RMS errors of CSLP are obtained from 90 hr with 6 hourly intervals those are 16.1, 18.6, 19.6, 13.2, 16.0, 15.1, 16.6, 20.0, 15.3, 17.2, 13.6, 18.2, 23.7, 21.8, 20.3 and 21.8 hPa in the case of WSM6, Kessler, Lin (Purdue), WSM3, WSM5, Eta, Thompson, Morrison2-mom, CAM 5.1, SBU-YL In, WDM5, WDM6, NSSL2-mom, NSSL2-mom-CNN, NSSL1-mom and NSSL1-momlfo schemes of MP respectively.

It has been observed from the above data that RMS maximum CSLP errors are obtained between 13.2 to 23.7 hPa and three microphysics schemes WSM3, Eta and WDM5 give the less errors those are 13.2, 15.1 and 13.6 hPa respectively whereas microphysics NSSL2-mom scheme gives the maximum CSLP error 23.7 hPa with respect to IMD observation. All the cases produce a strong cyclone.

Therefore, it may be concluded from the above discussion the combination of WSM3 for the microphysics Scheme gives least error 18.5 hPa with respect to IMD observation from the sixteen numerical experiments.

Finally from the RMS errors of track, wind and CSLP, the combination of WSM3 for the microphysics parameterization gives least error with respect to IMD observation from the sixteen numerical experiments. So WSM3 scheme has been chosen the best scheme for the next experiment.

4.2.2 Land surface model (LSM)

The land-surface models (LSMs) are responsible for the thermal and moisture fluxes in multiple layers of the soil and also vegetation, root, canopy effects and surface snow-cover. These models use atmospheric information from the surface layer scheme, radiative forcing from the radiation scheme, and precipitation forcing from the microphysics and convective schemes. Along with above schemes, the LSMs provide heat fluxes and moisture over the land points and sea-ice points and also give the lower boundary condition fluxes to the PBL schemes (Skamarock 2008). In this study, numerical experiments were conducted with six different land surface models along with the best schemes from previous experiments. These six models distinguish land soil inherently. In this set of experiments, six different land-surface model schemes have been considered along with the BMJ scheme for the cumulus, a combination of MRF for the PBL and MON for the surface layer parameterization and WSM3 for the microphysics parameterization. Various land-surface models options are UNLS, TDS, RUC, NLS, CLM4.0 and PXS schemes. The other physics options are kept fixed, as shown in table 3.4.

4.2.2.1 Effect of the land surface model on track

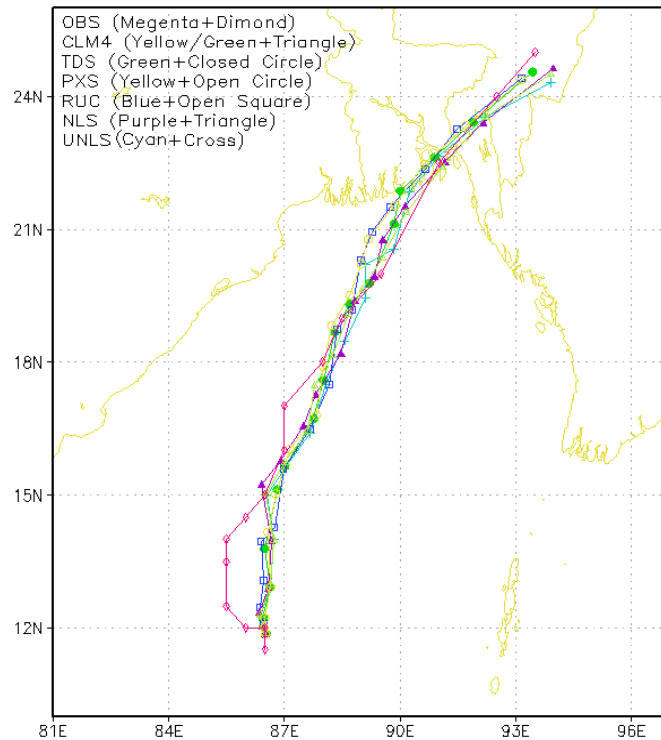


Figure 4.2.2.1(a): Model simulated track with IMD observed of TC Mahasen by using six different LSM schemes.

The propagation of tracks and observed with respect to IMD are shown in figure 4.2.2.1(a). All tracks show North-Easterly movement of the cyclone. Figure 4.2.2.1(b) has been shown the track error for all the land-surface models compared with IMD observation data. Track errors at 24, 48, 72 hours are shown in figure 4.2.2.1(c) as a histogram plot. As expected, for all the cases the track errors increase with forecast time and the RMS errors of track are obtained from 90 hr with 6 hr intervals those are 161, 168, 175, 157, 153 and 185 km are obtained in the case of UNLS, TDS, RUC, NLS, CLM4 and PXS schemes of LSM respectively. All tracks show North-Easterly movement of the cyclone.

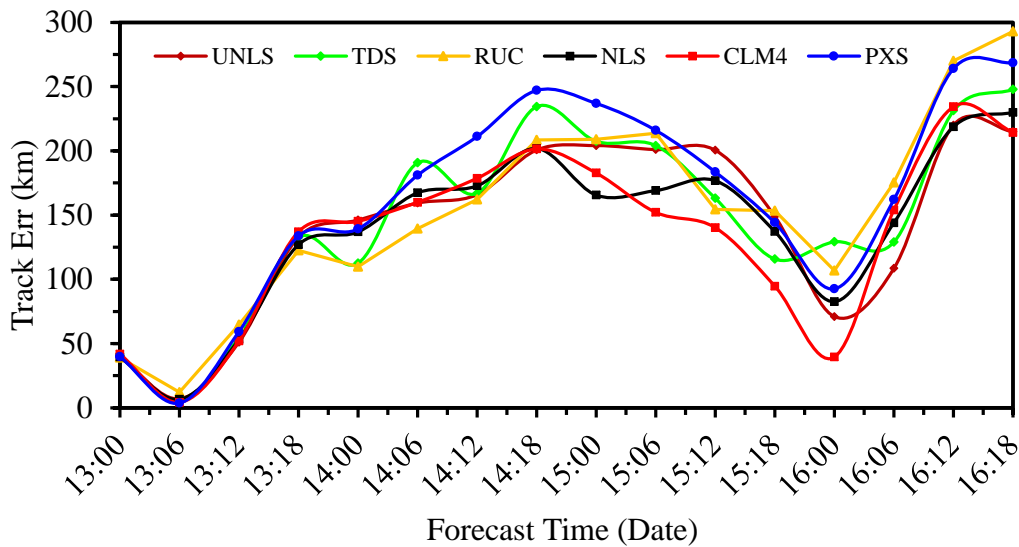


Figure 4.2.2.1(b): Model simulated track error with respect to IMD observed of TC Mahasen by using six different LSM schemes.

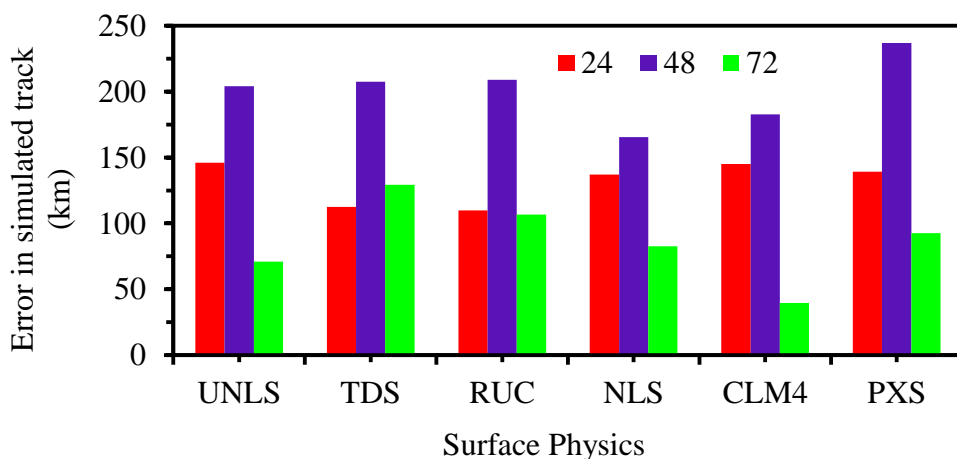


Figure 4.2.2.1(c): Model simulated track error in the 24, 48, and 72-hr forecasts with respect to IMD observed of TC Mahasen by using six different LSM schemes.

It has been observed from the above data that RMS track errors are obtained between 153 to 185 km and three land surface model schemes UNLS, NLS and CLM4 give the less errors those are 161, 157 and 153 km respectively whereas land surface model PXS scheme gives the maximum track error 185 km with respect to IMD observation.

Therefore, it may be concluded from the above discussion the combination of CLM4 for the land surface model schemes gives least error 153 km with respect to IMD observation.

4.2.2.2 Effect of the land surface model on wind speed

Figure 4.2.2.2(a) has been shown the wind speeds obtained from the six different simulations and the corresponding IMD wind data for every 6 hourly interval. From the figure, it has been shown that initially all the simulations over-predict the wind speed compared to IMD wind data. Figure 4.2.2.2(b) has been shown the wind speed error for all microphysics compared with IMD observation data. Wind speed errors at 24, 48, 72 hours are shown in figure 4.2.2.2(c) as a histogram plot. This parametrization also indicate that the model ‘produces’ a strong storm. All the cases produce a strong cyclone from the initial on 13 May from 00 UTC to 17 May 00 UTC.

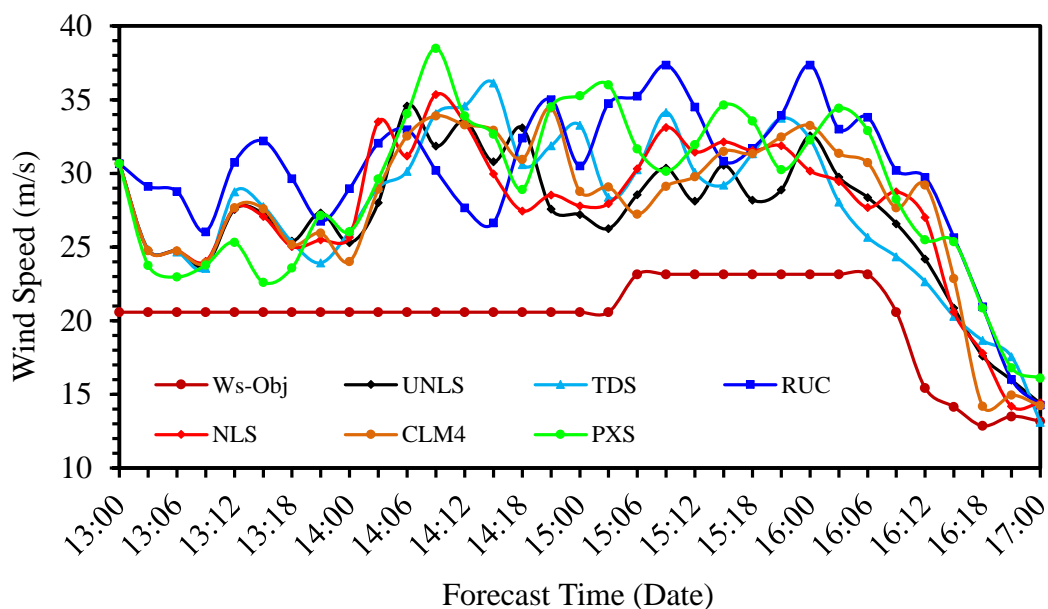


Figure 4.2.2.2(a): Model simulated wind speed with IMD observed of TC Mahasen by using six different LSM schemes.

For all the cases the RMS errors of WS are obtained from 90 hr with 6 hourly intervals those are 7.4, 7.7, 10.4, 7.4, 7.6 and 8.7 m/s in the case of UNLS, TDS, RUC, NLS, CLM4 and

PXS schemes of LSM respectively. The IMD data is showing a maximum wind speed of 23 m/s at 06 UTC on 15 May to 06 UTC on 16 May 2013.

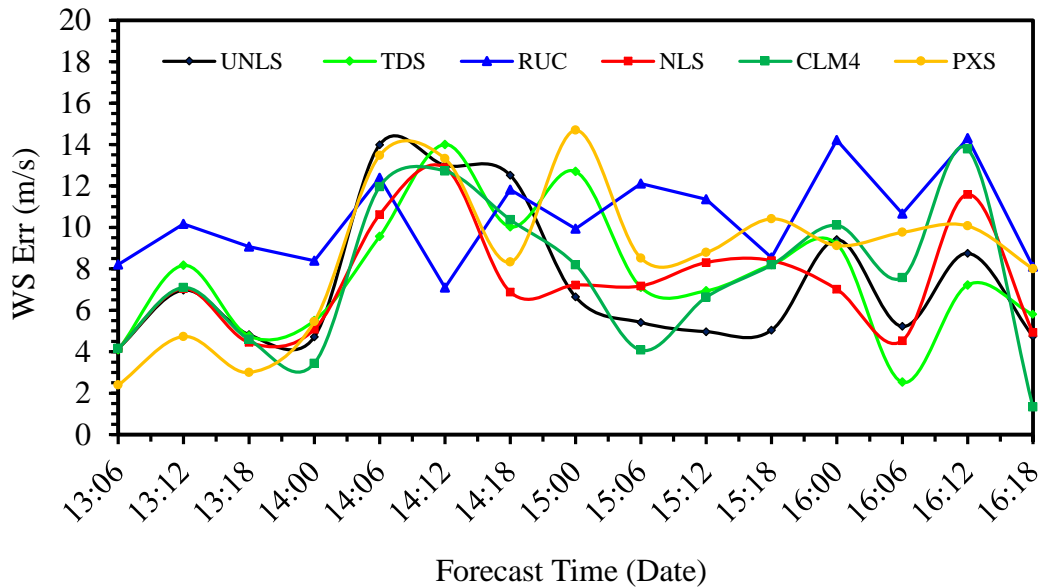


Figure 4.2.2.2(b): Model simulated wind speed error with respect to IMD observed of TC Mahasen by using six different LSM schemes.

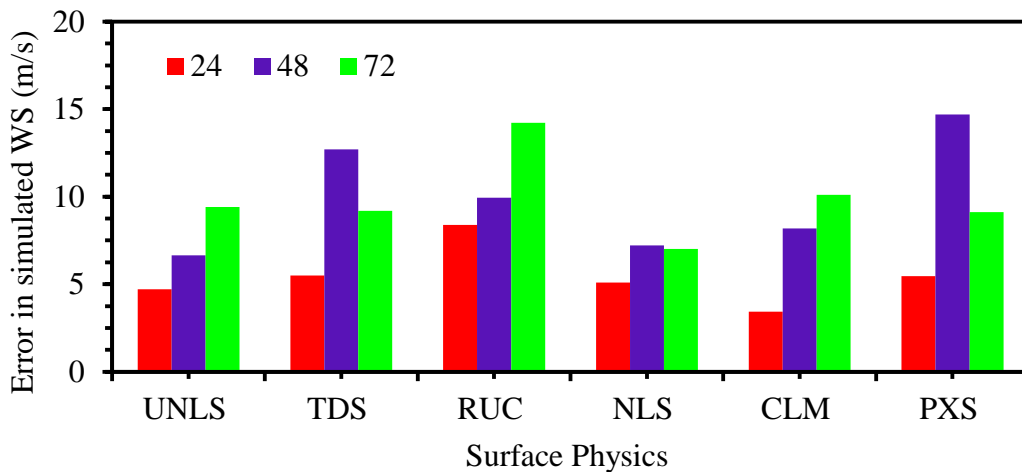


Figure 4.2.2.2(c): Model simulated wind speed error in the 24, 48, and 72-hr forecasts with respect to IMD observed of TC Mahasen by using six different LSM schemes.

It has been observed from the above data that RMS maximum wind speed errors are obtained between 7.4 to 10.4 m/s and three land surface model schemes UNLS, NLS and CLM4 scheme for the land surface model gives the less errors those are 7.4, 7.4 and 7.6 m/s

respectively whereas land surface model RUC scheme gives the maximum wind speed error 10.4 m/s with respect to IMD observation. All the cases produce a strong cyclone.

Therefore, it may be concluded from the above discussion the combination of NLS for the land surface model gives least error 7.4 m/s with respect to IMD observation.

4.2.2.3 Effect of the land surface model on CSLP

The intensity of the cyclone from the point of CSLP is generally over-predicted by all the schemes, as can be seen from the time series values which are too low for a category storm. The propagation of simulated cyclone CSLP for various combinations of land surface model with IMD observed have been presented in figure 4.2.2.3(a). Figure 4.2.2.3(b) has been shown the CSLP error for all LSM schemes compared with IMD observation data. CSLP errors at 24, 48, 72 hours are shown in figure 4.2.2.3(c) as a histogram plot.

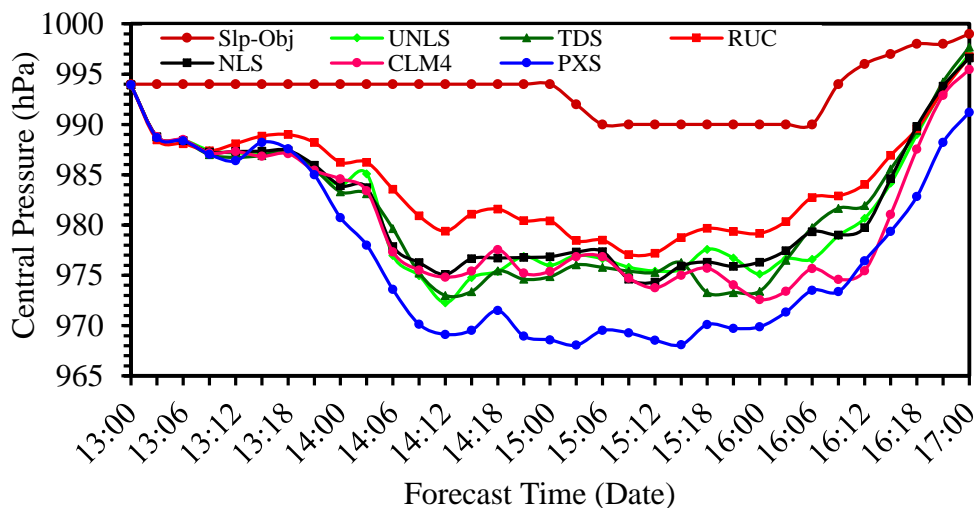


Figure 4.2.2.3(a): Model simulated CSLP with IMD observed of TC Mahasen by using six different LSM schemes.

This parametrization also indicate that the model ‘produces’ a strong storm. All the cases produce a strong cyclone from the initial on 13 May from 00 UTC to 17 May 00 UTC.

For all the cases the RMS errors of CSLP are obtained from 90 hr with 6 hourly intervals those are 13.2, 13.2, 9.9, 12.6, 13.7 and 17.3 hPa in the case of UNLS, TDS, RUC, NLS, CLM4 and PXS schemes of LSM respectively.

It has been observed from the above data that RMS maximum CSLP errors are obtained between 9.9 to 17.3 hPa and three land surface model UNLS, RUC and NLS give the less

errors those are 13.2, 9.9 and 12.6 hPa respectively whereas land surface model PXS scheme gives the maximum error 17.3 hPa with respect to IMD observation. All the cases produce a strong cyclone.

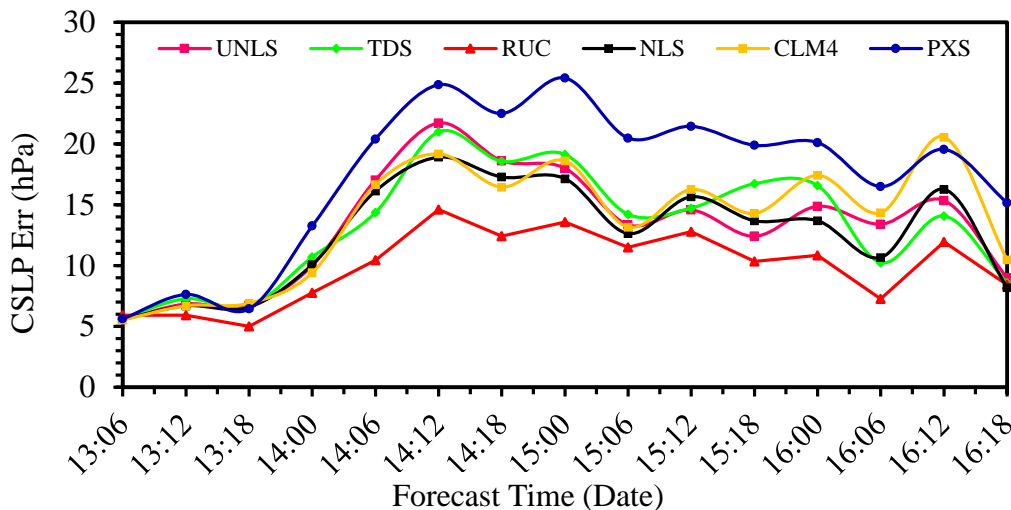


Figure 4.2.2.3(b): Model simulated CSLP error with respect to IMD observed of TC Mahasen by using six different LSM schemes.

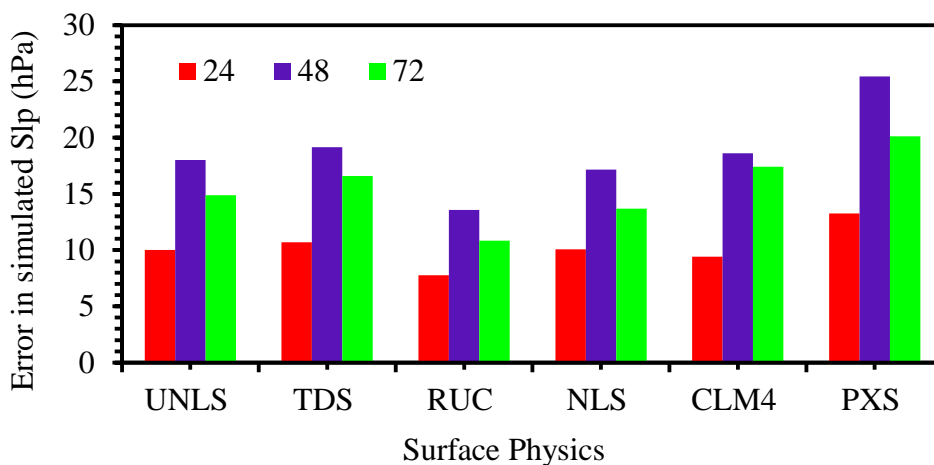


Figure 4.2.2.3(c): Model simulated CSLP error in the 24, 48, and 72-hr forecasts with respect to IMD observed of TC Mahasen by using six different LSM schemes.

Therefore, it may be concluded from the above discussion the combination of RUC for the land surface model gives least error 9.9 hPa with respect to IMD observation from the six numerical experiments.

From the six numerical experiments, it is clear that track propagation and RMS error among these six schemes have small variations, so the track prediction is indeed very sensitive to

land surface model. There is few significant variation in the RMS error is 153 and 157 km between the CLM4 and NLS schemes and from the point of view propagation of the track, CLM4 scheme is good. However, it is instructive to mention here that the NLS scheme over predicts the wind speed RMS as 7.4 m/s but CLM4 scheme is 7.6 m/s and UNLS scheme is 7.4 m/s with respect to the IMD wind speed data. On the another hand the RUC scheme over predicts the CSLP RMS error is 9.9 hPa but NLS scheme is 12.6 and UNLS scheme is 13.2 hPa with respect to the IMD CSLP data show as given in and they have small variation of those errors.

Finally it is strongly recommending that considering from the RMS errors of track, wind and CSLP, the combination of NLS for the land surface model gives least error with respect to IMD observation from the six numerical experiments. So NLS scheme has been chosen the best scheme for next experiment.

4.2.3 Short wave radiation schemes

The radiation schemes in the model provide the atmospheric heating due to radiation flux from the Sun and the short wave radiation schemes handle the process of absorption, reflection and scattering in the atmosphere and from the surface. In this study, numerical experiments were conducted with six different short wave radiation schemes. In this set of experiments, six different short wave radiation schemes have been considered along with the BMJ scheme for the cumulus, a combination of MRF for the PBL and MON for the surface layer parameterization, WSM3 for the microphysics scheme and NLS for the land surface model. Various short wave radiation schemes options are Dudhia, GSFC (ARW+Chem(τ)), CAM, RRTMG, New Goddard and FLG schemes. The other physics options are kept fixed, as shown in table 3.4.

4.2.3.1 Effect of the short wave radiation on track

The propagation of tracks are shown in figure 4.2.3.1(a). Figure 4.2.3.1(b) has been shown the track error for all the short wave radiation schemes compared with IMD observation data. Track errors at 24, 48, 72 hours are shown in figure 4.2.3.1(c) as a histogram plot.

As expected, for all the cases the track errors increase with forecast time and the RMS errors of track are obtained from 90 hr with 6 hr intervals those are 157, 147, 180, 156, 181 and

146 km are obtained in the case of Dudhia, GSFC, CAM, RRTMG, New, Goddard and FLG schemes respectively. All tracks show North-Easterly movement of the cyclone.

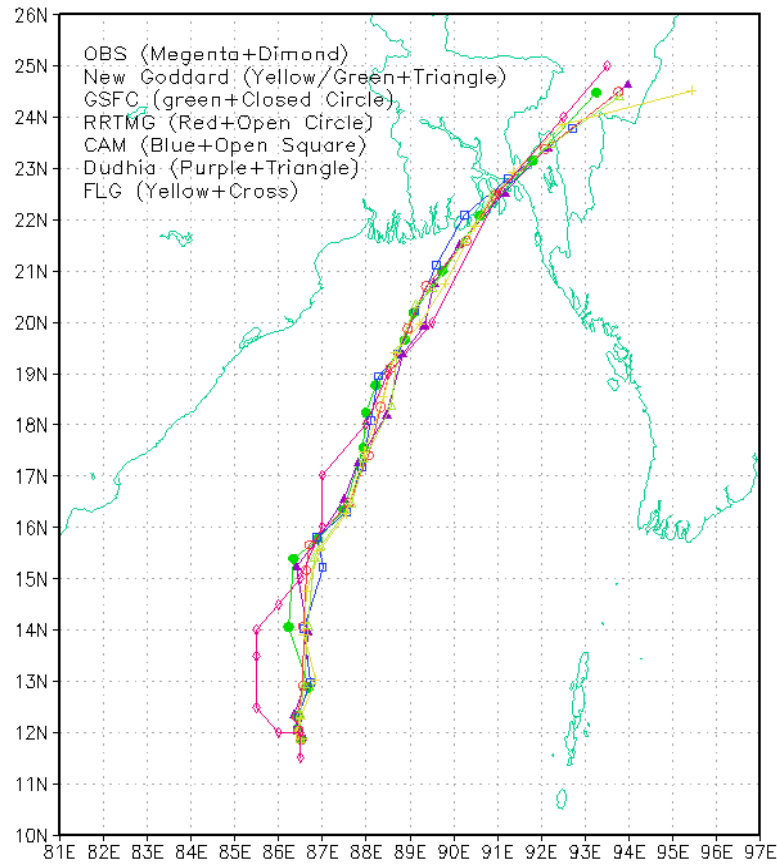


Figure 4.2.3.1(a): Model simulated track with IMD observed of TC Mahasen by using six different SWR schemes.

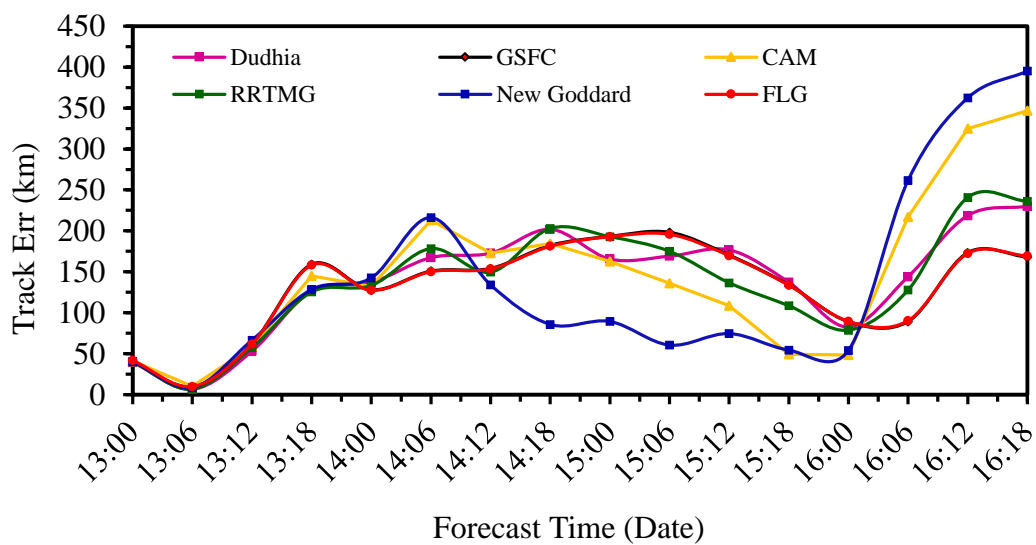


Figure 4.2.3.1(b): Model simulated track error with respect to IMD observed of TC Mahasen by using six different SWR schemes.

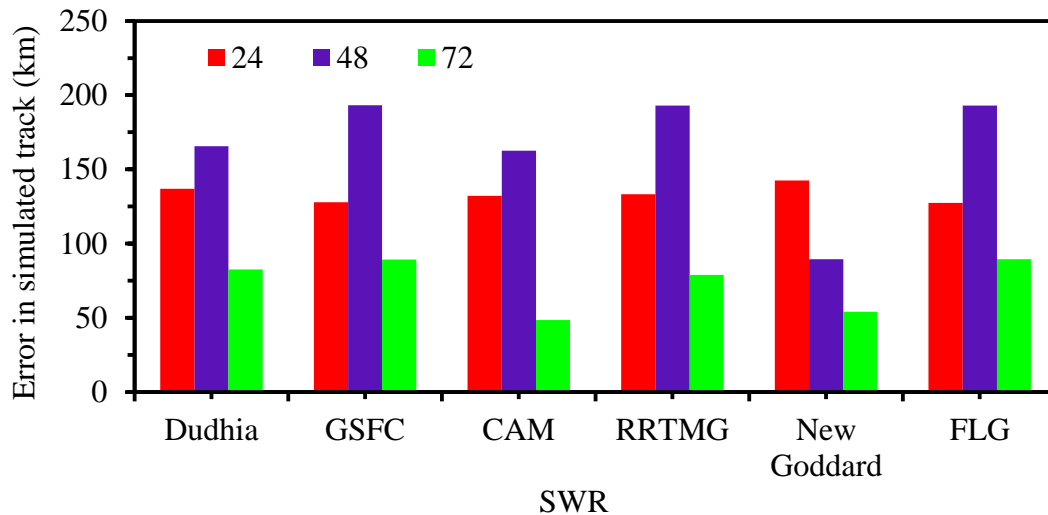


Figure 4.2.3.1(c): Model simulated track error in the 24, 48, and 72-hr forecasts with respect to IMD observed of TC Mahasen by using six different SWR schemes.

It has been observed from the above data that RMS track errors are obtained between 146 to 181 km and three short wave radiation schemes GSFC, RRTMG and FLG give the less errors those are 147, 156 and 146 km respectively whereas short wave radiation scheme New Goddard scheme gives the maximum track error 181 km with respect to IMD observation.

Therefore, it may be concluded from the above discussion the combination of FLG for the short wave radiation schemes gives least error 146 km with respect to IMD observation.

4.2.3.2 Effect of the short wave radiation schemes on wind speed

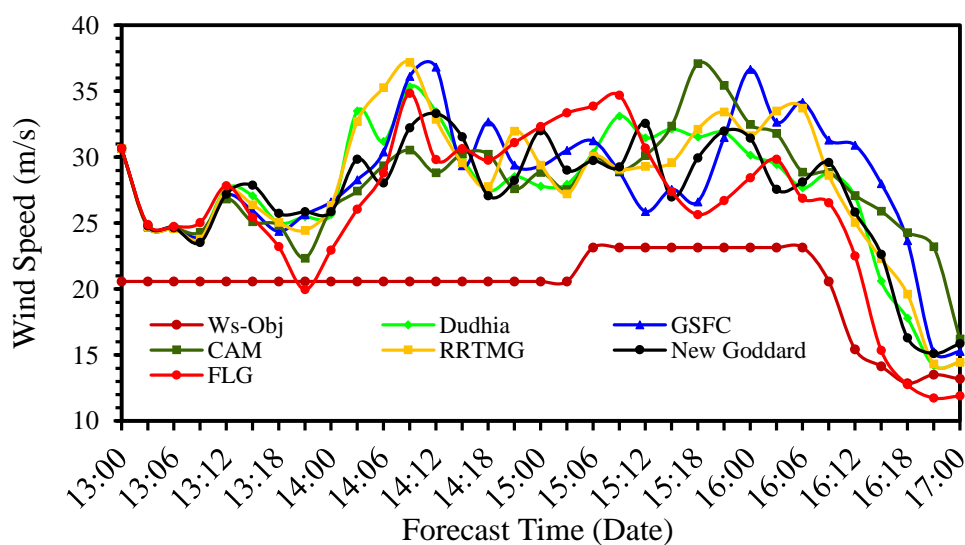


Figure 4.2.3.2(a): Model simulated wind speed with IMD observed of TC Mahasen by using six different SWR schemes.

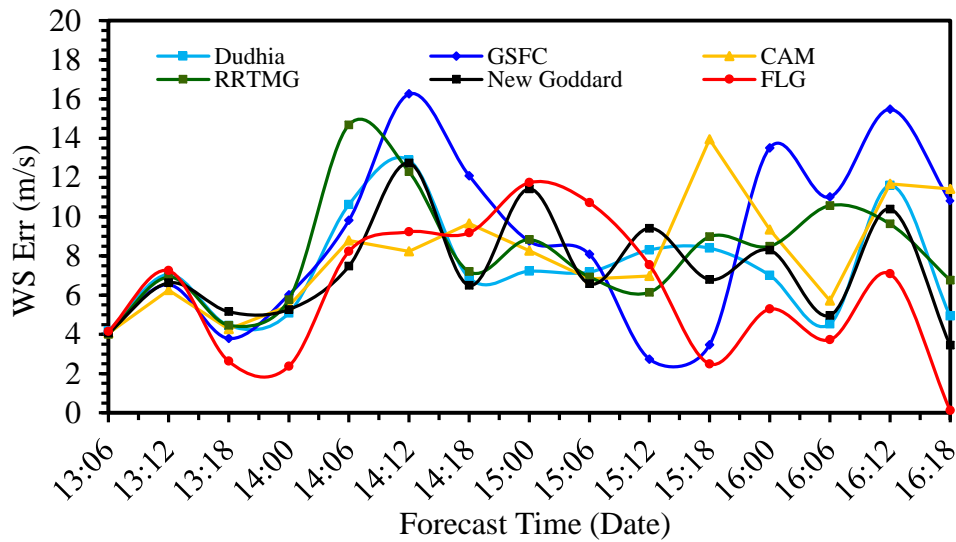


Figure 4.2.3.2(b): Model simulated wind speed error with respect to IMD observed of TC Mahasen by using six different SWR schemes.

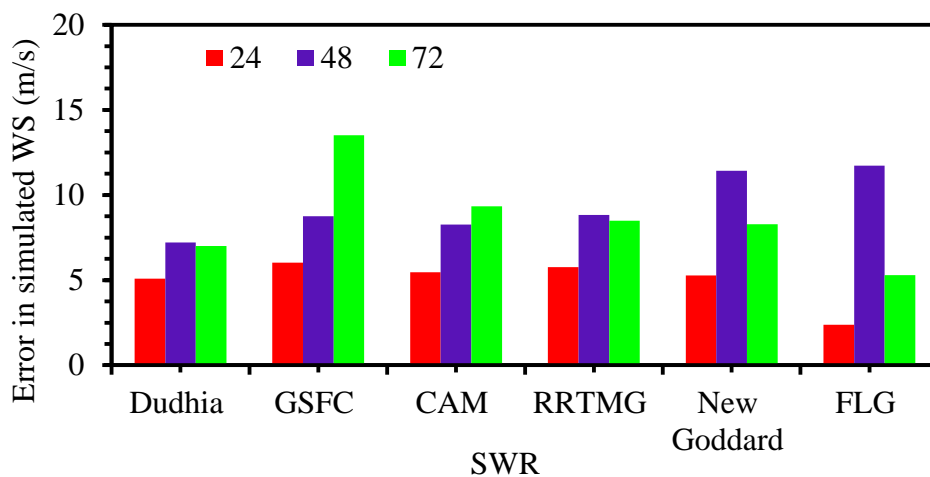


Figure 4.2.3.2(c): Model simulated wind speed error in the 24, 48, and 72-hr forecasts with respect to IMD observed of TC Mahasen by using six different SWR schemes.

Figure 4.2.3.2(a) has been shown the wind speeds obtained from the six different simulations and the corresponding IMD wind data for every 6 hourly interval. From the figure, it has been shown that initially all the simulations over-predict except FLG the wind speed compared to IMD wind data. Figure 4.2.3.2(b) has been shown the wind speed error for all short wave radiation schemes compared with IMD observation data. Wind speed errors at 24, 48, 72 hours are shown in figure 4.2.3.2(c) as a histogram plot. These experiments also indicate that the model ‘produces’ a strong storm. All the cases produce a strong cyclone from the initial on 13 May from 00 UTC to 17 May 00 UTC. For all the cases the RMS

errors of WS are obtained from 90 hr with 6 hourly intervals those are 7.4, 8.8, 8.1, 7.2 and 6.2 m/s in the case of Dudhia, GSFC, CAM, RRTMG, New Goddard and FLG schemes of SWR respectively. The IMD data is showing a maximum wind speed of 23 m/s at 06 UTC on 15 May to 06 UTC on 16 May 2013.

It has been observed from the above data that RMS maximum wind speed errors are obtained between 6.1 m/s to 8.8 m/s and three short wave radiation schemes FLG, Dudhia and New Goddard scheme for the short wave radiation give the less errors those are 6.2, 7.4 and 7.3 m/s respectively whereas short wave radiation GSFC scheme gives the maximum wind speed error 8.8 m/s with respect to IMD observation. All the cases produce a strong cyclone. Therefore, it may be concluded from the above discussion the combination of FLG for the short wave radiation scheme gives least error 4.6 m/s with respect to IMD observation.

4.2.3.3 Effect of the short wave radiation schemes on CSLP

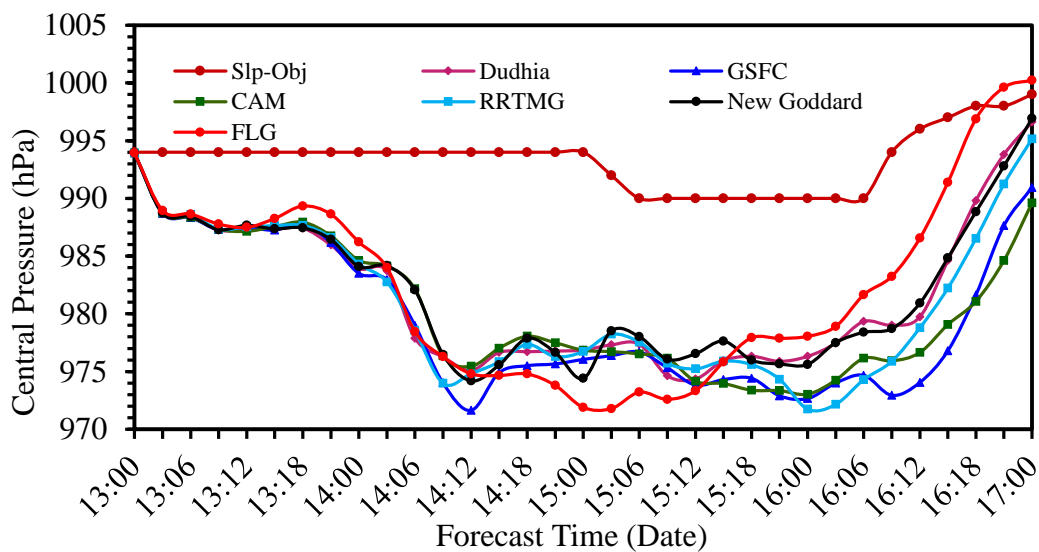


Figure 4.2.3.3(a): Model simulated CSLP with IMD observed of TC Mahasen by using six different SWR schemes.

The intensity of the cyclone from the point of CSLP is generally over-predicted by all the schemes, as can be seen from the time series values which are too low for a category storm. The propagation of simulated cyclone CSLP for various combinations of short wave radiation schemes have been presented in figure 4.2.3.3(a). Figure 4.2.3.3(b): has been shown the CSLP error for all short wave radiation schemes compared with IMD observation data. CSLP errors at 24, 48, 72 hours are shown in figure 4.2.3.3(c) as a histogram plot. This

parametrization also indicate that the model ‘produces’ a strong storm. All the cases produce a strong cyclone from the initial on 13 May from 00 UTC to 17 May 00 UTC. For all the cases the RMS errors of CSLP are obtained from 90 hr with 6 hourly intervals those are 12.6, 14.6, 13.6, 13.4, 12.4 and 11.8 hPa in the case of Dudhia, GSFC, CAM, RRTMG, New Godddard and FLG schemes of SWR respectively.

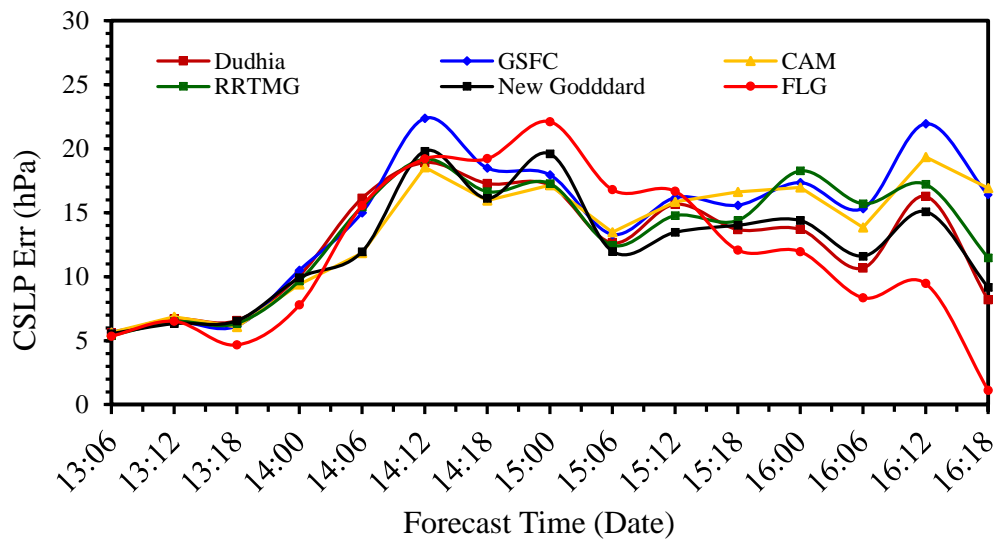


Figure 4.2.3.3(b): Model simulated CSLP error with respect to IMD observed of TC Mahasen by using six different SWR schemes.

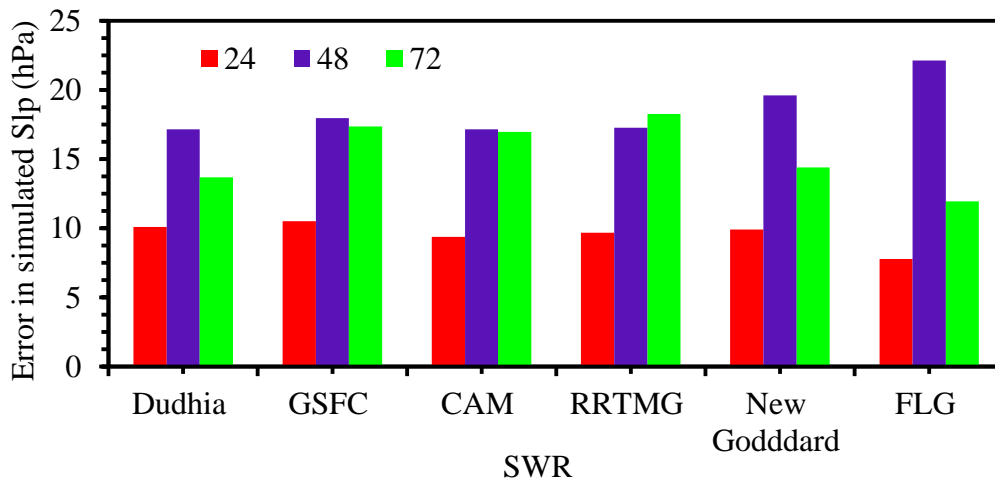


Figure 4.2.3.3(c): Model simulated CSLP error in the 24, 48, and 72-hr forecasts with respect to IMD observed of TC Mahasen by using six different SWR schemes.

It has been observed from the above data that RMS maximum CSLP errors are obtained between 11.8 to 14.6 hPa and three short wave radiation scheme FLG, Dudhia and New Godddard give the less errors those are 11.8, 12.6 and 12.4 hPa respectively whereas short

wave radiation GSFC scheme gives the maximum CSLP error 14.6 hPa with respect to IMD observation. All the cases produce a strong cyclone.

Therefore, it may be concluded from the above discussion the combination of FLG for the short wave radiation scheme gives least error 11.8 hPa with respect to IMD observation from the six numerical experiments.

From the six numerical experiments, it is clear that track propagation and track, WS and CSLP's RMS error among these six schemes have small variations. Finally considering from the RMS errors of track, wind and CSLP, the combination of FLG for the short wave radiation schemes gives least error with respect to IMD observation. So FLG scheme has been chosen the best scheme for the next experiment.

4.2.4 Long wave radiation schemes

The long wave radiation schemes handle the process of absorption and emission of infrared or thermal radiation by gases and surfaces. Simulations are carried out for five different long wave radiation scheme along with the best schemes determined from previous numerical experiments. In this study, numerical experiments were conducted with six different long wave radiation schemes. In this set of experiments, Six different long wave radiation schemes have been considered along with the BMJ scheme for the cumulus, a combination of MRF for the PBL and MON for the surface layer parameterization, WSM3 for the microphysics scheme, NLS for the land surface model and FLG scheme for the short wave radiation schemes. Various long wave radiation schemes options are RRTM, CAM Longwave (CAM), RRTMG, New Goddard, FLG and Held-Suarez scheme. The other physics options are kept fixed, as shown in table 3.4.

4.2.4.1 Effect of the long wave radiation on track

The propagation of tracks are shown in figure 4.2.4.1(a) and it has been shown that the propagation of simulated tracks closely follows the IMD observations. It is also showing the results for the track propagation and it has been shown that all the schemes produce a good match with the IMD observation track. Figure 4.2.4.1(b) has been shown the track error for all the long wave radiation schemes compared with IMD observation data.

Track errors at 24, 48, 72 hours are shown in figure 4.2.4.1(c) as a histogram plot. As expected, for all the cases the track errors increase with forecast time and the RMS errors of

track are obtained from 90 hr with 6 hr intervals those are 146, 156, 149, 139, 186 and 188 km are obtained in the case of RRTM, CAM, RRTMG, New Goddard, FLG and Held-Suarez schemes respectively. All tracks show North-Easterly movement of the cyclone.

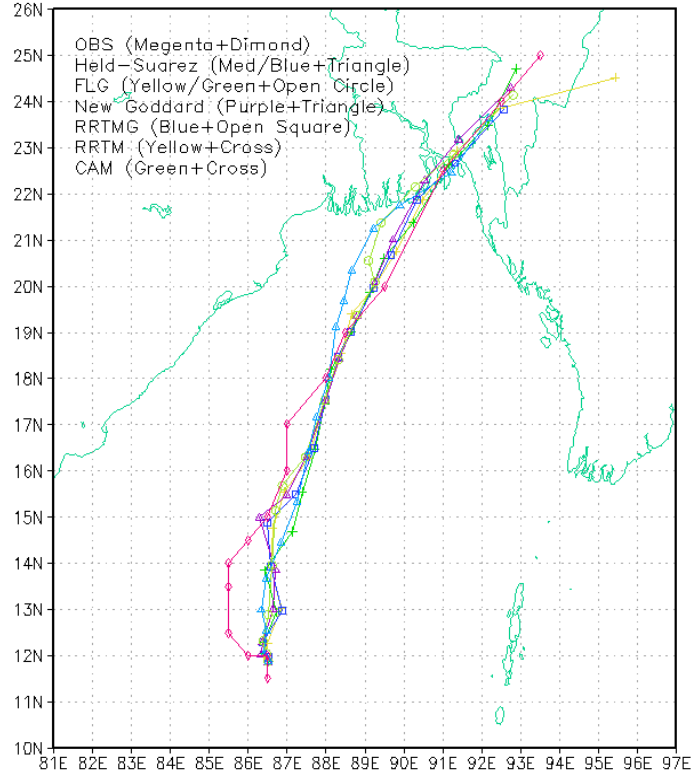


Figure 4.2.4.1(a): Model simulated track with IMD observed of TC Mahasen by using five different LWR schemes.

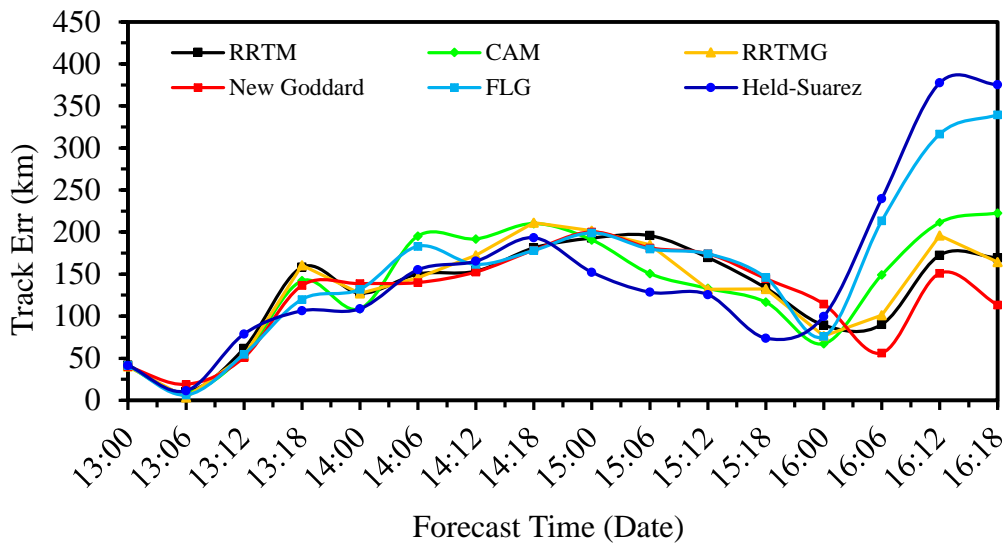


Figure 4.2.4.1(b): Model simulated track error with respect to IMD observed of TC Mahasen by using five different LWR schemes.

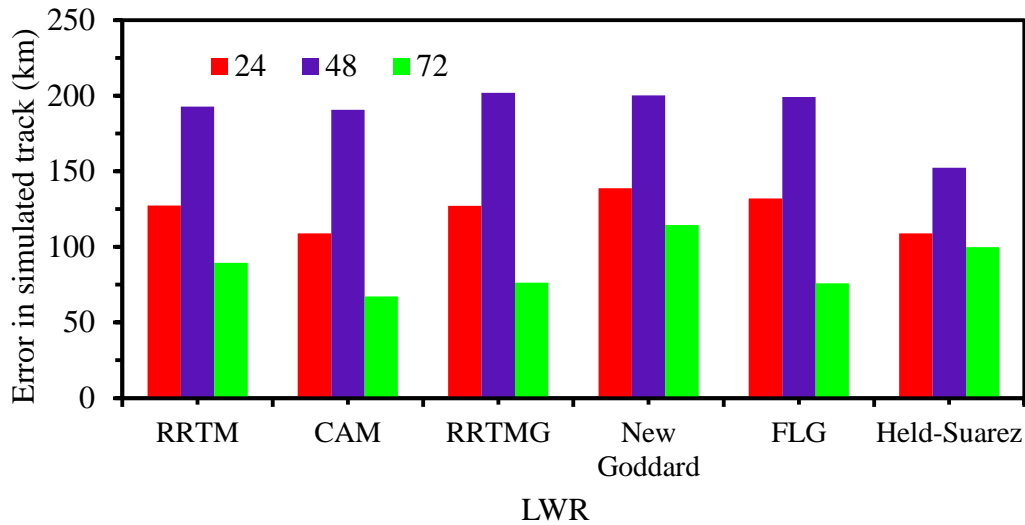


Figure 4.2.4.1(c): Model simulated track error in the 24, 48, and 72-hr forecasts with respect to IMD observed of TC Mahasen by using five different LWR schemes.

It has been observed from the above data that RMS track errors are obtained between 139 to 188 km and tree long wave radiation schemes RRTM, RRTMG and New Goddard give the less errors those are 146, 149 and 139 km respectively whereas long wave radiation scheme Held-Suarez gives the maximum track error 188 km with respect to IMD observation.

Therefore, it may be concluded from the above discussion the combination of New Goddard for the long wave radiation schemes gives least error 139 km with respect to IMD observation.

4.2.4.2 Effect of the long wave radiation schemes on wind speed

Figure 4.2.4.2(a) has been shown the wind speeds obtained from the six different simulations and the corresponding IMD wind data for every 6 hourly interval. From the figure, it has been shown that initially New Goddard, FLG and Held-Suarez the simulations over-predict but RRTM, CAM and RRTMG are predict the wind speed compared to IMD wind data. Figure 4.2.4.2(b) has been shown the wind speed error for all long wave radiation schemes compared with IMD observation data. Wind speed errors at 24, 48, 72 hours are shown in figure 4.2.4.2(c) as a histogram plot. This parametrization also indicate that the model ‘produces’ a strong storm. All the cases produce a strong cyclone from the initial on 13 May from 00 UTC to 17 May 00 UTC.

For all the cases the RMS errors of WS are obtained from 90 hr with 6 hourly intervals those are 6.1, 5.8, 6.4, 6.5, 8.8 and 6.8 m/s in the case of RRTM, CAM, RRTMG, New Goddard,

FLG and Hel-Suarez schemes of LWR respectively. The IMD data is showing a maximum wind speed of 23 m/s at 06 UTC on 15 May to 06 UTC on 16 May 2013.

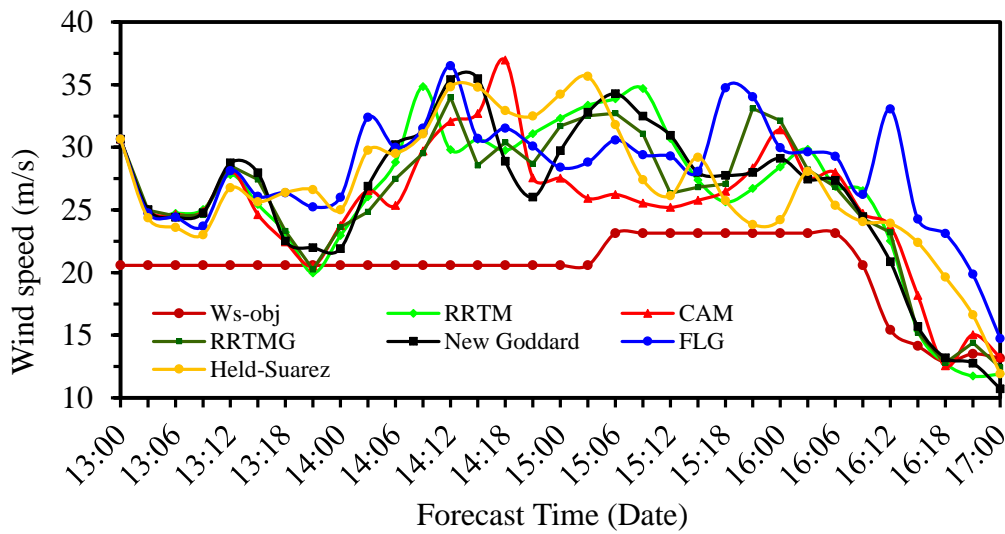


Figure 4.2.4.2(a): Model simulated wind speed with IMD observed of TC Mahasen by using five different LWR schemes.

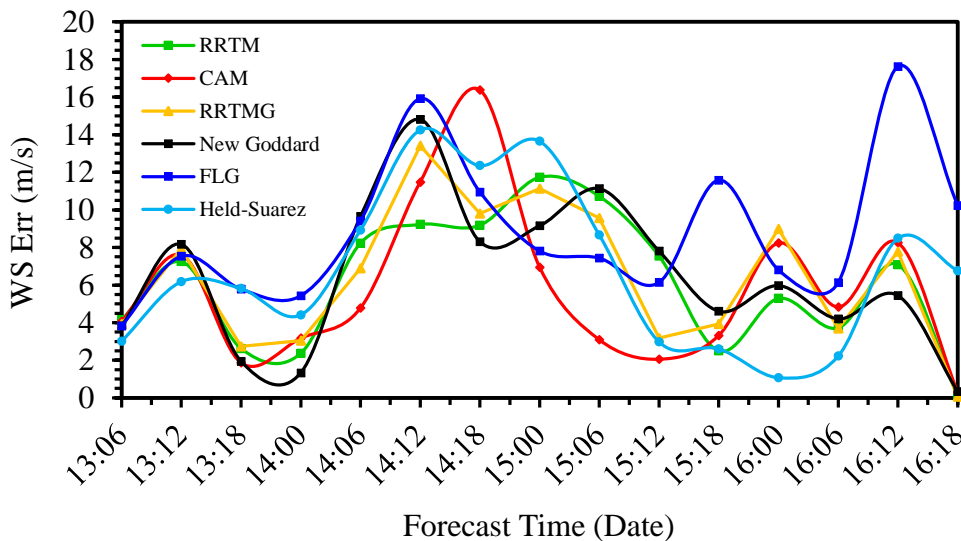


Figure 4.2.4.2(b): Model simulated wind speed error with respect to IMD observed of TC Mahasen by using five different LWR schemes.

It has been observed from the above data that RMS maximum wind speed errors are obtained between 5.8 to 8.8 m/s and three long wave radiation schemes RRTM, CAM and RRTMG scheme for the long wave radiation give the less errors those are 6.1, 5.8 and 6.4 m/s respectively whereas long wave radiation FLG scheme gives the maximum wind speed error 8.8 m/s with respect to IMD observation. All the cases produce a strong cyclone.

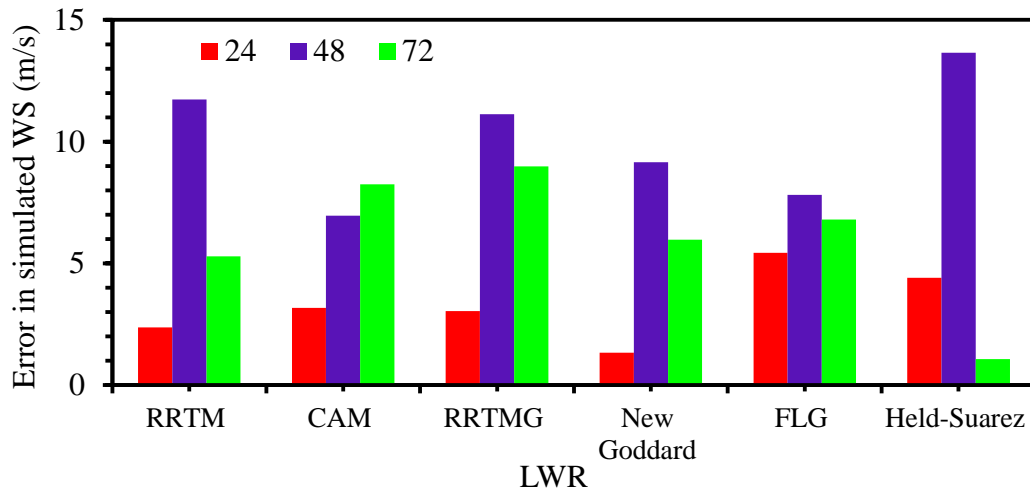


Figure 4.2.4.2(c): Model simulated wind speed error in the 24, 48, and 72-hr forecasts with respect to IMD observed of TC Mahasen by using five different LWR schemes.

Therefore, it may be concluded from the above discussion the combination of CAM for the long wave radiation scheme gives least error 5.8 m/s with respect to IMD observation.

4.2.4.3 Effect of the long wave radiation schemes on CSLP

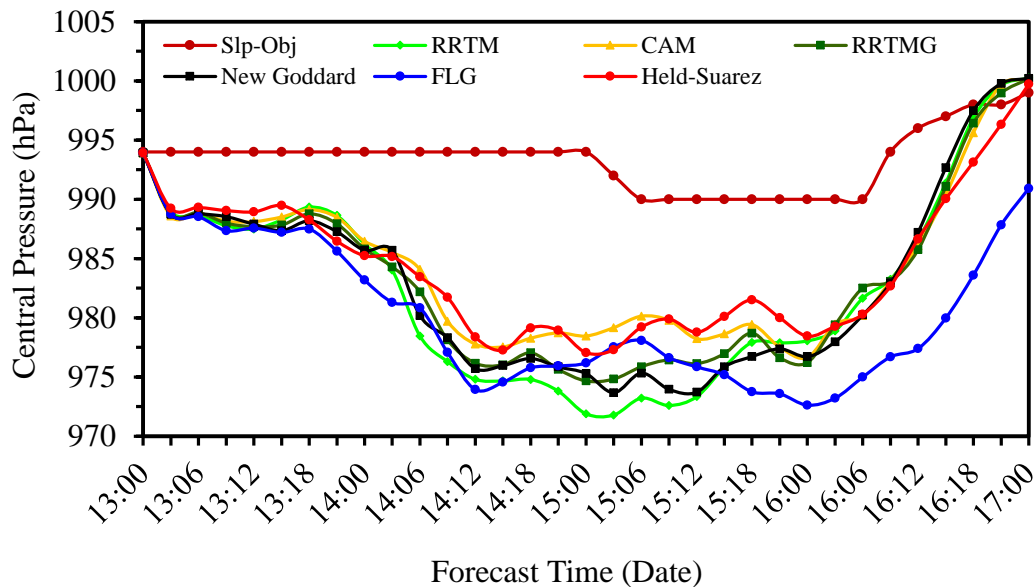


Figure 4.2.4.3(a): Model simulated CSLP with IMD observed of TC Mahasen by using five different LWR schemes.

The intensity of the cyclone from the point of CSLP is generally over-predicted by all the schemes, as can be seen from the time series values which are too low for a category storm. The propagation of simulated cyclone CSLP for various combinations of long wave radiation

schemes have been presented in figure 4.2.4.3(a). Figure 4.2.4.3(b) has been shown the CSLP error for all long wave radiation schemes compared with IMD observation data. CSLP errors at 24, 48, 72 hours are shown in figure 4.2.4.3(c) as a histogram plot. This parametrization also indicate that the model ‘produces’ a strong storm. All the cases produce a strong cyclone from the initial on 13 May from 00 UTC to 17 May 00 UTC.

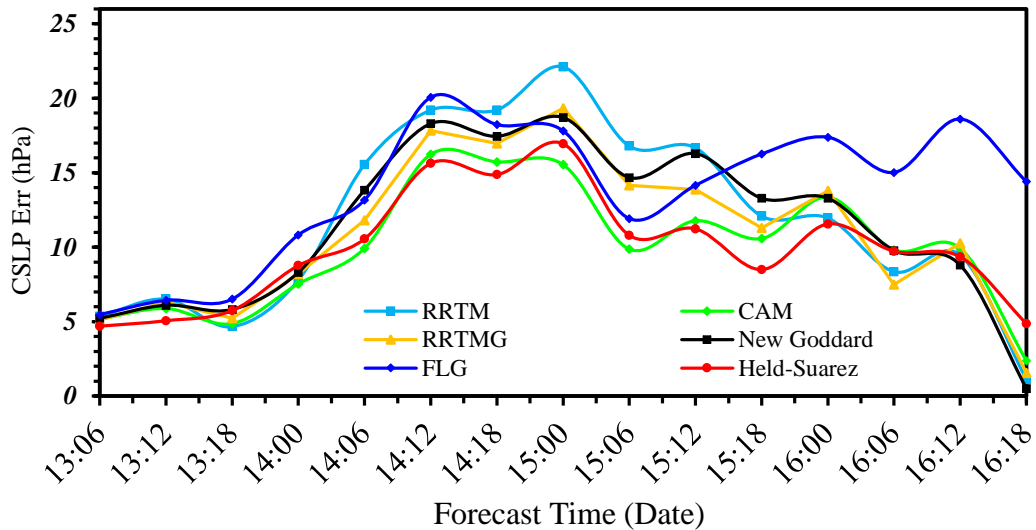


Figure 4.2.4.3(b): Model simulated CSLP error with respect to IMD observed of TC Mahasen by using five different LWR schemes.

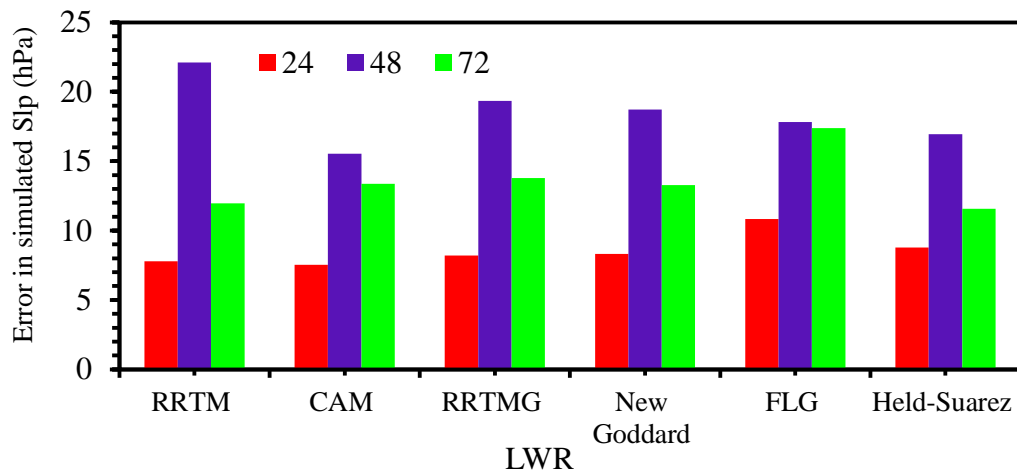


Figure 4.2.4.3(c): Model simulated CSLP error in the 24, 48, and 72-hr forecasts with respect to IMD observed of TC Mahasen by using five different LWR schemes.

For all the cases the RMS errors of CSLP are obtained from 90 hr with 6 hourly intervals those are 11.8, 9.9, 10.9, 11.4, 13.8 and 9.9 hPa in the case of RRTM, CAM, RRTMG, New Goddard, FLG and Held-Suarez schemes of LWR respectively.

It has been observed from the above data that RMS maximum CSLP errors are obtained between 9.9 to 14.6 hPa and three long wave radiation scheme CAM, RRTMG and Held-Suarez give the less errors those are 9.9, 10.9 and 9.9 hPa respectively whereas long wave radiation FLG scheme gives the maximum CSLP error 13.8 hPa with respect to IMD observation. All the cases produce a strong cyclone.

Therefore, it may be concluded from the above discussion the combination of Held-Suarez for the long wave radiation scheme gives least error 9.9 hPa with respect to IMD observation from the six numerical experiments.

From the six numerical experiments, it is clear that track propagation and RMS error among these six schemes have small variations, so the track prediction is indeed very sensitive to long wave radiation schemes. There is few significant variation in the RMS error is 139 and 146 km between the New Goddard and RRTM schemes and from the point of view propagation of the track, New Goddard scheme is good. However, it is instructive to mention here that the CAM scheme over predicts the wind speed RMS as 5.8 m/s but RRTM, RRTMG and New Goddard schemes are 6.1, 6.4 and 6.5 m/s with respect to the IMD wind speed data. On the another hand the Held-Suarez scheme over predicts the CSLP RMS error is 9.9 hPa but CAM, RRTMG and New Goddard schemes are 9.9, 10.9 and 11.4 hPa with respect to the IMD CSLP data and they have small variation of those errors.

Finally it is strongly recommending that considering from the RMS errors of track, wind and CSLP, the combination of New Goddard for the long wave radiation schemes gives least error with respect to IMD observation from the six numerical experiments.

Table 4.2.1: Compare final result of the two experiments

Set No.	Name of Physical parameterization	Cumulus	PBL	Microphysics	LSM	SWR	LWR
1 st	Name of Schemes	BMJ	MRF	WSM3	UNLS	Dudhia	RRTM
	Track (RMS err km)	212	174	123	123	123	123
	WS (RMS err m/s)	12.1	8.8	4.6	4.6	4.6	4.6
	CSLP (RMS err hPa)	18.5	11.4	6.6	6.6	6.6	6.6

	Name of Scheme	BMJ	MYNN2	WSM3	NLS	FLG	New Goddard
2 nd	Track (RMS err km)	212	184	161	157	146	139
	Ws (RMS err m/s)	12.1	10.1	7.4	7.4	6.1	6.5
	CSLP (RMS err hPa)	18.5	16.1	13.2	12.6	11.8	11.4

Above discussion and from the table 4.2.1, it is clear that the least RMS error values are 1st set then the 2nd set obtained of the experiments. So it is clear that 1st set of experiment is the best determine.

CHAPTER V

Conclusions

In this research, WRF-ARW model has been used to simulate the sensitivity of TC Mahasen that formed in the Bay of Bengal and crossed the coasts of Bangladesh- Myanmar in the month of May 2013. Final Reanalysis (FNL) data ($1^\circ \times 1^\circ$) collected from National Centre for Environment Prediction (NCEP) is used as initial and lateral boundary conditions (LBCs) which is updated at six hours interval i.e. the model is initialized with 0000, 0600, 1200 and 1800 UTC initial field of corresponding date. The model has been integrated for 96 hr from 2013-05-13_00:00:00 to 2013-05-17_00_00_00 for TC Mahasen. To understand the knowledge about the sensitivity of tropical cyclone Mahasen, two sets of experiments have been conducted using different parameterization schemes available in WRF model. Firstly 48 and secondly 49 experiments have been conducted in TC Mahasen by using five different cumulus, ten different PBL, sixteen different microphysics, six different LSM, six different SWR and six different LWR schemes except first set of experiment without CAM.

To examine the effect on the track, wind speed at 10m height and central sea level pressure of TC Mahasen, the model domain which covered the region 2.05° - 26.48° N & 73.96° - 97.04° E are used. Through this, several physical parameterizations in the WRFV3 model were exhaustively tested.

On the basis of the present study, the following conclusions are drawn:

- ❖ For the sensitivity study for the cyclone track, all cumulus schemes could predict North-Easterly movement for the cyclone Mahasen as like as observed track obtained from IMD. For the prediction of track, Wind and SLP, least RMS errors are obtained from GF, BMJ and BMJ cumulus schemes respectively. Finally, considering the RMS error of the CU, BMJ scheme Performance is consider the best one.
- ❖ For the sensitivity study for the cyclone track, all PBL schemes could predict North-Easterly movement for the cyclone Mahasen as like as observed track obtained from IMD. For the prediction of track, Wind and SLP, least RMS errors are obtained using MRF, PBL schemes for all the cases. Finally, considering the RMS error of the PBL, MRF scheme Performance is consider the best one.
- ❖ For the sensitivity study for the cyclone track, all microphysics schemes could predict North-Easterly movement for the cyclone Mahasen as like as observed track obtained from IMD. For the prediction of track, Wind and SLP, least RMS errors are obtained

WSM3 microphysics schemes for all cases. Another set of experiments considering for the prediction of track, Wind and SLP, least RMS errors are also obtained using WSM3 microphysics schemes but the RMS error value of track, Wind and CSLP for 1st set experiments are lower than that obtained using 2nd set of experiments. Finally considering the RMS error compared with both sets of the MP, WSM3 scheme Performance is considered the best one.

- ❖ For the sensitivity study for the cyclone track, all LSM schemes could predict North-Easterly movement for the cyclone Mahasen as like as observed track obtained from IMD. For the prediction of track, Wind and SLP, least RMS errors are obtained from UNLS, UNLS and RUC LSM schemes respectively and considering the RMS error, UNLS scheme is consider the best one. Another set of experiments considering for the prediction of track, Wind and SLP, least RMS errors are obtained from CLM4, NLS and NLS LSM schemes respectively and considering the RMS error, NLS scheme is the best one. Finally considering the RMS error compared with both sets of the LMS, UNLS scheme Performance is considered the best one.
- ❖ For the sensitivity study for the cyclone track, all SWR schemes could predict North-Easterly movement for the cyclone Mahasen as like as observed track obtained from IMD. For the prediction of track, Wind and SLP, least RMS errors are obtained from Dudhia, Dudhia and FLG SWR schemes respectively and considering the RMS error, Dudhia scheme is consider the best one. Another set of experiments considering for the prediction of track, Wind and SLP, least RMS errors are obtained FLG scheme and considering the RMS error, FLG scheme is the best one. Finally considering the RMS error obtained from both sets of the SWR, Dhudhia scheme performance is considered the best one.
- ❖ For the sensitivity study for the cyclone track, all LWR schemes could predict North-Easterly movement for the cyclone Mahasen as like as observed track obtained from IMD. For the prediction of track, Wind and SLP, least RMS errors are obtained from RRTM, RRTM and RRTMG LWR respectively and considering the RMS error, RRTM scheme is consider the best one. Another set of experiments considering for the prediction of track, Wind and SLP, least RMS errors are obtained from New Goddard, CAM and Held-Suarez and considering the RMS error, New Goddard scheme is the best one. Finally considering the RMS error obtained from both sets of the LWR, RRTM scheme Performance is considered the best one.

Reference

1. Ali, A., (1999); “Climate change impacts and adaptation assessment in Bangladesh.”
Climate Research, 12: 109-116.
2. Ali, A., 1999a: Ghurnijhar, BanglaAcademy, Dhaka.
3. Angevine, Hongli Jiang and Thorsten Mauritsen, 2010; “Performance of an Eddy
Diffusivity–Mass Flux Scheme for Shallow Cumulus Boundary Layers.”
Cooperative Institute for Research in Environmental Sciences, University of
Colorado, and NOAA/Earth System Research Laboratory, Boulder, Colorado.
NOAA/Earth System Research Laboratory, Boulder, and Cooperative Institute
for Research in the Atmosphere, Colorado State University, Fort Collins,
Colorado. Max Planck Institute for Meteorology, Hamburg, Germany.
4. Arakawa and Wayne Howard Schubert, 1974; “Interaction of a Cumulus Cloud
Ensemble with the Large-Scale Environment, Part I.” Dept. of Meteorology,
University of California, Los Angeles 90024. Journal of the Atmospheric
Sciences, Vol. 31: 674-701.
[doi.org/10.1175/1520-0469\(1974\)031<0674:IOACCE>2.0.CO;2](https://doi.org/10.1175/1520-0469(1974)031<0674:IOACCE>2.0.CO;2)
5. Arakawa J.-H. Jung, 2011; “Multiscale modeling of the moist-convective atmosphere
— A review.” University of California, Los Angeles, CA, USA Colorado State
University, Fort Collins, CO, USA.
doi.org/10.1016/j.atmosres.2011.08.009Get rights and content
6. Betts and M. J. Miller, (1986); “A new convective adjustment scheme. Part 11: Single
column tests using GATE wave, BOMEX, ATEX and arctic air-mass data sets.”
West Pawlet, VT 05775, U.S.A and *Quart. J. R. Met. Soc.*, 112, pp. 693-709.
7. Bougeault, P. and Lacarrere, P.: 1989, “Parameterization of Orography-Induced
Turbulence in a Mesobeta-Scale Model.” *Mon. Wea. Rev.* 117, 1872–1890.
[doi.org/10.1175/1520-0493\(1989\)117<1872:POOITI>2.0.CO;2](https://doi.org/10.1175/1520-0493(1989)117<1872:POOITI>2.0.CO;2)
8. Bretherton, C.S. and Park, S., (2009); “A New Moist Turbulence Parameterization in
the Community Atmosphere Model.” *Journal of Climate*, 22, 3422-3448.
doi.org/10.1175/2008JCLI2556.1
9. Brian Eaton NCAR, “User’s Guide to the Community Atmosphere Model CAM-
5.1.”: 1-34.

10. Canuto, Y. Cheng and A. M. Howard, 2008; "A new model for Double Diffusion + Turbulence." *GEOPHYSICAL RESEARCH LETTERS*, VOL. 35, L02613.
doi: 10.1029/2007GL032580,
11. Chen, S. H., and W. Y. Sun, 2002; "The applications of the multi grid method and a flexible hybrid coordinate in a non-hydrostatic model." *Mon. Wea. Rev.* 129, 2660–2676.
12. Chou, M. D., Suarez, M. J., Liang, X. Z., and Yan, M. M. H., 2001: "A thermal infrared radiation parameterization for atmospheric studies, NASA Tech." Memo, 104606, 56.
doi: dopu.cs.auc.dk, available online at ftp://climate.gsfc.nasa.gov/chou/clirad lw/.
13. Chou, M.-D., and M. J. Suarez, 1999: A shortwave radiation parameterization for atmospheric studies. NASA Tech. Memo., 15(104606), 40 pp.
14. Choudhury, M.A., 2009: *Protecting Bangladesh from Natural Disasters*, Academic Press and publishers Library, Dhaka.
15. Collins, W. D., Rasch, P. J., Boville, B. A., Hack, J. J., McCaa, J. R., Williamson, D. L., Kiehl, J. T., Briegleb, B., Bitz, C., Lin, S., and *et al.* 2004; "Description of the NCAR community atmosphere model (*CAM 3.0*), NCAR Tech." nCAR/TN-464+ STR.
16. Deshpande M, Pattnaik S and Salvekar P, 2010; "Impact of physical parameterization schemes on numerical simulation of super cyclone Gonu." *Nat Hazards*, No.55: 211–231.
DOI: 10.1007/s11069-010-9521-x DOI:10.2151/jmsj.87.895
17. Dudhia, J., 1989; "Numerical Study of convection observed during the winter Monsoon experiment using a mesoscale two-dimensional model." *J. Atmos. Sci.*, 46: 3077-3107.
18. Dudhia, J., S-y Hong, and K.-S. Lim, 2008; "A new method for representing mixed phase particle fall speeds in bulk microphysics parameterizations." *J. Met. Soc. Japan*, in press.
19. Evans, J.L., 1992: Comment on "Can existing climate models be used to study anthropogenic changes in tropical cyclone climate?" *Geophys. Res. Lett.*, 19, 1523-1524
doi: 10.1029/92GL01120

20. Fu and K. N. Liou, 1993; "Parameterization of the Radiative Properties of Cirrus Clouds." JOURNAL OF THE ATMOSPHERIC SCIENCES. Vol-50, No-13:2008-2025.
doi.org/10.1175/1520-0469(1993)050<2008:POTRPO>2.0.CO;2
21. Fu and Liou, 1992; "On the Correlated k-Distribution Method for Radiative Transfer in Nonhomogeneous Atmospheres." Department of Meteorology/CARSS, University of Utah, Salt Lake City, Utah.
doi.org/10.1175/1520-0469(1992)049<2139:OTCDMF>2.0.CO;2
22. Fu, K. N. Liou, M. C. Cribb, T. P. Charlock and A. Grossman, 1997; "Multiple Scattering Parameterization in Thermal Infrared Radiative Transfer" Atmospheric Sciences Division, Lawrence Livermore National Laboratories, Livermore, California.
doi.org/10.1175/1520-0469(1997)054<2799:MSPITI>2.0.CO;2
23. Grell and S. R. Freitas, 2014; "A scale and aerosol aware stochastic convective parameterization for weather and air quality modeling." Earth Systems Research Laboratory of the National Oceanic and Atmospheric Administration (NOAA), Boulder, Colorado 80305-3337, USA. Center for Weather Forecasting and Climate Studies, INPE, Cachoeira Paulista, Sao Paulo, Brazil.
24. Grell, G. A., 1993; "Prognostic evaluation of assumptions used by cumulus parameterizations." Monthly Weather Review, 121, 764-787.
doi: 10.1175/1520-0493(1993)121<0764:PEOAUB>2.0.CO;2.
25. Grenier and Christopher S. Bretherton, 2001; "A Moist PBL Parameterization for Large-Scale Models and Its Application to Subtropical Cloud-Topped Marine Boundary Layers." Department of Atmospheric Sciences, University of Washington, Seattle, Washington.
doi.org/10.1175/1520-0493(2001)129<0357:AMPPFL>2.0.CO;2
26. Han and Pan, 2011; "Revision of Convection and Vertical Diffusion Schemes in the NCEP Global Forecast System." Wyle Information Systems LLC, and National Centers for Environmental Prediction/Environmental Modeling Center, Camp Springs, Maryland. National Centers for Environmental Prediction/Environmental Modeling Center, Camp Springs, Maryland.
doi.org/10.1175/WAF-D-10-05038.1

27. Henderson-Sellers, A., H. Zhang, G. Berz, K. Emanuel, W. Gray, C. Landsea, G. Holland, J. Lighthill, S.-L. Shieh, P. Webster, and K. McGuffie, 1998; "Tropical Cyclones and Global climate change: A. Post-IPCC Assessment. Bull. Amer. Meteor. Soc., 79, 19.
28. Holtslag and B. A. Boville, 1993; "Local Versus Nonlocal Boundary-Layer Diffusion in a Global Climate Model." Royal Netherlands Meteorological Institute (KNMI), De Bilt, the Netherlands National Center for Atmospheric Research, Boulder, Colorado.
doi.org/10.1175/1520-0442(1993)006<1825:LVNBLD>2.0.CO;2
29. Hong and Lim, 2006; "The WRF single-moment 6-class microphysics scheme (WSM6)." Global Environment Laboratory, Department of Atmospheric Sciences, Yonsei University, Seoul, South Korea.
30. Hong, S. Y., and J. O. J. Lim, 2006; "The WRF Single Moment 6-Class Microphysics Scheme (WSM6)." J Korean Meteorol. Soc., 42, 2: 129-151
31. Hong, S.-Y., 2007; "Stable Boundary Layer Mixing in a Vertical Diffusion Scheme." The Korea Meteor. Soc., Fall conference, Seoul, Korea, Oct. 25-26.
32. Hong, S.-Y., H.-M. H. Juang, and Q. Zhao, 1998; "Implementation of prognostic cloud scheme for a regional spectral model." Mon. Wea. Rev., 126, 2621–2639.
33. Hong, Song-You, and Hua-Lu Pan, 1996; "Nonlocal boundary layer vertical diffusion in a medium-range forecast model." Monthly weather review 124, 10: 2322-2339.
34. Hong, S-Y., J. Dudhia, and S-H. Chen, 2004; "A revised approach to ice microphysical processes for the bulk parameterization of clouds and precipitation." Mon. Wea. Rev., 132, 103–120.
doi.org/10.1175/1520-0493(2004)132<0103:ARATIM>2.0.CO;2
35. Iacono, Jennifer S. Delamere, Eli J. Mlawer, Mark W. Shephard, Shepard A. Clough, and William D. Collins, 2008; "Radiative forcing by long-lived greenhouse gases: Calculations with the AER radiative transfer models." JOURNAL OF GEOPHYSICAL RESEARCH, VOL. 113, D13103.
doi: 10.1029/2008JD009944
36. Janjic and J. P. Gerrity Jr, 2001; "An Alternative Approach to Non hydrostatic Modeling." Monthly Weather Review, volume 129; 1164-1178.
Doi.org/10.1175/1520-0493 (2001)129<1164:AAATNM>2.0.CO;2

37. Janjic Z.I, 1996; "The surface layer parameterization in the NCEP Eta Model." World Meteorological Organization-Publications-WMO TD, ICSU, WMO, UNESCO.
38. Janjic Z.I, 1990; "The step-mountain coordinate: Physical package. Mon." *Wea. Rev.*, 118, 1429–1443.
doi.org/10.1175/1520-0493(1990)118<1429:TSMCPP>2.0.CO;2
39. Janjic Zavisla I., 2000; "Development and Evaluation of a Convection Scheme for Use in Climate Models." Volume 57 *Journal of The Atmospheric Sciences* National Centers for Environmental Prediction, Camp Springs, Maryland.
doi.org/10.1175/1520-0469(2000)057<3686:CODAEO>2.0.CO;2
40. Janjic, Z. I., 1994; "The step-mountain Eta coordinate model: Further developments of the convection, viscous sub layer, and turbulence closure schemes." *Mon. Wea. Rev.*, 122: 927–945.
41. Janjic, Z. I., 2002; "Nonsingular Implementation of the Mellor-Yamada Level 2.5 Scheme in the NCEP Meso model." NCEP Office Note, No 437: 61 pp.
42. Kain J. S. and J. M., Fritsch, 1990; "A one-dimensional entraining/detraining plume model and its application in convective parameterization." *J. Atmos. Sci.*, 47: 2684-2702.
43. Kain, J. S. and J. M. Fritsch, 1993; "Convective parameterization for mesoscale models: The Kain-Fritsch scheme, the representation of cumulus convection in numerical models, K.A. Emanuel and D.J. Raymond." Eds. *Amer. Meteor. Soc.*: 246 pp.
44. Kain, J. S., 2004; "The Kain-Fritsch convective Parameterization." An update. *J. Appl. Meteor.*, 43: 170-181.
45. Kessler, E., 1969; "On the distribution and continuity of water substance on atmospheric circulation." *Meteorol. Monogr.*, 10, 32: 84.
46. Khain, A. P., N. BenMoshe, and A. Pokrovsky, 2008: Factors determining the impact of aerosols on surface precipitation from clouds: Attempt of classification. *J. Atmos. Sci.*, 65, 1721–1748.
47. Krieger JW, 2009; "Single versus multiple sets of resistance exercise: a meta-regression." *J Strength Cond Res.* 2009 Sep; 23(6):1890-901.
Doi: 10.1519/JSC.0b013e3181b370be.
48. Lacis, A. A., and J. E. Hansen, 1974; "A parameterization for the absorption of solar radiation in the earth's atmosphere." *J. Atmos. Sci.*, 31, 118–133.

49. Lighthill, J., G. J. Holland, W.M. Gray, C. Landsea, K. Emanuel, G. Craig, J. Evans, Y. Kurihara, and C. P. Guard, 1994: Global climate change and tropical cyclones. *Bull. Amer. Met. Soc.*, 75, 2147-2157
50. Lim and Hong S-Y, 2010; "Development of an Effective Double-Moment Cloud Microphysics Scheme with Prognostic Cloud Condensation Nuclei (CCN) for Weather and Climate Models." Global Environment Laboratory, Department of Atmospheric Sciences, Yonsei University, Seoul, South Korea.
doi.org/10.1175/2009MWR2968.1
51. Lin, Y.L., R. D. Farley, and H. D., Orville, 1983; "Bulk parameterization of the snow field in a cloud model." *J. Climate Appl. Meteor.*, 22: 1065-1092.
52. Liou, Thomas P. Ackerman, Francisco P. J. Valero and Leonhard Pfister, 1988; "Heating Rates in Tropical Anvils." *Journal of the atmospheric sciences* 45 (10), 1606-1623.
doi.org/10.1175/1520-0469(1988)045<1606:HRITA>2.0.CO;2
53. Loh W, Juneng L and Tangang F, 2010; "Sensitivity of Typhoon Vamei simulation to planetary boundary layer parameterization using PSU/NCAR MM5." *Pure Appl. Geophys.*, 168(10) 1799–1811.
54. Mandal M, Mohanty U and Raman S, 2004; "A study on the impact of parameterization of physical processes on prediction of tropical cyclones over the Bay of Bengal with NCAR/PSU mesoscale model." *Natural Hazards*, 31(2): 391–414.
55. Martilli, Alain Clappier and Mathias W. Rotach, 2002; "An Urban Surface Exchange Parameterization for Mesoscale Models," *Boundary-Layer Meteorology*, Volume 104, Issue 2, pp 261–304.
56. Mellor and Tetsuji Yamada, 1982; "Development of a turbulence closure model for geophysical fluid problems." *Reviews of Geophysics and Space Physics*, Vol. 20, NO. 4: 851-875.
DOI: 10.1029/RG020i004p00851
57. Mishra, D. K., and G.R Gupta, 1976; "Estimation of maximum wind speed in tropical cyclones occurring in India Sea." *Indian J. Hydr. And Geophys.*, vol. 27 No.3: 285-290.

58. Mlawer, E. J., S. J. Tubman, P. D. Brown, M. J. Lacono, and S. A. Clough, 1997; “Radiative transfer for inhomogeneous atmosphere: RRTM, a validated correlated-k model for the long wave.” *J. Geophys. Res.*, 102(D14): 16663-16682.
59. Morcrette J. M., Howard W. Barker, Jason S. Cole, Michael J. Iacono, and Robert Pincus, 2008, “Impact of a new radiation package, McRad, in the ECMWF Integrated Forecasting System.” *Monthly Weather Review*, Vol. 136, pages 4773-4798.
Doi: 10.1175/2008MWR2363.1.
60. Morrison and J. O. Pinto, 2006; “Inter comparison of Bulk Cloud Microphysics Schemes in Mesoscale Simulations of Springtime Arctic Mixed-Phase Strati form Clouds.” Department of Aerospace Engineering, University of Colorado, Boulder, Colorado, Department of Aerospace Engineering, University of Colorado, and NCAR, Boulder, Colorado.
doi.org/10.1175/MWR3154.1
61. Morrison H, Thompson G, Tatarskii V, (2008); “Impact of cloud microphysics on the development of trailing strati form precipitation in a simulated squall line: Comparison of one- and two-moment schemes.” *Monthly Weather Review*: In Press.
62. Morrison, J. A. Curry, and V. I. Khvorostyanov, 2005: “A new double-moment microphysics parameterization for application in cloud and climate models. Part I: Description.” *J. Atmos. Sci.*, 62, 1665–1677.
63. Noh, Y., W.G. Cheon, S.-Y. Hong, and S. Raasch, 2003; “Improvement of the K-profile model for the planetary boundary layer based on large eddy simulation data.” *Bound.-Layer Meteor.*, 107, 401–427.
64. Noilhan, J., and S. Planton, 1989; “A simple parameterization of land surface processes for Meteorological models.” *Mon. Wea. Rev.*, 117, 536–549.
65. Oreopoulos, L., E.J. Mlawer, J.S. Delamere, T. Shippert, J. Cole, B. Fomin, M.J. Iacono, Z. Jin, J. Li, J. Manners, P. Räisänen, F.G. Rose, Y.-C. Zhang, M.J. Wilson, and W.B. Rossow, 2012; “The Continual Inter comparison of Radiation.” *Codes: Results from Phase I. J. Geophys. Res.*, 117, no. D6, D06117.
doi:10.1029/2011JD016821.

66. Pattnaik and T. N. Krishnamurti, 2007; “Impact of cloud microphysical processes on hurricane intensity, part 2: Sensitivity experiments.” *Meteorology and Atmospheric Physics*, Vol. 97, No. 1: 127–147.
DOI: 10.1007/s00703-006-0248-x
67. Pleim, J. E. and A. Xiu, 1995; Development and testing of a surface flux and planetary boundary layer model for application in mesoscale models. *J. Appl. Meteor.*, 34, 16–32.
68. Pleim, J. E., and A. Xiu, 2003; “Development of a land surface model. Part II: Data Assimilation.” *J. Appl. Meteor.*, 42, 1811–1822.
69. Pleim, J., 2007; “A combined local and non-local closure model for the atmospheric boundary layer. Part II: Application and evaluation in a mesoscale meteorological model.” *J. Applied Meteor. Climatology*, 46: 1396–1409.
70. Pleim, J.E. and R.C. Gilliam, 2008: An indirect data assimilation scheme for deep soil temperature in the Pleim-Xiu land surface model. Submitted to *J. Appl. Meteor. Climatology*.
71. Prater B and Evans J, 2002; “Sensitivity of modeled tropical cyclone track and structure of Hurricane Irene (1999) to the convective parameterization scheme.” *Meteorol. Atmos. Phys*, 80(1): 103–115.
72. Ramanathan, V., P. J. Crutzen, J. T. Kiehl and D. Rosenfeld, 2001; “Aerosols, climate, and the hydrological cycle.” *Science*, 294, 2119–2124.
73. Rao D and Prasad D, 2007; “Sensitivity of tropical cyclone intensification to boundary layer and convective processes.” *Natural Hazards*, 41(3) 429–445.
74. Rutledge and Hobbs, 1984; “The Mesoscale and Microscale Structure and Organization of Clouds and Precipitation in Midlatitude Cyclones. XII: A Diagnostic Modeling Study of Precipitation Development in Narrow Cold-Frontal Rainbands.” Atmospheric Sciences Department, University of Washington, Seattle, WA 98195.
[doi.org/10.1175/1520-0469\(1984\)041<2949:TMAMSA>2.0.CO;2](https://doi.org/10.1175/1520-0469(1984)041<2949:TMAMSA>2.0.CO;2)
75. Ryan, B. F., 1996: On the global variation of precipitating layer clouds. *Bull. Amer. Meteor. Soc.*, 77, 53–70.
76. Shi, Y., K. J. Davis, C. J. Duffy, and X. Yu, 2011: A Watershed Scale Groundwater-Land-Surface Model Poster. *25th Conference on Hydrology, Seattle, WA. American Meteorological Society*.

77. Skamarock, W.C., J.B. Klemp, J. Dudhia, D.O. Barker, M.G. Duda, X-Y. Huang, W. Wang and J.G. Powers, 2008; "A description of the Advanced Research WRF Version 3." NCAR Technical Notes, NCAR/TN-475+STR, Boulder, Colorado, USA.
78. Srinivas C, Venkatesan R, Bhaskar Rao D and Hari Prasad D, 2007; "Numerical simulation of Andhra severe cyclone (2003): Model sensitivity to the boundary layer and convection parameterization," *Pure Appl. Geophys.* 164(8–9) 1465–1487.
79. Stephens, G. L., 1978; "Radiation profiles in extended water clouds. Part II: Parameterization schemes, *J. Atmos. Sci.*, 35, 2123–2132.
80. Tao and William K.-M. Lau, 1989; "Convective-Radiative- -Mixing Processes in the Tropical Ocean-Atmosphere." Laboratory for Atmospheres goddard Space Flight Center, Greenbelt, Maryland, USA.
81. Thompson, G., R. M Rasmussen, and K. Manning, 2004; "Explicit forecasts of winter precipitation using an improved bulk microphysics schemes Part I." Description and sensitivity analysis. *Mon. Wea. Rev.*, 132: 519-542.
82. Wang, C., 2005: A modeling study of the response of tropical deep convection to the increase of cloud condensation nuclei concentration: 1. Dynamics and microphysics. *J. Geophysics. Res.*, 110, D21211.
doi:10.1029/2004JD005720.
83. Wicker and Wilhelm son, 1995; "Simulation and Analysis of Tornado Development and Decay within a Three-Dimensional Super cell Thunderstorm." Department of Atmospheric Science and National center for upper computing Applications, University of Illinois, Urbana - Champaign, Illinois.
84. Xiu, A. and J. E. Pleim, 2001; "Development of a land surface model part 1." Application in a mesoscale meteorology mode. *J. Appl. Meteor.*, 40: 192-209
85. Yang, M. J., and L. Ching, 2005; "A Modeling study of typhoon Toraji (2001): Physical Parameterization sensitivity and topographic effect." *Terrestrial, Atmospheric and Oceanic Sciences*, 16(1): 177-213.